Understanding and Exploiting MYCN Addiction in High-Risk Neuroblastoma Using the Example of CDK13

Dissertation

Mona Soledad Friedrich, M. Sc.

Biowissenschaften

Dissertation

submitted to the
Combined Faculty of Natural Sciences and Mathematics
of the Ruperto Carola University Heidelberg, Germany
for the degree of
Doctor of Natural Sciences

Presented by
Mona Soledad Friedrich, M.Sc.
Born in: Karlsruhe
Oral Examination: 03.06.2019

Understanding and Exploiting MYCN Addiction in High-Risk Neuroblastoma Using the Example of CDK13

Referees: Prof. Dr. Thomas Höfer

PD Dr. Frank Westermann

Sperrvermerk

für die Dissertation „Understanding and Exploiting MYCN Addiction in High-Risk Neuroblastoma Using the Example of CDK13"
von Mona Soledad Friedrich, M. Sc.

Declaration

The work presented in this thesis was carried out from March 2014 until March 2019 in the group of Neuroblastoma Genomics at the German Cancer Research Center (DKFZ) in Heidelberg, Germany. It was supervised by PD Dr. Frank Westermann.

I declare that this thesis, and the research to which it refers, are the product of my own work that has not yet been submitted for a degree or a diploma at any university. To the best of my knowledge this thesis contains no material previously published or written by another person except where due acknowledgement is made in the thesis itself.

_____

Mona Friedrich
Heidelberg, April 10, 2019

SUMMARY

Neuroblastoma (NB) is an extracranial childhood cancer and accounts for 15 % of all childhood cancer-related deaths. It is a remarkably heterogeneous disease and cases range from spontaneous regression to aggressive high risk disease. Amplification of the oncogene *MYCN* occurs in 20-30 % of cases and is an indicator of poor prognosis. As a transcription factor, MYCN drives several cellular programs favoring malignant behavior, for example proliferation, angiogenesis and metastasis. In order to gain a better understanding of direct and secondary transcriptional targets of MYCN, gene expression was analyzed in a time course experiment using cell cycle-synchronized cells with regulatable MYCN level. This approach revealed the continued upregulation of a number of cell cycle driver genes as well as genes involved in protein and DNA biosynthesis in MYCN high cells. Differences in the expression of other cell cycle and DNA replication genes occurred only in specific phases of the cell cycle. On the other hand, genes involved in alternative splicing and cell adhesion were constantly downregulated. The expression of snoRNAs strongly increased in the MYCN low condition towards the end of the observation period. An analysis of miRNA expression revealed that many differentially regulated miRNAs targeted genes involved in ribosome biogenesis, cancer processes and signaling pathways. Taken together, this data set indicates that MYCN directly regulates the expression of genes and miRNAs which contribute to accelerated proliferation, metabolism and metastatic growth in NB cells. As a consequence of the induced phenotype, a larger number of secondary targets are deregulated.

As MYCN heavily contributes to tumor malignancy, *MYCN*-amplified NB cells become addicted to high amounts of the protein. However, MYCN itself is notoriously difficult to target, therefore two siRNA screens were performed to detect synthetic lethal relationships with high MYCN levels. The second part of this thesis deals with the transcriptional kinase CDK13, which was identified as a potential candidate for novel targeted therapies. *CDK13* and its highly homologous family member *CDK12* were knocked down by several technical approaches. In a cellular *MYCN* overexpression model, *CDK13* repression induced strong cell death only in *MYCN* high cells. *CDK12* repression also elicited a small amount of cell death comparing *MYCN* high with low cells. Inducible *CDK13* knockdown in a *MYCN*-amplified cell line caused modest reductions in cellular viability and colony formation capacity. *CDK13,* but not *CDK12,* knockout induced by the clustered regularly interspaced short palindromic repeats (CRISPR) technique reduced viability and caused a small increase in cells arrested in G_1. However, analysis of *CDK13* mRNA level revealed significant residual expression, suggesting that the majority of the polyclonal culture might be heterozygous for the induced mutation. A novel small

compound inhibitor against CDK12 and CDK13 (BAY-587) was tested in a panel of eight NB cell lines and the effects were compared to that of a commercially available inhibitor, THZ531. BAY-587 was active at lower concentrations than THZ531. Both compounds strongly reduced viability, colony formation capacity and disrupted cell cycle distributions. BAY-587 treatment reduced the level of CDK12 protein and further induced apoptosis. Gene expression analysis revealed that CDK12/13 inhibition by BAY-587 caused downregulation of genes involved in alternative splicing and DNA damage repair, while transcription regulation genes were upregulated. In summary, CDK13 emerged as a promising new therapeutic candidate for the treatment of high risk NB patients.

ZUSAMMENFASSUNG

Das Neuroblastom ist ein extrakranialer Tumor, der im Kindesalter auftritt und für 15 % der Todesfälle im Zusammenhang mit Krebserkrankungen bei Kindern verantwortlich ist. Der Verlauf dieser Erkrankung ist sehr heterogen, es gibt Fälle, bei denen sich der Tumor spontan zurückbildet, aber auch sehr aggressive Hochrisikofälle. In 20 – 30 % der Fälle liegt eine Amplifizierung des Onkogens *MYCN* vor, was mit einer deutlich schlechteren Prognose verbunden ist. MYCN ist ein Transkriptionsfaktor und reguliert verschiedene zelluläre Programme, die bösartiges Wachstum begünstigen, wie zum Beispiel Proliferation, Angiogenese und Metastasierung. Um mehr über direkte und indirekte transkriptionelle Ziele von MYCN zu erfahren, wurde die Genexpression synchronisierter Zellen mit regulierbarem MYCN Level über einen längeren Zeitraum gemessen. Dabei wurden Gene identifiziert, die über die gesamte Beobachtungsdauer hinweg stärker in Zellen mit viel MYCN Protein exprimiert wurden. Darunter fanden sich mehrere Zellzyklusgene sowie vermehrt Gene der Protein- und DNA-Biosynthese. Bei einigen anderen Zellzyklusgenen und DNA Replikationsgenen unterschied sich die Expression in Zellen mit viel oder wenig MYCN Protein nur in spezifischen Zellzyklusphasen. Im Gegensatz dazu wurden Gene des alternativen Spleißens und der Zelladhäsion in Zellen mit viel MYCN konstant niedriger exprimiert. In Zellen mit wenig MYCN gab es zudem einen starken Anstieg in der Expression von snoRNAs gegen Ende des Beobachtungszeitraumes. Eine Analyse der miRNA Expression ergab, dass MYCN vorwiegend miRNAs beeinflusst, welche Gene der Ribosom Biogenese, Tumorbiologie und Signalwege regulieren. Zusammenfassend zeigt der vorliegende Datensatz, dass MYCN durch die direkte Regulierung von Gen- und miRNA-Expression zu beschleunigter Proliferation, Metabolismus und metastasierendem Wachstum beiträgt. Der daraus resultierende Phänotyp bedingt die Deregulierung weiterer, sekundärer Zielgene.

Da MYCN einen großen Anteil an der Bösartigkeit des Tumors trägt, werden *MYCN*-amplifizierte Neuroblastomzellen abhängig von großen Mengen des Proteins in der Zelle. Bislang ist es problematisch, MYCN selbst durch Wirkstoffe anzugreifen. Aus diesem Grund wurden zwei siRNA Screens durchgeführt, die zum Ziel hatten, synthetisch-letale Interaktionen mit erhöhtem MYCN Protein zu ermitteln. Der zweite Teil dieser Arbeit beschäftigt sich mit der Charakterisierung eines Kandidaten aus diesen Screens, der transkriptionellen Kinase CDK13. Knockdowns von *CDK13* sowie einer verwandten Kinase aus derselben Proteinfamilie, *CDK12*, wurden mittels verschiedener Techniken erzielt. In einem Zellmodell zur Überexpression von *MYCN* führte der Knockdown von *CDK13* zu starkem sowie der Knockdown von *CDK12* zu leichtem Zelltod. *CDK13* Knockdown in einer *MYCN*-amplifizierten Zelllinie führte zu einer leichten Verminderung

von Viabilität und der Fähigkeit, aus Einzelzellen Kolonien zu bilden. Darüber hinaus wurde mittels CRISPR (clustered regularly interspaced short palindromic repeats) ein Knockout von *CDK13* erzielt, was zu einer Reduktion der Viabilität sowie einem leichten G_1-Arrest führte, nicht jedoch bei einem Knockout von *CDK12*. Allerdings war die *CDK13* mRNA Expression um weniger als 50 % reduziert, was auf das Vorliegen einer polyklonalen Zellkultur mit vermutlich vorwiegend heterozygoten Mutationen zurückzuführen war. Des Weiteren wurde ein neuartiger Inhibitor von CDK12 und CDK13 (BAY-587) in acht verschiedenen Neuroblastom Zelllinien getestet und mit dem kommerziell erhältlichen Inhibitor THZ531 verglichen. Alle Zelllinien reagierten sensitiver auf BAY-587 als auf THZ531 und wiesen niedrigere IC50 Werte auf. Beide Inhibitoren verminderten die Zellviabilität und die Fähigkeit, Kolonien zu bilden und riefen Veränderungen der Zellzyklusprofile hervor. Die Behandlung mit BAY-587 verminderte den CDK12 Proteingehalt und induzierte außerdem Apoptose. Eine Analyse der Genexpression nach CDK12/13 Inhibition durch BAY-587 zeigte, dass Gene des alternativen Spleißens und der DNA-Schadensreparatur weniger stark exprimiert wurden. Die Expression von Genen, welche die Transkription regulieren, war erhöht. Zusammengefasst konnte gezeigt werden, dass CDK13 ein vielversprechender Kandidat für die Entwicklung neuer Therapien für Patienten mit Hochrisiko-Neuroblastom darstellt.

TABLE OF CONTENTS

LIST OF FIGURES

LIST OF TABLES

°C	Degrees Celsius
µ	Micro
A	Alanine
AAVS1	Adeno-Associated Virus Integration Site 1
act. transl.	Activating translocation
ALK	Anaplastic Lymphoma Kinase
Amp	Amplified
APS	Ammonium persulfate
ATM	Ataxia Telangiectasia Mutated
ATP	Adenosine 5′-triphosphate
ATR	Ataxia Telangiectasia And Rad3 Related
ATRX	Alpha Thalassemia/Mental Retardation Syndrome X-linked
Baf A1	Bafilomycin A1
bp	Basepair(s)
BrdU	Bromdesoxyuridin
BSA	Bovine serum albumin
Cas9	CRISPR Associated Protein 9
CCN(D)	Cyclin (D) (gene name)
CDC25A	Cell Division Cycle 25A
CDK	Cyclin-Dependent Kinase
CDKI	CDK inhibitor
CDKN1A	CDK Inhibitor 1A
cDNA	Complementary DNA
cm	Centimeter
c-MYC	V-Myc Avian Myelocytomatosis Viral Oncogene Homolog
CPM	Count per million
CRISPR	Clustered regularly interspaced short palindromic repeats
CRISPRi	CRISPR interference
C_T	Threshold cycle
CTB	CellTiter-Blue Assay
CTD	Carboxyterminal domain
DAPI	4,6-diamidino-2-phenylindol
dCas	Deactivated Cas
ddH2O	Double-distilled water
DDR	DNA damage repair
DEG	Differentially expressed genes
DKFZ	German Cancer Research Center
DMSO	Dimethyl sulfoxide
DNA	Deoxyribonucleic acid
dNTP	Deoxynucleoside triphosphate
Doxy	Doxycycline
DTT	Dithiothreitol
EDTA	Ethylenediaminetetraacetic acid
Escherichia coli	*E. coli*
Et al.	*Et alii* (and others)
EtOH	Ethanol

EZH2	Enhancer of Zeste 2
FACS	Fluorescence-activated cell sorting
FCS	Fetal calf serum
FDR	False discovery rate
Fer-1	Ferrostatin-1
FOXM1	Forkhead Box Protein M1
FSC	Forward scatter
GFP	Green fluorescent protein
GO	Gene ontology
H	Histone
h	Hour(s)
IC50	Half maximal inhibitory concentration
IC50	Half-maximal inhibitory concentration
INRG	International neuroblastoma risk group
INRG	International Neuroblastoma Risk Group
K	Lysine
kDa	Kilodalton
KDM	Kinase-dead mutant
KEGG	Kyoto Encyclopedia of Genes and Genomes
KRAB	Krüppel Associated Box
l	Liter
LB	Lysogeny broth
M phase	Mitosis
M	Molar
MAD	MYC Dimerization Protein 1
MAX	MYC-associated Factor X
MeOH	Methanol
microRNA	miRNA
min	Minute(s)
MIZ1	Myc-Interacting Zinc-finger Protein 1
ml	Milliliter
MNA	MYCN-amplified/amplification
MPER	Mammalian protein extraction reagent
mut	Mutant
MYC	V-Myc Avian Myelocytomatosis Viral Oncogene Homolog
MYCN	V-Myc Avian Myelocytomatosis Viral Oncogene Neuroblastoma Derived Homolog
n	Nano
NB	Neuroblastoma
Nec-1	Necrostatin-1
NHDF	Non-transformed fibroblasts
NOP56	Nucleolar Protein 56
n.s.	not significant
OE	Overexpression
P	Proline
PAA	Polyacrylamide
PAGE	Polyacrylamide gelelectrophoresis
PBS	Phosphate-buffered saline
PCAP	Phospho-CTD Associating Proteins

PHOX2B	Paired-like Homeobox 2B
PI	Propidium iodide
PKMYT1	Protein Kinase Membrane Associated Tyrosine/Threonine 1
PNK	Polynucleotide kinase
PRC2	Polycomb Repressive Complex 2
pSer	Phosphorylated serine residue
pTEF-ß	Positive Transcription Elongation Factor ß
R	Arginine
RB	Retinoblastoma Protein
RNA Pol II	RNA polymerase II
RNA	Ribonucleic acid
RNAi	RNA interference
rRNA	Ribosomal RNA
RT-qPCR	Quantitative real-time polymerase chain reaction
S / Ser	Serine
s	Second(s)
SDS	Sodium dodecyl sulfate
SEM	Standard error of the mean
sgRNA	Single guide RNA
shRNA	Short hairpin RNA
siRNA	Small interfering RNA
SKP2	S-Phase Kinase Associated Protein 2
snoRNA	Small nucleolar RNA
snRNA	Small nuclear RNA
SP1	Specific Protein 1
SSC	Side scatter
TALEN	Transcription activator-like effector nuclease
TBS-T	Tris-buffered saline-Tween
TERT	Telomerase Reverse Transcriptase
TGFß	Transforming Growth Factor ß
TMM	Trimmed mean of M values
TR	Tetracycline repressor
TUNEL	Terminal deoxynucleotidyl transferase -mediated dUTP-biotin nick end labeling
V	Volt
wt	Wildtype

1.1 Basics of Cancer

To this day, cancer represents one of the leading causes of death. According to the World Cancer Report, in 2012 there were 1820 per million people diagnosed with cancer worldwide, which corresponds to a total number of 14.1 million cases (Stewart and Wild, 2014). In the same year, 1020 per million people died from the disease (a total of 8.2 million). The incidence of childhood cancer ranges between 50 and 200 cases per million per year, representing up to 4.5 % of all cancer cases. Growing globalization and human development involve changes in lifestyle that will likely lead to an even higher cancer burden. In 2025, the cancer incidence is predicted to rise above 20 million cases.

Decades of intense cancer research have shed some light on origin and development of this complex disease and given rise to novel concepts of treatment. Despite this, many aspects still remain poorly understood. The following chapter will touch upon the most important concepts in tumor biology.

Cancer is a disease where cells become able to divide uncontrollably and to spread to other tissues (Cooper, 2000). In a landmark article, Hanahan and Weinstein described six distinctive hallmarks that enable previously normal cells to acquire a malignant phenotype (2000). First, the ability to produce mitogenic signals renders cells independent from stimuli by the surrounding tissues. Second, malignant cells override anti-growth signals from the surroundings that in normal tissues maintain quiescence and homeostasis. Third, tumor cells are able to escape programmed cell death, which constitutes a natural barrier to cancer development. Fourth, cells replicate without being limited intrinsically by telomere shortening and ensuing states of senescence or crisis. Fifth, continuous angiogenesis ensures sufficient supply of oxygen and nutrients to the tumor, and sixth, cells invade locally and metastasize to distant tissues.

These traits are acquired stepwise and facilitated by increasing genomic instability (Hanahan and Weinberg, 2011). A series of such genetic changes confers a selective growth advantage to a cell (Nowell, 1976). These changes include somatic mutations as well as chromosome instability associated with losses or gains of chromosome parts or translocations. In addition, epigenetic changes like DNA methylation or histone modifications can impact on gene expression. In tumorigenesis, two classes of genes are of particular importance: proto-oncogenes and tumor suppressor genes. Proto-oncogenes regulate proliferation or inhibit cell death and genetic changes turn them into constitutively active oncogenes (Croce, 2008). Opposed to that, tumor suppressor gene products have a protective function by negatively regulating the cell cycle or promoting cell death. Only a

biallelic inactivation of such a tumor suppressor gene promotes tumorigenesis (Sherr, 2004).

Even though cells need to accumulate several mutations in order to become tumorigenic, several research groups observed that abolishing a single key oncogene may be enough to stop cell growth and induce differentiation or cell death (Jain *et al.*, 2002; Pelengaris *et al.*, 1999). This observation gave rise to the concept of oncogene addiction, which was first described by Weinstein (2002). He postulated that malignant cells depend on the aberrant expression of one or only a few oncogenes to maintain their cancerous behavior. Evidence from clinical studies backs up this concept (Weinstein and Joe, 2006). For instance, breast cancer patients with *HER2* overexpression can successfully be treated with antibodies against HER2 (Vogel *et al.*, 2002). Also, reactivation of a key tumor suppressor gene may be sufficient to prevent a cancer cell from proliferating (Weinstein, 2002). This is called tumor suppressor gene hypersensitivity. Both aspects of tumor cell biology bear great potential for the development of new molecularly targeted therapies. In most cases, it will be beneficial to combine targeted drugs or add standard therapy in order to avoid the development of resistances, as observed in targeted therapy studies where tumors relapsed after an initial response. Analysis of the relapsed tumors revealed that they had acquired additional mutations, which blocked the administered antibody from binding (Weinstein and Joe, 2006). Thus, the cells likely depend so heavily on the oncogene in question that selective pressure favors mutations circumventing targeted therapy.

1.2 Neuroblastoma

Neuroblastoma (NB) is a common childhood tumor originating from neural crest precursor cells. Usually, the primary tumor is found in tissues of the nervous system, adrenal medulla or the paraspinal ganglia (Huang and Weiss, 2013). Approximately one in 100,000 children is diagnosed with NB each year and 15 % of all childhood cancer deaths are NB cases (Stewart and Wild, 2014). However, neuroblastoma biology and its clinical manifestation are remarkably heterogeneous. Low-risk cases oftentimes regress spontaneously without any treatment. On the other hand, high-risk cases still have survival rates below 50 % despite multimodal, intense treatment (Smith and Foster, 2018). It is therefore important to assign the best suitable treatment strategy to each patient and to avoid unnecessary strains through aggressive therapies in patients with a good prognosis. New staging and classification systems were developed by the International Neuroblastoma Risk Group (INRG) in 2009 to reach a worldwide consensus for risk stratification (Cohn *et al.*, 2009; Monclair *et al.*, 2009). Staging is based on image analysis prior to surgery and comprises the stages very low (localized tumors), low, intermediate

and high (metastatic disease) (L1, L2, M and MS) (Monclair *et al.*, 2009). Classification takes into account stage, age, histology, extent of tumor differentiation, *MYCN (V-Myc Avian Myelocytomatosis Viral Oncogene Neuroblastoma-Derived Homolog)* status, chromosome 11q status and DNA ploidy (Cohn *et al.*, 2009).
The current standard of care for high-risk patients includes chemotherapy followed by resection (induction phase), high-dose chemotherapy with autologous stem cell rescue and radiation (consolidation phase) and immunotherapy and retinoic acid treatment (maintenance phase) (Smith and Foster, 2018). These therapies come with strong side effects and induce considerable damage. In order to develop less harmful, targeted therapies, a better understanding of the underlying tumor biology of neuroblastoma is indispensable.

1.2.1 Somatic Aberrations in Neuroblastoma

The most common aberration in NB is the amplification of the *MYCN* oncogene, which occurs in 20-30 % of all cases (Brodeur *et al.*, 1984; Matthay *et al.*, 2016; Schwab *et al.*, 1983). Additionally, amplifications of *Anaplastic Lymphoma Kinase (ALK)* are frequently correlated with that of *MYCN* (Miyake *et al.*, 2002; Trigg and Turner, 2018).
Generally, NBs display relatively few recurrent somatic mutations when compared to adult tumors. Mutations in the *ALK* gene have been observed in up to 10 % of sporadic NB and in half the cases of hereditary NB (2 % of total cases) (Y. Chen *et al.*, 2008; Janoueix-Lerosey *et al.*, 2008; Mosse *et al.*, 2008). Moreover, germline or sporadic mutations in the *Paired-like Homeobox 2B (PHOX2B)* gene have been identified in a small number of NB tumors (Trochet *et al.*, 2004; van Limpt *et al.*, 2004).
Although mutations of the tumor suppressor gene *TP53* occur in less than 2 % of primary NB tumors, they are found in approximately 15 % of relapsed tumors (Carr-Wilkinson *et al.*, 2010).

1.2.2 MYCN in Neuroblastoma and Beyond

MYCN is a basic helix-loop-helix leucine zipper transcription factor and belongs to the same protein family as the highly homologous oncogene *MYC* (also known as *c-MYC*). While both MYCN and MYC deficiency lead to embryonic lethality in mice, it is possible to rescue the effect by introducing *MYCN* at the *MYC* locus (Malynn *et al.*, 2000). However, these mice suffer from growth deficits and muscular dystrophies. Apparently, MYC and MYCN can assume similar functions, including in proliferation, differentiation and apoptosis, but not completely replace each other. Their exact impact depends on distinct temporal and spatial expression patterns. For example, *MYCN* is expressed rather early

during development and necessary for neurogenesis in healthy mouse embryos (Knoepfler *et al.*, 2002; Zimmerman *et al.*, 1986).

MYCN amplification in NB is highly predictive of a poor prognosis (Brodeur *et al.*, 1984). Moreover, targeted *MYCN* overexpression in neural crest cells of mice is sufficient to cause NB development (Weiss *et al.*, 1997). Apart from NB, amplification and aberrant *MYCN* expression occur in medulloblastoma, retinoblastoma, astrocytoma, non-small cell lung cancer and glioblastoma (Schwab, 2004). High levels of MYC(N) have been correlated with several oncogenic processes, such as malignant transformation and proliferation (Schwab *et al.*, 1985), angiogenesis (Baudino *et al.*, 2002), genome instability (Felsher and Bishop, 1999), metastasis (Megison *et al.*, 2013) or the inhibition of differentiation (Freytag and Geddes, 1992). Somewhat contradictory, tumor inhibiting functions have also been documented, such as sensitization to apoptosis (Fulda *et al.*, 1999).

MYC and MYCN act as transcription factors through different mechanisms. They dimerize with the protein MYC-associated factor X (MAX) to reinforce expression of a large set of target genes by binding to a consensus sequence, the E-Box (Blackwood and Eisenman, 1991). However, at abundant protein levels, the complex is also able to bind to non-canonical sequences (Fernandez *et al.*, 2003). The complex then recruits further proteins to the gene, such as histone acetyltransferase proteins ensuring active chromatin states and positive transcription elongation factor (pTEF-β) for transcript elongation (Frank *et al.*, 2003; Majello *et al.*, 1999). Instead of MYC, MAX can also form a heterodimer with another protein named MAX dimerization protein 1 (MAD), which leads to transcriptional repression of MYC target genes (Ayer *et al.*, 1993).

Beside this, MYC itself also functions as a transcriptional repressor in two scenarios. It forms complexes with MYC-interacting zinc-finger protein 1 (MIZ1), thereby indirectly binding to the DNA (Peukert *et al.*, 1997). MYC-MIZ1 represses the expression of certain cell cycle inhibitory genes, for example *cyclin-dependent kinase inhibitor 1A* (*CDKN1A,* also known as *p21*) or *MAD4* (Kime and Wright, 2003; S. Wu *et al.*, 2003). Furthermore, MYC also interacts with Specific Protein 1 (SP1) (Gartel *et al.*, 2001). SP1 recognizes GC-rich regions and is involved in a range of cellular processes, such as differentiation, growth, cell death and DNA damage response. To achieve this, the MYC(N)-SP1 complex recruits histone deacetylases to its target genes (Iraci *et al.*, 2011). The removal of acetylation marks induces a closed chromatin structure characteristic of transcriptional repression. MYCN also indirectly affects other epigenetic repressors, such as Enhancer of Zeste 2 (EZH2) and other parts of the Polycomb Repressive Complex 2 (PRC2), which is responsible for histone 3 lysine 27 (H3K27) trimethylation (Kaur and Cole, 2013; Neri *et al.*, 2012).

In addition, both MYC and MYCN alter the expression of microRNAs (miRNAs), small non-coding RNAs that repress expression of a whole set of target proteins (Chang *et al.*, 2008; Schulte *et al.*, 2008). Therefore, the impact range of MYC(N) is extensive. For example, several miRNAs from the oncogenic miR-17-92 cluster are regulated by MYC. This cluster controls expression of cell cycle progression protein *E2F1*, chromatin modifiers and apoptosis regulator *BIM* (Li *et al.*, 2014; O'Donnell *et al.*, 2005).

Recent publications argued that MYC(N) acts as a transcriptional amplifier of already transcribed genes (Lin *et al.*, 2012; Nie *et al.*, 2012). In contrast, Duffy and colleagues overexpressed *MYCN* in a non-amplified NB cell line and reported that more genes were downregulated than upregulated in this setting. In addition, a pulse chase experiment revealed that differential gene regulation does not depend on the previous level of expression (Duffy *et al.*, 2015).

Due to its broad effect on gene expression programs, *MYCN*-amplified (MNA) NB and other cancers are dependent on high levels of the protein. According to the oncogene addiction theory, removal of MYCN should therefore critically hit the tumor. In fact, reducing the MYCN level by short hairpin RNAs (shRNAs) in NB cell lines and mouse models reduces proliferation and tumor incidence (Burkhart *et al.*, 2003). However, targeting MYC or MYCN has proven very difficult in the past (Westermark *et al.*, 2011). Even though some small molecules against MYC-MAX complex formation have been identified recently, they lack *in vivo* efficiency and are rapidly metabolized (Prochownik and Vogt, 2010). To date, no small molecules targeting MYCN are known. Others tried targeting the bromodomain of putative MYC(N) binding partners by small molecule JQ1, which had anti-proliferative effects and provided a survival advantage *in vivo* (Delmore *et al.*, 2011; Puissant *et al.*, 2013). While reduction of *MYCN* expression by RNA interference exhibited promising effects *in vitro* and in mouse models, there are still technical limitations in the clinic (Westermark *et al.*, 2011). Another strategy aims at identifying genes that are part of the MYCN regulatory network and required for oncogenic activity so that inactivation results in synthetic lethality (Chayka *et al.*, 2015). The inhibition of such a gene will cause tumor cell death but leave normal cells without *MYCN* amplification (MNA) unaffected.

1.2.3 Chromosomal Instability in Neuroblastoma

Deletions or gains of chromosome parts occur rather frequently in NB, such as gains of 17q (>80 % of cases) or deletion of the 11q or 1p chromosome arms (around 30% of cases) (Brodeur *et al.*, 1977; Schleiermacher *et al.*, 2012; Theissen *et al.*, 2014). These alterations are indicators of poorer prognosis. Oftentimes, 17q gain is linked to chromosomal loss at the partner chromosome. For example, 17q may translocate and

attach to chromosome arm 1p (Savelyeva *et al.*, 1994). The recurrence of such events suggests that they might contribute to NB tumorigenesis, for example through the loss of tumor suppressor genes or gain of oncogenes located on the concerned chromosomal arms.

1.2.4 Telomere Lengthening Mechanisms

In recent years, several aberrations affecting telomere maintenance have been identified in NB. In 31 % of high-risk cases, the 5p chromosome region is rearranged, which causes very high expression of the neighboring gene for *telomerase reverse transcriptase* (*TERT*) (Peifer *et al.*, 2015). High *TERT* expression also occurs in tumors with *MYCN* amplification, which is mutually exclusive with *TERT* rearrangement.
Inactivating mutations in the *ATRX (alpha thalassemia/mental retardation syndrome X-linked)* gene occur predominantly in older patients with chronic disease and adverse outcome (Cheung *et al.*, 2012). They are only found in cases without MNA or *TERT* rearrangements and are associated with the phenotype of alternative lengthening of telomeres.
Taken together, telomere maintenance, which is central to the cancer hallmark unlimited replication, appears to play an essential role in high-risk NB tumorigenesis (Hertwig *et al.*, 2016).

1.3 The Cell Cycle

Cellular proliferation is a tightly regulated process. In order to divide, cells go through a fixed succession of steps and have to pass several checkpoints (Harper and Brooks, 2005). As described above, several of the hallmarks of cancer disrupt aspects of controlled proliferation.

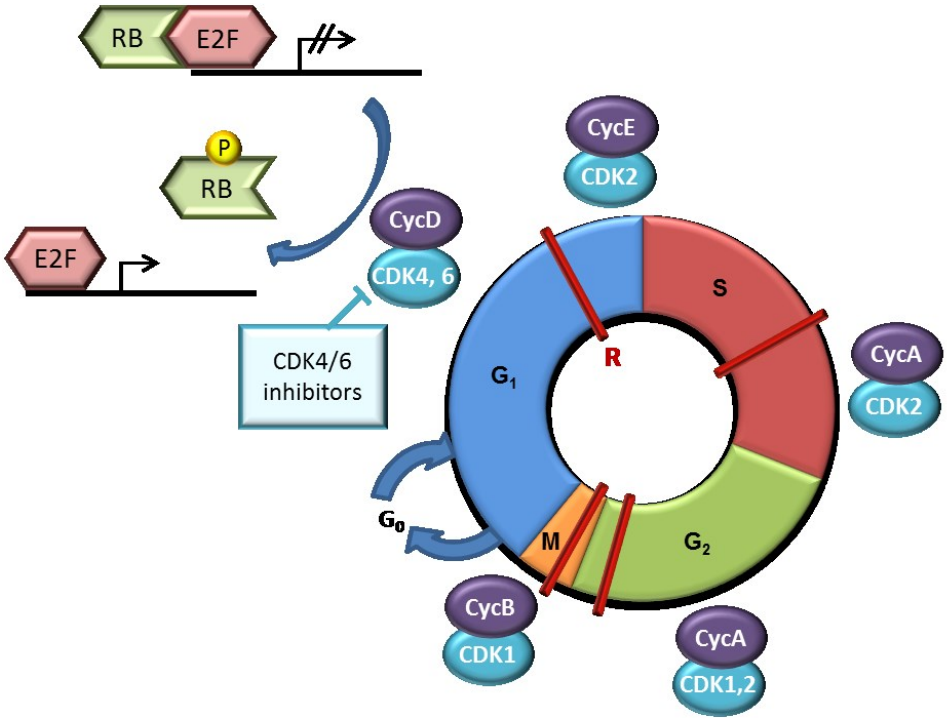

Figure 1: **CDKs in the Course of the Cell Cycle**
Progression through the cell cycle phases is driven by specific CDKs and their partner cyclins. Several checkpoints (red bars) prevent cells from proceeding in the event of DNA damage or insufficient growth. R - restriction point. Adapted from Aleem and Arcerci (2015).

Quiescent cells reside in G_0, making up the majority of an organism's cells. When a quiescent cell receives certain mitogenic growth signals, it re-enters the cell cycle at G_1 phase (Figure 1). In this phase, RNA and proteins are synthesized. Before progressing to S phase, the cell has to pass the restriction point. At this point, cells commit to completing the cell cycle independent of any further growth signals (Pardee, 1974). In the S phase, the cell's DNA and its centrosomes are duplicated and several checkpoints ensure that replication is complete and potential DNA damage is repaired (Harper and Brooks, 2005). If DNA damage is beyond repair, cell death is initiated as a protective mechanism. In healthy cells, G_2 phase ensues, where the cell prepares for mitosis (M phase) by further protein synthesis and cell growth. During mitosis, nucleus and cytoplasm are divided to form two daughter cells. Progression through the cell cycle is mainly driven by an enzyme family called cyclin-dependent kinases (CDKs).

1.4 Cyclin-Dependent Kinases

1.4.1 Cyclin-Dependent Kinases in the Cell Cycle

CDKs are a family of 20 serine/threonine kinases that share a conserved catalytic core consisting of an ATP-binding pocket (Adenosine triphosphate), a cyclin-binding domain

and an activating T-loop (Lim and Kaldis, 2013). In their classical function, they need to form a complex with a regulatory subunit from the cyclin family to become activated.
The first CDK named Cdc2 was discovered in yeast (Beach 1982, Nurse 1980). Since then, a wealth of research has identified more and more family members, binding partners and functions, as summarized by Malumbres (2014). During the cell cycle, the CDK level remains rather constant, while the different cyclin levels oscillate depending on the cell cycle phase. In the G_1 phase, different cyclin D isoforms interact with CDK4 and CDK6. The active complex then phosphorylates Retinoblastoma Proteins (RB), thus liberating transcription factor E2F and allowing expression of genes like cyclin E and A that are necessary for cell cycle progression (Figure 1). CDK2/cyclin E complexes drive transition from G_1 into S phase, whereas CDK1/cyclin A complexes are responsible for the initiation of the prophase at G_2:M transition. Entry into mitosis is controlled by CDK1/cyclin B complexes, which also regulate centrosome separation (Lindqvist *et al.*, 2007).
The activity of cell cycle CDKs is further controlled through activating phosphorylations by CDK7 and through CDK inhibitors (CDKIs) from the INK4 and the CIP/KIP protein family (Kaldis, 1999; Sherr and Roberts, 1999). For example, in the case of DNA damage, p53 binds to the DNA and induces the transcription of $p21^{Cip1}$. This protein in turn binds to and inhibits CDK2, thereby preventing the transition from G_1 to S phase. To abolish G_1:S phase arrest, $p21^{Cip1}$ is sequestered by the CDK4,6/cyclin D complex (Sherr and Roberts, 1999).
While the sequence of events in the cell cycle is finely tuned, knockout mouse models have proven that the function of many CDKs can be taken over by other members of the family (Gopinathan *et al.*, 2011).

1.4.2 Cyclin-dependent Kinases and the Cell Cycle in Cancer

In many cancer entities, one or more players of the cell cycle are deregulated. Frequently, *CDKs 4* or *6* or *cyclin D (CCND)* or *CCNE* are overexpressed or the expression of *CDKIs* or *RB* is lost due to mutations or chromosomal alterations (Malumbres and Barbacid, 2001). These deregulated components may represent attractive targets in cancer therapy. In the early 2000s, several small molecule CDKIs were developed, such as Flavopiridol and Selicilib. Unfortunately, first clinical studies with CDKIs as single agents showed only very limited effects with suboptimal pharmacokinetics but high toxicity (Diaz-Padilla *et al.*, 2009). All of these CDKIs targeted CDK2 amongst other CDKs, which proved to be replaceable by other family members during cell cycle progression (Ortega *et al.*, 2003). Follow-up studies investigated combination therapies of CDKIs with chemotherapeutics which showed at least some synergies. More potent second-generation CDKIs were designed to be more specific towards single CDKs (Diaz-Padilla *et al.*, 2009). Three

CDK4/6 inhibitors have since demonstrated good activity and have been approved for treatment in advanced breast cancer (Vijayaraghavan *et al.*, 2018). In a range of other solid tumors, ongoing clinical studies are testing the efficiency of CDK4/6 inhibitors.

Recent studies demonstrated that up to one third of primary NBs harbor chromosomal aberrations affecting a cell cycle gene (Molenaar *et al.*, 2012). Particularly in high-risk cases, the expression of many cell cycle components is deregulated (Krasnoselsky *et al.*, 2005). Amplifications of *CDK4* or *CCND1* and loss of CDK inhibitor *CDKN2* have been detected in tumors as well as in MNA cell lines (Gogolin *et al.*, 2013; Molenaar *et al.*, 2012). In case of DNA damage, an impaired G_1:S arrest has been shown in MNA cell lines despite functional p53 (McKenzie *et al.*, 1999). Most likely, this is due to low levels of $p21^{Cip1}$ and disturbed downstream signaling (Gogolin *et al.*, 2013; Tweddle *et al.*, 2001). Also, high-risk MNA cases frequently overexpress *S-Phase Kinase Associated Protein 2* (*SKP2)* (Westermann *et al.*, 2007). This protein induces the degradation of cell cycle inhibitors $p21^{Cip1}$ and $p27^{kip1}$, thereby promoting G_1:S and G_2:M phase transition. In p53 wildtype (wt) MNA cell lines, *CDK4* suppression via RNA interference (RNAi) or small molecules triggered G_1:S arrest and reduced viability (Gogolin *et al.*, 2013). In addition, CDK4 as well as cyclin D inhibition led to neuronal differentiation (Molenaar *et al.*, 2008). Ribociclib (LEE011), a specific CDK4/6 inhibitor, significantly delayed tumor growth in mouse models (Rader *et al.*, 2013). It was further tested in a phase I clinical study, where it achieved stable disease in 47 % of NB patients (Geoerger *et al.*, 2017).

Molenaar and colleagues also showed that CDK2 is synthetically lethal with high MYCN in NB – a finding that stands in contrast to other entities (2009). A small molecule CDK2 inhibitor was able to reduce tumor size and improve survival in a *MYCN* transgene mouse model (Dolman *et al.*, 2015). However, these effects cannot be attributed solely to CDK2 inhibition, as it also targets CDKs 1, 4, 5, 6 and 9.

1.4.3 Transcriptional Cyclin-Dependent Kinases

Besides cell cycle regulation, many CDK family members have diverse, often tissue-specific functions, as reviewed by Lim and Kaldis (2013). This includes DNA damage repair (CDK1, 3), epigenetic mechanisms (CDK1, 2), metabolism (CDK5, 8), stem cell renewal (CDK1), spermatogenesis (CDK2, 4, 16) and neuronal function (CDK5, 16). Moreover, a number of CDKs are involved in transcriptional regulation.

Several CDKs sequentially phosphorylate the heptapeptide repeats (YSPTSPS) of the carboxyterminal domain (CTD) of RNA polymerase II (RNA Pol II) during transcription and create a characteristic pattern, the CTD code. Thereby, they impact on RNA Pol II activity, the recruitment of complex members and co-transcriptional processing of pre-mRNA (Sanso and Fisher, 2013). Shortly after transcription is initiated, CDK7/cyclin H within the

Transcription Factor IIH complex phosphorylate serine residues 5 (Ser5) and 7 of the CTD and induce promoter-proximal pausing of RNA Pol II. Next, CDK7 activates CDK9, which together with cyclin T is part of the positive transcription elongation factor b complex (P-TEFb). CDK9 in turn causes pause release and the initiation of elongation by phosphorylating Ser2 (Larochelle *et al.*, 2012). As elongation takes place, Ser5 residues are dephosphorylated, while the amount of phosphorylated Ser2 residues increases (Kohoutek and Blazek, 2012). When transcription terminates, all phosphorylations are removed, which (next to complex interactions with several proteins) primes RNA Pol II for the next round of transcription. During elongation and termination, CDK7, CDK9 and CDK12 activity has been implicated, but the exact mechanisms are still unclear (Fisher, 2017).

CDK8 controls transcriptional repression by preventing the mediator complex from binding RNA Pol II and thereby activating gene expression (Knuesel *et al.*, 2009). In addition, CDK8 and also CDK14 are involved in the WNT/ß-catenin signaling pathway (G. Davidson *et al.*, 2009; Firestein *et al.*, 2008). Even cell cycle CDKs can indirectly impact on gene expression by regulating transcription factors, such as E2F and Forkhead Box Protein M1 (FOXM1) (Lim and Kaldis, 2013). Transcriptional regulation also occurs independently from the kinase function, as is the case for CDK10, which binds to and represses the ETS2 transcription factor (Kasten and Giordano, 2001).

CDK7 inhibition by a covalent inhibitor in NB cells resulted in downregulation of MYCN levels and a decrease in the expression of MYCN target genes (Chipumuro *et al.*, 2014). In a mouse model of high-risk NB, this translated to slower tumor growth.

1.4.4 Cyclin-Dependent Kinases 12 and 13

CDK13 (previously CDC2L5) and the highly homologous CDK12 (previously CrkRS) belong to the group of transcriptional CDKs. Both proteins contain a central kinase domain with 92 % shared sequence identity (H. H. Chen *et al.*, 2007). In addition, CDK12 and CDK13 are characterized by serine arginine (SR) and proline-rich motifs in the N-terminus and a low complexity C-terminus with a proline-rich domain, indicating areas of protein-protein interactions (Greenleaf, 2018) (Figure 2). In comparison to other CDKs, CDK12 and 13 are large proteins of around 164 kDa. While early studies claimed cyclin L to be the partner of both CDK12 and CDK13, it turned out that it is in fact cyclin K (Bartkowiak *et al.*, 2010; Blazek *et al.*, 2011). So far, most studies have focused on elucidating CDK12 function and much less is known about CDK13.

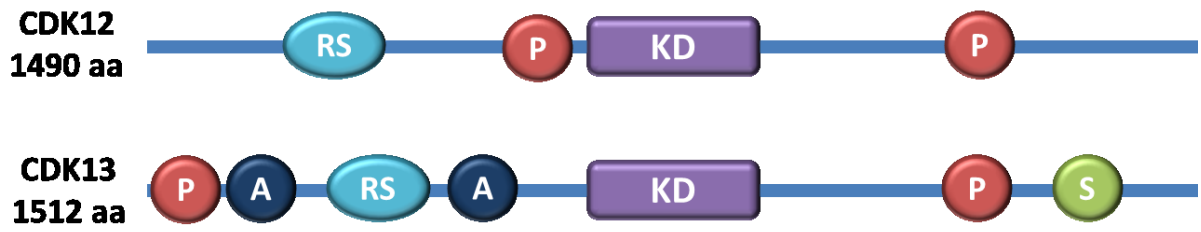

Figure 2: Domain Composition of CDK12 and CDK13
The kinase domains (KD) of CDK12 and CDK13 are flanked by arginine-serine (RS), proline (P), alanine (A) and serine (S) rich domains. Adapted from Kohoutek and Blazek (2012).

Knockdown of CDK12 and CDK13 by RNA interference (RNAi) in Drosophila and in human cells changes the phosphorylation status of RNA Pol II, arguing for their role as CTD kinases (Bartkowiak *et al.*, 2010; Blazek *et al.*, 2011). Also, chromatin immunoprecipitation experiments demonstrated that CDK12 is found in the middle and at the 3' end of actively transcribed genes, whereas CDK9 localizes more to the 5' end. However, the preferred substrate of CDK12/13 is still a matter of debate. Greifenberg and colleagues reported that CDK13 preferentially phosphorylated CTDs with existing phosphorylation marks at Ser7 (2016). They also claimed that CDK13 and CDK12 phosphorylated Ser2 and Ser5 residues, but not Ser7. Davidson et al. suggested that CDK12 might phosphorylate Ser2 and thus contribute to 3 prime end cleavage and polyadenylation (2014). Another study showed that upon CDK12 knockdown, the Ser2 phosphorylation level decreased (Bartkowiak *et al.*, 2010). These conclusions on substrate specificity were based on immunoblotting with pSer antibodies. However, Greenleaf recently pointed out in his review that the extent of antibody binding is influenced by phosphorylation of nearby residues (2018). Consequently, an altered signal only identifies general changes in CTD phosphorylation, but not where exactly these occur. Therefore, conclusions concerning the substrate of CDK12 and CDK13 need to be regarded cautiously. More recently, *in vitro* phosphorylation studies were able to confirm that CDK12 and CDK13 in complex with cyclin K target predominantly Ser2 and Ser5 (Bosken *et al.*, 2014; Greenleaf, 2018).

Both CDK12 and CDK13 induce alternative splicing when overexpressed *in vitro* (H. H. Chen *et al.*, 2006; H. H. Chen *et al.*, 2007). This finding is backed up by the observation that the two kinases localize to nuclear speckles (Even *et al.*, 2016; Ko *et al.*, 2001). Also, pull-down assays identified pre-mRNA processing proteins to be associated with CDK12 (Bartkowiak and Greenleaf, 2015). Apart from splicing mechanisms, CDK12 and CDK13 have also been implicated in the regulation of axonal elongation and the maintenance of self-renewal in stem cells (H. R. Chen *et al.*, 2014; Dai *et al.*, 2012).

Several authors performed gene expression analyses to better understand transcriptional targets of CDK12 and CDK13. Blazek et al. found that CDK12/cyclin K particularly

regulated long genes with many exons (2011). In their study using human embryonic kidney cells, genes involved in DNA damage repair (DDR) mechanisms were enriched in the set of downregulated genes after knockdown of *CDK12* or *CCNK*, but not *CDK13*. *CDK12* and *CCNK* knockdown also induced sensitivity towards DNA damaging agents. Greifenberg et al. reported that in colon cancer cells, *CDK13* knockdown resulted in the up- and downregulation of a similar number of genes, while *CDK12* knockdown induced more downregulation than upregulation (2016). There were relatively few commonly up- or downregulated genes (~25 % of CDK13 target genes). *CDK12* knockdown mainly downregulated expression of genes involved in DNA replication and DNA damage, while *CDK13* knockdown regulated extracellular and growth signaling pathways and metabolic processes. A different study by Liang and colleagues reported that both *CDK12* and *CDK13* knockdown by shRNAs almost exclusively led to target gene downregulation (2015). They also reported a much larger overlap of target genes (74 % of CDK13 genes). *CDK12* knockdown affected genes involved in RNA processing, DNA repair, chromosome organization and the cell cycle, whereas *CDK13* knockdown also affected RNA processing and in addition translation, energy metabolism genes and the expression of small nuclear RNA (snRNA) and small nucleolar RNA (snoRNA). The large discrepancies between these gene expression studies leave open the question in how far CDK12 and CDK13 assume the same or distinct functions in the cell.

Both kinases have been implicated in cancer. *CDK13* is amplified in in approximately 30% of hepatocellular carcinomas (Kim *et al.*, 2012). Alterations of the *CDK12* gene, such as mutations, rearrangements and amplifications occur in a large number of cancer entities, for example in breast and ovarian cancer (Chila *et al.*, 2016). For instance, a study on ovarian cancer revealed homozygous mutations in about 3% of examined cases, suggesting that *CDK12* functions as a tumor suppressor gene. Most *CDK12* mutations identified were located in the kinase domain, rendering the protein dysfunctional. As a consequence, the expression of CDK12 target genes was decreased. This was observed for genes involved in DDR like *ATM (Ataxia Telangiectasia Mutated), ATR (Ataxia Telangiectasia And Rad3 Related) or RAD51C* (Ekumi *et al.*, 2015). In contrast, two other studies in ovarian and prostate cancers with CDK12 inactivation found that DDR genes were not downregulated (Popova *et al.*, 2016; Y. M. Wu *et al.*, 2018). It appears that nonfunctional CDK12 leads to genomic instability in ovarian and prostate cancer in the form of random tandem duplications.

1.5 Aim and Objectives of the Study

Particularly high-risk NB patients with amplification of the *MYCN* transcription factor face a bad prognosis despite intensive therapy. Therefore, new treatment strategies based on a better understanding of neuroblastoma biology are desperately needed.

High abundance of MYCN protein deeply alters the transcriptional signature of affected cells (Oberthuer *et al.*, 2015). Proliferation and especially progression through the cell cycle are accelerated regardless of checkpoints (Bell *et al.*, 2006; Lutz *et al.*, 1996). While it seems obvious that the tumor cells depend on this MYCN signature to maintain this malignant phenotype, the exact transcriptional consequences of high MYCN levels are not completely understood yet.

The first part of this study deals with the gene expression analysis of synchronized NB cells with regulatable MYCN levels as they progress through the cell cycle. It takes into account both RNA and miRNA expression. The use of synchronized cells facilitates the discrimination between cell cycle and MYCN effects at distinct stages of the cell cycle.

A promising approach for the identification of new targets is to exploit potential vulnerabilities that arise from high MYCN. A synthetic lethal screen was performed in order to identify vulnerabilities connected to aberrant MYCN and revealed several interesting candidates. The second part of this study deals aims at the validation and ensuing characterization of the candidate CDK13 and the highly homologous CDK12 as potential novel therapeutic targets in MNA tumors.

2.1 Materials

2.1.1 Chemicals

4,6-diamidino-2-phenylindol (DAPI)	Sigma Aldrich / Merck, Darmstadt
Agar agar, Kobe I	Carl Roth, Karlsruhe
Agarose NEED Ultra-Qualität	Carl Roth, Karlsruhe
Ammonium persulfate (APS)	Merck, Darmstadt
b-Mercaptoethanol	Merck, Darmstadt
Bacto-tryptone	Carl Roth, Karlsruhe
Boric acid	Sigma Aldrich / Merck, Darmstadt
Bovine serum albumin (BSA)	Sigma Aldrich / Merck, Darmstadt
Bromphenol blue	Sigma Aldrich / Merck, Darmstadt
Bicine	Sigma Aldrich / Merck, Darmstadt
BIS-TRIS	Sigma Aldrich / Merck, Darmstadt
Chloroform	Sigma Aldrich / Merck, Darmstadt
Citric acid monohydrate	Sigma Aldrich / Merck, Darmstadt
Dimethyl sulfoxide (DMSO)	Sigma Aldrich / Merck, Darmstadt
Disodium hydrogen phosphate	Sigma Aldrich / Merck, Darmstadt
Dithiothreitol (DTT)	Carl Roth, Karlsruhe
Ethylenediaminetetraacetic acid (EDTA)	Carl Roth, Karlsruhe
Ethanol (EtOH)	Sigma Aldrich / Merck, Darmstadt
Formaldehyde	Sigma Aldrich / Merck, Darmstadt
Giemsa Azure Eosin Methylene Blue	Merck, Darmstadt
Glutaraldehyde	Sigma Aldrich / Merck, Darmstadt
Glycine	Sigma Aldrich / Merck, Darmstadt
Goat serum	Jackson ImmunoResearch, West Grove, USA
HEPES KOH	Sigma Aldrich / Merck, Darmstadt
Isopropanol	Sigma Aldrich / Merck, Darmstadt
Lipofectamine RNAiMAX	Thermo Fisher Scientific, Waltham, USA
Magnesium acetate	Sigma Aldrich / Merck, Darmstadt
Methanol (MeOH)	Sigma Aldrich / Merck, Darmstadt
Milk powder	Sigma Aldrich / Merck, Darmstadt
Propidium iodide staining solution (PI)	Miltenyi Biotec, Bergisch Gladbach

Polyacrylamide (PAA)	Serva Electrophoresis, Heidelberg
Potassium acetate	Sigma Aldrich / Merck, Darmstadt
Potassium chloride	Carl Roth, Karlsruhe
Ponceau S Solution	Sigma Aldrich / Merck, Darmstadt
Sodium acetate	Carl Roth, Karlsruhe
Sodium chloride	Sigma Aldrich / Merck, Darmstadt
Sodium dodecyl sulfate (SDS)	Sigma Aldrich / Merck, Darmstadt
Sodium hydroxide	Sigma Aldrich / Merck, Darmstadt
Sucrose	Sigma Aldrich / Merck, Darmstadt
TEMED	AppliChem, Darmstadt
Tris base	AppliChem, Darmstadt
Tris-HCl	AppliChem, Darmstadt
Triton X-100	AppliChem, Darmstadt
Trypan Blue	Sigma Aldrich / Merck, Darmstadt
Tween 20	Sigma Aldrich / Merck, Darmstadt
Yeast extract	GERBU, Heidelberg

2.1.2 Kits & Ready-Made Reagents

Agencourt AMPure XP	Beckman Coulter, Sinsheim
Agilent Kits (High Sensitivity DNA, RNA 6000 Nano, Small RNA)	Agilent, Santa Clara, USA
APO-BrdU TUNEL assay kit	Invitrogen / Thermo Fisher Scientific, Waltham, USA
Caspase-Glo 3/7 Assay	Promega, Madison, USA
CellTiter-Blue® Cell Viability Assay	Promega, Madison, USA
Clarity Western ECL Substrate	Bio-Rad, Munich
cOmplete, Mini Protease Inhibitor Tablets	Roche / Merck, Darmstadt
CytoTox ONE Homogeneous Membrane Integrity Assay	Promega, Madison, USA
ECL Select Western Blot Detection Reagent	GE Healthcare, Munich
Effectene Transfection Reagent	Qiagen, Hilden
Expand Long Range dNTPack	Roche / Merck, Darmstadt
GeneArt Site Directional Mutagenesis Plus Kit	Invitrogen / Thermo Fisher Scientific, Waltham, USA
LabChip XT DNA 300	PerkinElmer, Waltham, USA
Laemmli Sample buffer x4	Bio-Rad, Munich

Lipofectamine RNAiMAX	Thermo Fisher Scientific, Waltham, USA
Mammalian Protein Extraction Reagent (M-PER)	Thermo Fisher Scientific, Waltham, USA
NEBNext Ultra RNA Library Prep Kit for Illumina	NEB, Ipswich, USA
NEBNext Small RNA Library Prep Set for Illumina	NEB, Ipswich, USA
NuPAGE 3-8% Tris-Acetate Midi Gels	Invitrogen / Thermo Fisher Scientific, Waltham, USA
NuPAGE Tris-Acetate SDS Running Buffer (20X)	Invitrogen / Thermo Fisher Scientific, Waltham, USA
PhosSTOP Phosphatase Inhibitor Cocktail Tablets	Roche / Merck, Darmstadt
Platinum SYBR Green PCR SuperMix UDG (2x)	Invitrogen / Thermo Fisher Scientific, Waltham, USA
Protein Assay Dye Reagent Concentrate	Bio-Rad, Munich
Qiagen Plasmid Maxi Kit	Qiagen, Hilden
QIAPrep Spin Miniprep Kit	Qiagen, Hilden
QIAquick Gel Extraction Kit	Qiagen, Hilden
QIAquick PCR Purification Kit	Qiagen, Hilden
miRNeasy Kit	Qiagen, Hilden
Qiazol Lysis Reagent	Qiagen, Hilden
Qubit Assay Kits (dsDNA BR, dsDNA HS, RNA BR, RNA HS, microRNA)	Invitrogen / Thermo Fisher Scientific, Waltham, USA
Ribo-Zero Gold rRNA Removal Kit	Illumina, San Diego, USA
RNase-free DNase Set	Qiagen, Hilden
SOC medium	Invitrogen / Thermo Fisher Scientific, Waltham, USA

2.1.3 Enzymes

Accu-Prime Pfx	Invitrogen / Thermo Fisher Scientific, Waltham, USA
DNA restriction enzymes	NEB, Ipswich, USA
DNase I	Fermentas, St.Leon-Rot, NEB, Ipswich, USA
RNase A	Roche / Merck, Darmstadt
SuperScript IV Reverse Transcriptase	Invitrogen / Thermo Fisher Scientific, Waltham, USA
T4 Polynucleotide Kinase (PNK)	NEB, Ipswich, USA

T7 DNA ligase	NEB, Ipswich, USA

2.1.4 Drugs and Inhibitors

Bafilomycin A1	Abcam, Cambridge, England
BAY-587	kindly provided by Bayer AG
Ferrostatin-1	Sigma Aldrich / Merck, Darmstadt
Necrostatin-1	Abcam, Cambridge, England
RiboLock RNase Inhibitor	Thermo Fisher Scientific, Waltham, USA
RNaseOUT Recombinant Ribonuclease Inhibitor	Invitrogen / Thermo Fisher Scientific, Waltham, USA
THZ-531	kindly provided by Bayer AG
z-VAD-FMK	Sigma Aldrich / Merck, Darmstadt

2.1.5 Buffers and Solutions

1x PBS	137 mM NaCl 2.7 mM KCl 10 mM Na_2HPO_4 pH 7.4	**LB medium**	5 g/l yeast extract 10 g/l bacto tryptone 5 g/l NaCl
Versene	0.02 % EDTA 1x PBS		

2.1.5.1 Agarose Gel Electrophoresis (DNA Separation)

Agarose gel	x% Agarose 1x TBE	**1x TBE**	89 mM Tris 89 mM Boric acid 2 mM EDTA

2.1.5.2 Immunoblotting

Lysis buffer	10 ml M-PER 40 µl EDTA [2 mM] 1x cOmplete Mini 1x PhosSTOP	**1x TBS-T**	50 mM Tris, pH 7.6 150 mM NaCl 5 % Tween 20

NuPAGE transfer buffer (10x)
25 mM Bicine
25 mM Bis-Tris (free base)
1 mM EDTA
pH 7.2
prepare 1x solution with 10 % MeOH

Blocking solution
5 % milk powder or BSA in 1x TBS-T

Complex blocking solution
20 % milk powder
20 % FCS
3 % BSA
1 % goat serum
0.2 % Tween 20
in 1x TBS

2.1.5.3 Flow Cytometry

Citric acid buffer
2.1 g citric acid
500 µl Tween 20
100 ml H_2Odd

2.1.5.4 Molecular Cloning

Annealing buffer
100 mM potassium acetate
30 mM HEPES KOH
2 mM magnesium acetate

2.1.6 Neuroblastoma Cell Lines

CHP-134	Schlesinger *et al.* (1976)
HCT116	Brattain *et al.* (1981)
IMR-32	Tumilowicz, et al. (1970)
IMR-5-75	Tumilowicz *et al.* (1970)
NB-69	Mena, et al. (1989)
SH-EP TET21N	Lutz *et al.* (1996)
SH-EP	Ross, et al. (1983)
SK-N-BE(2)c	Biedler and Spengler (1976)
SK-N-DZ	Sugimoto, et al. (1984)
TR-14	Cowell and Rupniak (1983)

Table 2.1: Cell Culture Media Composition

Purpose	Additive	Final Concentration
Basic medium	RPMI 1640 (500 ml)	
	FCS	10 %
	P/S	1%
Freezing medium	RPMI 1640	40%
	FCS	50%
	DMSO	10%
IMR-5-75 6TR, IMR-32 6TR	Blasticidin	5 µg/ml
IMR-5-75 6TR *XY*sh, IMR-32 6TR *XY*sh	Zeocin	50 µg/ml
	Blasticidin	5 µg/ml
IMR-5-75 6TR dCas9	Blasticidin	5 µg/ml
	G418	400 µg/ml
IMR-5-75 6TR dCas9 sg*XY*	Blasticidin	5 µg/ml
	G418	400 µg/ml
	Puromycin	5 µg/ml
IMR-5-75 6TR dCas sg6 pcDNA5/TO	Blasticidin	5 µg/ml
	G418	400 µg/ml
	Puromycin	5 µg/ml
	Hygromycin B	150 µg/ml

2.1.7 Antibodies

Table 2.2: Primary Antibodies for Immunoblotting

Specificity	Host	Dilution	Supplier	Catalogue No.
alpha Tubulin (DM1A) - HRP	Mouse monoclonal	1:10000	Abcam, Cambridge, England	ab40742
CDK12 (CrkRS)	Rabbit polyclonal	1:8000	Novus, Minneapolis, USA	NB100-87011
CDK12 (CrkRS)	Mouse monoclonal	1:1000	Abcam, Cambridge, England	ab57311
CDK12 (CrkRS)	Rabbit polyclonal	1:500	Cell Signaling Technology, Danvers, USA	#11973
CDK13 (CDC2L5)	Rabbit polyclonal	1:8000	Novus, Minneapolis, USA	NB100-68268
CDK13 (CDC2L5)	Mouse monoclonal	1:1000	Abcam, Cambridge, England	ab58309
CDK13 (CDC2L5)	Rabbit polyclonal	1:1000	Sigma Aldrich / Merck, Darmstadt	SAB 2700810
Vinculin (7F9) - HRP	Mouse monoclonal	1:1000	Santa Cruz, Dallas, USA	sc-73614

Table 2.3: Secondary Antibodies for Immunoblotting

Specificity	Host	Supplier	Catalogue No.
Anti-mouse-HRP	Goat, polyclonal	Dianova, Hamburg	115-035-003
Anti-rabbit-HRP	Goat, polyclonal	Dianova, Hamburg	115-035-144
Anti-rat IgG-HRP	Goat	Santa Cruz, Dallas, USA	sc-2065

2.1.8 *E.coli* Cultivation

One Shot Top10	Invitrogen / Thermo Fisher Scientific, Waltham, USA
One Shot MAX Efficiency DH5α-T1R	Invitrogen / Thermo Fisher Scientific, Waltham, USA
One Shot ElectroMAX Stbl4	Invitrogen / Thermo Fisher Scientific, Waltham, USA

Table. 2.4: Antibiotics Used for the Cultivation of *E.coli*

Antibiotic	Final concentration	Supplier
Ampicillin	100 µg/ml	Serva, Heidelberg
Kanamycin	50 µm/ml	Serva, Heidelberg
Spectinomycin	50 µg/ml	Serva, Heidelberg

2.1.9 Nucleic Acids

GeneRuler 1 kb (Plus) DNA Ladder	Thermo Fisher Scientific, Waltham, USA
ERCC RNA Spike-In Control Mix 1	Thermo Fisher Scientific, Waltham, USA
NEBNext Multiplex Oligos for Illumina (Index Primers Set 1 + 2)	NEB, Ipswich, USA
Adenosine 5′-Triphosphate (ATP)	NEB, Ipswich, USA

Table 2.5: Vectors

Vector	Specification	Supplier
pcDNA6/TR	Tetracycline repressor (TR) protein	Invitrogen, Thermo Fisher Scientific, Waltham, USA
pcDNA5/TO	Tetracycline-regulated expression	Invitrogen, Thermo Fisher Scientific, Waltham, USA
pTER+	Tetracycline-regulated shRNA expression	Van de Wetering, et al. (2003)
pT-RexTM-DEST30	Tetracycline-regulated expression	Invitrogen, Thermo Fisher Scientific, Waltham, USA
pLKO.1-puro U6 sgRNA BfuAI stuffer	sgRNA cloning vector	Kearns, et al. (2014), Addgene plasmid # 50920
AAVS1 TALEN F	Homodimeric TALEN, right pair	Mandegar, et al. (2016)
AAVS1 TALEN R	Homodimeric TALEN, left pair	Mandegar, et al. (2016)
pAAVS1-NDi-CRISPRi (Gen1)	Dox-inducible CRISPRi knock-in construct w. mCherry marker	Mandegar, et al. (2016)

Table 2.6: Oligonucleotides for Short Hairpin RNA (shRNA) Vectors

shRNA oligonucleotides	Sequence 5'-3'
CDK12 sh1 for	GATCCGCCGAAGAAGCAATATCGAATTCAAGAGATTCGATATTGCTTCTTCGGTTTTTTGGAAA
CDK12 sh1 rev	CGCCGAAGAAGCAATATCGAATTCAAGAGATTCGATATTGCTTCTTCGGTTTTTTGGAAAAGCT
CDK12 sh3 for	GATCCGGACTTGCTCGGCTCTATATTCAAGAGATATAGAGCCGAGCAAGTCCTTTTTTGGAAA

shRNA oligonucleotides	Sequence 5'-3'
CDK12 sh3 rev	CGGACTTGCTCGGCTCTATATTCAAGAGATATAGAGCCGA GCAAGTCCTTTTTTGGAAAAGCT
CDK13 sh1 for	GATCCGGAACTTGCACAACTAGAATTCAAGAGATTCTAGT TGTGCAAGTTCCTTTTTTGGAAA
CDK13 sh1 rev	CGGAACTTGCACAACTAGAATTCAAGAGATTCTAGTTGTG CAAGTTCCTTTTTTGGAAAAGCT
CDK13 sh3 for	GATCCGCAGATTGTCTAGATCCAGATTCAAGAGATCTGGA TCTAGACAATCTGTTTTTTGGAAA
CDK13 sh3 rev	CGCAGATTGTCTAGATCCAGATTCAAGAGATCTGGATCTA GACAATCTGTTTTTTGGAAAAGCT
Scramble for	CTAGCGCAGTCGCGTTTGCGACTGGTTCAAGAGACCAGT CGCAAACGCGACTGTTTTTTGGAAG
Scramble rev	CGCAGTCGCGTTTGCGACTGGTTCAAGAGACCAGTCGCA AACGCGACTGTTTTTTGGAAGCGGCC

Table 2.7: Silencer Select Small Interfering RNAs (siRNAs) for Transient Gene Knockdown (Ambion)

Target gene	Sequence 5'-3'	siRNA ID
CDK12 (CRKRS) si1	CCGAAGAAGCAAUAUCGAAtt	s28621
CDK12 (CRKRS) si3	GGACUUGCUCGGCUCUAUAtt	s28623
CDK13 (CDC2L5) si1	GGAACUUGCACAACUAGAAtt	s16399
CDK13 (CDC2L5) si3	CAGAUUGUCUAGAUCCAGAtt	s16397
Silencer Select Neg Ctl 1	Proprietary	4390843
Silencer Select Neg Ctl 2	Proprietary	4390846

Table 2.8: Oligonucleotides for Single Guide RNA (sgRNA) Vectors

Primer	Sequence 5'-3'
sgRNA_scr2 _rev	AAACCCGTCAGGGCACGTTTGGCGC
sgRNA_scr2_fw	ACCGGCGCCAAACGTGCCCTGACGG
sgRNA_scr3_fw	ACCGGCACTACCAGAGCTAACTCA
sgRNA_scr3_rev	AAACTGAGTTAGCTCTGGTAGTGC
sgRNA10_fw	ACCGTGGTGGCGGCGACACACCGC
sgRNA10_rev	AAACGCGGTGTGTCGCCGCCACCA
sgRNA6_fw	ACCGTGACAACAACTCCCGGCCTAGGG
sgRNA6_fw neu	ACCGTGACAACAACTCCCGGCCT
sgRNA6_rev	AAACCCCTAGGCCGGGAGTTGTTGTCA
sgRNA6_rev neu	AAACTAGGCCGGGAGTTGTTGTCA
sgRNA8_fw	ACCGGGAGGACGACGTCGACGCCGAGG
sgRNA8_fw neu	ACCGGGAGGACGACGTCGACGCCG
sgRNA8_rev	AAACCCTCGGCGTCGACGTCGTCCTCC
sgRNA8_rev neu	AAACCGGCGTCGACGTCGTCCTCC
CDK12 2b_fw	CACCGACTGACCGACTGCCTTCTCG
CDK12 2b_rev	AAACCGAGAAGGCAGTCGGTCAGTC
CDK13 I1_fw	CACCGATCACAAACAAACCATGTGA
CDK13 I1_rev	AAACTCACATGGTTTGTTTGTGATC
scramble 8.2_fw	CACCGAAAAAGCTTCCGCCTGATGG
scramble 8.2_rev	AAACCCATCAGGCGGAAGCTTTTTC

Table 2.9: Sequencing Primers

Primer	Sequence 5'-3'
BGH_rev	TAGAAGGCACAGTCGAGG
CDK12 Amp Zusatz fw	GCAGCAAAGATGGATGGAAAGG
CDK12 Amp Zusatz rev	TTCAGCTCCCGTTCTTTCCTG
CDK12 Ersatz 1	GATCGCCCAGTCCCTATGGT
CDK12 Ersatz 2	CTCAGGCAAATTCTCAGCCC
CDK13 fw Zusatz 1	CGACGTGTCCCCTAGTCCC
CDK13 fw Zusatz 2	CCAAAGAAAAAGATATTGACTGG
CDK13 Zusatz3	GTGGCCGCAGCAAGGA
CDK13 Zusatz4	ACCAAAGAAGCAATATCGTCGAA
H1 fw	TCGCTATGTGTTCTGGGAAA

Table 2.10: Amplification Primers

Primer	Sequence 5'-3'
CDK12 Amp V4 fw	GTCACTCTTAAGGCCACCATGCCCAATTCAGAGAGA
CDK12 Amp V4 rev	AGTAGCGGATCCCTAGTAAGGAACTCCTCTCCCT
CDK13 Amp V4 fw	CTTACACTTAAGGCCACCATGCCGAGCAGCT
CDK13 Amp V4 rev	GTGCATCTCGAGCTAGTATGGTAACCCTCTGCCTCT

Table 2.11: Site-Directed Mutagenesis Primers

Primer	Sequence 5'-3'
CDK12_3252_FW	GAACTAGTGGCTCTGGCGAAGGTGAGACTAGA
CDK12_3252_RV	TCTAGTCTCACCTTCGCCAGAGCCACTAGTTC
CDK12_3615_FW	CAAATCAAACTAGCAAATTTTGGACTTGCTC
CDK12_3615_RV	GAGCAAGTCCAAAATTTGCTAGTTTGATTTG
CDK13 Mut fw1	CTGGAGAAATGGTAGCCTTAGCAAAAGTACGTCTGGATAATG
CDK13 Mut fw2	GAGGGCAGATAAAACTTGCAAACTTTGGACTTGCTCGATTG
CDK13 Mut rev1	CATTATCCAGACGTACTTTTGCTAAGGCTACCATTTCTCCAG
CDK13 Mut rev2	CAATCGAGCAAGTCCAAAGTTTGCAAGTTTTATCTGCCCTC

2.1.10 Laboratory Equipment

Analytical Balances PM 4600	Mettler, Gießen
ChemiSmart 5100	Vilber Lourmat, Marne-la-Vallée, France
CO_2 Incubator Steri-Cult	Thermo Fisher Scientific, Waltham, USA
Criterion Vertical Electrophoresis Cell	Bio-Rad, Munich
Criterion Blotter	Bio-Rad, Munich
Gel documentation system (Geldoc)	Bio-Rad, Munich
Horizontal mini-gel systems	GIBCO/BRL Eggenstein Renner, Darmstadt
Horizontal mixer RM5	CAT, Staufen
iBlot 2 Gel Transfer Device	Thermo Fisher Scientific, Waltham, USA
Incubator Function Line	Heraeus, Wehrheim
Incubator Shaker, Innova 4300	New Brunswick Scientific, Enfield, USA
LightCycler 480	Roche / Merck, Darmstadt
Luna Automated Cell Counter	Logos biosystems, Annandale, USA
MACSQuant VYB flow cytometer	Miltenyi Biotec, Bergisch Gladbach
Magnetic Mixers	Heidolph-Elektro, Kehlheim

Mini Trans-Blot Cell	Bio-Rad, Munich
Mini-PROTEAN 3 electrophoresis system	Bio-Rad, Munich
NanoDrop Spectrophotometer ND-1000	Peqlab, Erlangen
pH-Meter Ph 540 GLP	WTW, Weilheim
Platereader FLUOstar OPTIMA	BMG Labtech, Ortenberg
Power supply units, Phero-stab 500	Biotec Fischer, Reiskirchen
Shaking platform, IKA KS250	Janke & Kunkel, Staufen
Spark Microplate Reader	Tecan, Männedorf, Switzerland
Spectrophotometer GeneQuant 1300	GE Healthcare, Munich
Sterile bench SAFE 2020	Thermo Fisher Scientific, Waltham, USA
Thermo block mixer compact	Eppendorf, Hamburg
Thermo water bath GFL 1083	GFL, Burgwedel
Thermocycler GeneAmp 9700	Applied Biosystems, Darmstadt
Vacuum concentrator, RVC2-18	Christ, Osterode am Harz
Vortex Reax top	Heidolph Instruments, Schwabach

Centrifuges and Rotors

Avanti-JS-25-I	Beckman Coulter, Sinsheim
Allegra X-12	Beckman Coulter, Sinsheim
Biofuge fresco	Heraeus, Wehrheim
J2-21 M/E	Beckman Coulter, Sinsheim
Mini Star	Neolab, Heidelberg
Rotor JA-10	Beckman Coulter, Sinsheim
Rotor JA-20	Beckman Coulter, Sinsheim
Rotor JS-4.2	Beckman Coulter, Sinsheim

Microscopes

Olympus IX81	Olympus, Hamburg
Olympus CKX41	Olympus, Hamburg

2.1.11 Further Materials

Cell culture dishes	TPP, Trasadingen, Switzerland
Cell culture flasks	TPP, Trasadingen, Switzerland
Nunc CryoTubes (2 ml)	Nalgene / Thermo Fisher Scientific, Waltham, USA
Cuvettes Semi-Micro	Greiner Bio-One, Kremsmünster, Austria
FACS tubes with cell-strainer cap	Corning / Merck, Darmstadt
Filter tips, graduated (10, 100, 200, 1000 µl)	Star Lab, Hamburg
Luna Cell Counter Slides	Logos biosystems, South Korea
Mr. Frosty Freezing Container	Nalgene / Thermo Fisher Scientific, Waltham, USA
Nitrocellulose membrane 0.45 µm	GE Healthcare, Munich
Plastic pipettes (5, 10, 25, 50 ml)	Corning / Merck, Darmstadt
qPCR 96 well plates, white	Biozym, Hessisch Oldendorf
qPCR optical adhesive film	Applied Biosystems, Darmstadt
Reaction tubes (0.5, 1.5, 2.0, 5.0 ml)	Eppendorf, Hamburg
Reaction tubes (15, 50 ml)	Greiner Bio-One, Kremsmünster, Austria
Tissue culturing plates (black, flat bottom 96 wells)	Corning / Merck, Darmstadt
Tissue culturing plates (transparent, 6, 24, 96 wells)	TPP, Trasadingen, Switzerland
Whatman 3MM paper	Whatman, Dassel

2.1.12 Software

Cell B Image Software	Olympus, Hamburg
Chromas Lite 2.1	Technelysium Ltd., Brisbane, Australia
FlowJo version 10	FlowJo, LLC, Ashland, USA
FLUOstar Optima	BMG Labtech, Ortenberg
IGV viewer	Broad Institute, Cambridge, USA
ImageJ version 1.51d	Wayne Rasband
Microsoft Office package 2010	Microsoft Corp., Redmond, USA
R studio	Comprehensive R Archive Network
ScanR acquisition software	Olympus, Hamburg

Sigma Plot 13.0	SPSS Inc., Chicago, USA

2.1.13 Web Resources

Addgene	https://www.addgene.org
DAVID functional annotation tool 6.8	https://david.ncifcrf.gov
Ensembl genome browser	http://www.ensembl.org/index.html
IC50 Calculator	https://www.aatbio.com/tools/ic50-calculator/
mirPath v.3 algorithm	http://snf-515788.vm.okeanos.grnet.gr/
National Center for Biotechnology	http://www.ncbi.nlm.nih.gov/
R2	https://hgserver1.amc.nl/cgi-bin/r2/main.cgi
UCSC Genome Browser	http://genome.ucsc.edu/

2.2 Methods

2.2.1 Cell Culture Methods

2.2.1.1 Culture and Cryoconservation of Human Neuroblastoma Cells

Neuroblastoma cells were cultured in basic medium with the appropriate selective markers as listed in Table 2.1 in a humidified cell incubator at 37 °C and 5 % CO_2. Every four to seven days the cells were subcultured at ratios from 1:4 to 1:15, according to the individual cell confluence and proliferation rate. Versene or fresh medium were employed to detach the cells from the surface of the culture vessel. Cells were collected for cryoconservation when they reached around 70 % confluence; after centrifugation at 800 rpm for 5 min, they were resuspended in freezing medium and aliquoted into cryovials. The vials were stored in a freezing container and immediately transferred to -80 °C. Cells were stored in liquid nitrogen tanks at -196 °C for the long term. To recultivate cells, they were thawed quickly and dispensed into pre-warmed basic medium. After 48 hours, the medium was replaced with basic medium containing selective markers as applicable.

For experiments, the cell number was determined with a Luna Automated Cell Counter after trypan blue staining (1:1 dilution of 0.1 % trypan blue in PBS). Cells were seeded and, if applicable, doxycycline was directly added to the medium for the induction of

regulatable vectors unless otherwise specified. After completion of the experiment, medium and attached cells were collected for further processing.

2.2.1.2 Cell Cycle Synchronization

IMR-5-75 MYCN shRNA cells were synchronized according to the protocol developed by Emma Bell (Ryl *et al.*, 2017). 24 hours after seeding, 1 µg/ml tetracycline or 70 % EtOH was added to the medium. Another 24 hours later, 2 mM thymidine were added. After 18 hours, the medium containing thymidine was removed and cells were washed once before adding fresh medium containing tetracycline. Cells were harvested at regular intervals for the next 22 hours to analyze cell cycle, RNA and miRNA expression.

2.2.1.3 Cell Transfection and Selection

DNA vectors were introduced into our cell lines with Effectene Transfection Reagent. Cells of a low passage were plated on a 15 cm dish so that they would reach around 40 % confluence the following day. 3 µg plasmid DNA were diluted in 450 µl EC buffer plus 24 µl Enhancer. After a 2 min incubation step, 90 µl of Effectene Transfection Reagent were added and the DNA mix was vortexed and incubated again for 15 min. Then, 4.5 ml basic medium were added gently to the mix. The medium was removed from the cell culture plate, and 10.5 ml fresh basic medium were added. The DNA transfection mix was added dropwise. After 24 h, the medium was replaced. After another 48 to 72 h, cells were detached from the plate and the full amount was replated, now with the appropriate selection marker. A non-transfected control plate was also exposed to the selection marker in order to determine the time point when all cells not carrying the corresponding resistance gene were killed. After 1-3 weeks, when transfected positive cells had regrown, they were seeded onto 96 well plates at one cell/100 µl for single clone selection. After 6 days, true single clones were identified by visual inspection due to circular, even colony shape and the absence of further colonies in one well. Single clones were raised and analyzed with regard to the expression of the introduced vectors by immunoblotting (chapter 2.2.4).

2.2.1.4 Lentiviral Transduction

IMR-5-75 cells were seeded in a 12-well plate ($2.5*10^5$ cells). The following day, medium was removed and replaced by 500 µl of RPMI + FCS + 8 µg / µl polybrene. Lentivirus containing the lentiCRISPRv.2-706 vector was slowly added to the cells (provided by Friederike Herbst). After 16 hours, the medium was removed, cells were washed once

and fresh medium was added. The polyclonal culture was expanded for validation of the knockout and further use in experiments.

2.2.1.5 Gene Knockdown with siRNA

Cells were seeded in 10 cm dishes 24 h before the transfection and doxycycline was directly added where shRNA induction was desired. For transfection, the siRNA stock was diluted in 500 µl serum- and antibiotic-free Opti-MEM medium to a final concentration of 100 nM. Depending on the cell line, 4-5 µl Lipofectamine RNAiMAX were diluted in 500 µl medium in a second tube. The solutions were incubated on the bench for 5 minutes. Then they were combined and incubated for 15 min to allow complex formation. Meanwhile, the medium of the pre-seeded dishes was exchanged with 9 ml RPMI / FCS plus doxycycline, where applicable. The transfection solution was added drop-wise to the dishes. After 72 h, the cells were harvested for further analysis of the achieved knockdown (immunoblotting, cell cycle, cell death).

2.2.1.6 CDK12/13 Inhibition

Inhibition of CDK12/13 was achieved using the tool compound BAY-587 or the commercially available THZ531. At first, the IC50 values were determined individually for each cell line. Cells were seeded and after 24 hours treated with a dilution series of the inhibitors. Another 96 hours later, a CellTiter-Blue Assay (CTB) was performed to determine viability. The relative IC50 values were calculated with the four parameter logistic regression model using the online tool “IC50 Calculator” by AAT Bioquest. For experiments, cells were treated with multiples of the IC50 as described above. Cell cycle, cell death and cell confluence were assayed after 96 hours. Apoptosis was assayed after 24 hours, RNA and protein expression after 8 hours.

2.2.1.7 Viability Assays

After an experiment, such as treatment with siRNAs or induction of shRNAs, viability of the cells was established by CTB. The reagent was added at a 1:10 ratio to the cells and incubated for 4 hours. Fluorescence resulting from metabolic activity of the cells was recorded using a 540/580 filter with a FLUOstar platereader (0.2 s acquisition time, automatic gain) or Tecan Spark reader (flashes: 30, integration time: 40 µs, gain: 58).
A second measure of viability after treatment was cell confluence. Here, cells were seeded and treated in 96-well plates in a volume of 100 µl. After completion of the experiment, 50 µl of 11 % glutaraldehyde in PBS were added for 30 min to fix the cells.

Subsequently, cells were washed two times with 1x PBS before overnight staining with 10 % Giemsa Azure Eosin Methylene Blue solution in 1x PBS. This was followed by two washes with 1x PBS and a final wash with H_2Odd. After drying, the plates were scanned and confluence was determined with the help of the colony formation plugin of the ImageJ software.

2.2.1.8 Colony Formation Assay

Single cells were seeded at very low density in 6-well plates. They were incubated for 7-10 days, depending on the cell line's proliferation rate. When colonies could be detected macroscopically, the cells were fixed and stained with Giemsa solution as described above.

2.2.1.9 Rescue from Cell Death

In order to determine the mode of cell death, several inhibitors were used. 30 µM Z-VAD-FMK was employed as an inhibitor of apoptosis, 2.5 – 5 µM ferrostatin-1 as an inhibitor of ferroptosis, 10 – 20 µM necrostatin-1 as an inhibitor of necroptosis and 1.5 nM bafilomycin as an inhibitor of autophagy. For each inhibitor, a cell line-specific maximum tolerable concentration without effect on viability was determined. The rescue experiment was performed by applying the inhibitors at the same time as the treatment and by assessing viability after 96 hours.

2.2.1.10 Cytotox Membrane Integrity Assay

The CytoTox-ONE Homogeneous Membrane Integrity Assay by Promega was used according to the manufacturer's instructions. Cells were cultured in 5 % FCS to reduce background fluorescence and protein knockdown was induced for 96 hours. Cells were then incubated with the CytoTox-One Reagent for 10 minutes. The fluorescence was recorded with the Tecan Spark reader using the 540/580 filter. Gain was adjusted based on the maximum lactate dehydrogenase release control.

2.2.1.11 Caspase 3/7 Assay

The Caspase-Glo 3/7 Assay by Promega was performed 24 h after treatment of cells in a 96-well format according to the manufacturer's instructions. Luminescence was recorded with the Tecan Spark reader after 2 h 30 min. The net signal was calculated by subtracting the negative control (basic medium + DMSO) from each sample.

2.2.2 Nucleic Acids Manipulation

2.2.2.1 RNA Extraction for RNA Sequencing

Cells were grown according to the experimental question and harvested. 3 x 10^6 cells per condition were pelleted and dissolved in 700 µl QIAzol lysis reagent and stored at -80 °C until further processing. RNA was isolated with the miRNeasy kit by Qiagen according to the manufacturer's instructions to isolate separate fractions of > 200 nt and small RNA. After ethanol precipitation, the column was further processed for the isolation of total RNA. A DNase I digestion step on the spin column was included into the protocol. RNA was eluted into a volume of 50 µl of RNase-free H_2O. The integrity of the isolated RNA was controlled on a bioanalyzer with a RNA Nano 6000 chip and the RNA concentration was determined with the Qubit RNA broad range assay.

2.2.2.2 RNA Library Preparation

Prior to library preparation, the ERCC RNA Spike-In Control Mix 1 was introduced to allow for accurate quantification of the libraries. 1 µl of a 1:10 spike-in dilution was added to a 25 µl volume containing 5 µg total RNA. Next, ribosomal RNA (rRNA) was depleted with the Ribo-Zero Gold rRNA Removal Kit. Afterwards, the sample volume was adjusted to 180 µl and RNA was precipitated by adding 18 µl of 3 M sodium actetate, 2 µl glycogen (10 mg/ml) and 600 µl EtOH (100%) and by incubating it at -20 °C for at least 60 min. This was followed by a centrifugation step at 13000 rpm for 30 min. The supernatant was removed and the pellet was washed with 70% EtOH twice. The pellet was air-dried and dissolved in 11.5 µl ddH_2O. The success of rRNA removal was controlled by measuring the new concentration with the Qubit RNA high sensitivity assay and calculating the percentage of mRNA retrieved.

For library preparation, the NEBNext Ultra RNA Library Prep Kit for Illumina was used in combination with Agencourt AMPure XP beads according to the manufacturer's instructions with the following exceptions. Fragmentation of intact RNA was performed for 20 min at 94 °C. First strand complementary DNA (cDNA) was synthesized during 10 min at 25 °C, 50 min at 42 °C and 15 min at 70 °C. Size selection was done for insert sizes of 300 – 450 bp. For PCR library enrichment, each sample was assigned a unique index primer (NEBNext Multiplex Oligos for Illumina). After library purification, its quality was assessed on the bioanalyzer with a DNA high sensitivity chip. If adapter dimer peaks were visible at <150 bp, the final purification step was repeated. The libraries were then pooled prior to submission to the DKFZ core facility "Genomics & Proteomics" for sequencing. Every sample was adjusted to a concentration of 10 nmol/l in a volume of 10 µl.

The average region size of the library determined by the bioanalyzer was taken as a basis for the calculation of the library concentration. HiSeq 2000 pair-end 100 or 125 bp sequencing was performed on the Illumina platform.

2.2.2.3 RNA Extraction for Small RNA Sequencing

Cells were grown according to the experimental question and harvested. 2.5 x 10^6 cells per condition were pelleted and dissolved in 350 µl QIAzol lysis reagent and stored at -80°C until further processing. RNA was isolated with the miRNeasy kit by Qiagen according to the manufacturer's instructions to isolate total RNA. RNA was eluted in two steps into a total volume of 90 µl RNAse-free H_2O. Subsequently, DNA was digested with the RNase-free DNase set by Qiagen for 30 min at 37 °C:

36 µl	sample
50.5 µl	H_2O
10 µl	10x buffer RDD
2.5 µl	RiboLock RNase Inhibitor
1 µl	DNase I

The RNA was precipitated by adding 10 µl sodium actetate, 2 µl glycogen and 300 µl EtOH and storing it at -20 °C for at least 60 min. It was then centrifuged at 13000 rpm for 30 min. After discarding the supernatant, the pellet was washed with 70% EtOH. The pellet was air-dried and dissolved in 15 µl ddH_2O.

2.2.2.4 Small RNA Library preparation

The kit NEBNext Small RNA Library Prep Set for Illumina was used to create microRNA (miRNA) libraries from 1 µg of the isolated total RNA according to the manufacturer's instructions. The libraries were purified using the QIAquick PCR Purification Kit before the recommended size selection step with AMPure XP Beads. To remove also small fragments, samples were run on a LabChip XT DNA 300. Quality of the libraries was controlled with a bioanalyzer high sensitivity DNA chip. The libraries were pooled and sent for sequencing to the DKFZ core facility "Genomics & Proteomics". HiSeq 2000 single read 50 bp sequencing was performed on the Illumina platform.

2.2.2.5 Quantitative Real-Time Polymerase Chain Reaction (RT-qPCR)

Total RNA was isolated from cells and reversely transcribed to cDNA. Samples were kept constantly on ice. Each reaction contained:

11 µl	RNA (1 µg)
1 µl	Oligo (dT)20
1 µl	dNTP Mix (10 mM)

The mix was incubated for 5 minutes at 65 °C and 1 minute on ice. Then, the following components were added:

4 µl	5x Superscript IV Buffer
1 µl	DTT (0.1 M)
1 µl	RNaseOUT
1 µl	Superscript IV Reverse Transcriptase

50 °C	10 min
80 °C	10 min

From each sample of the experiment, 2 µl were pooled and the final volume adjusted to 70 µl. A serial dilution of the cDNA mix by 1:4, 1:16, 1:64 and 1:256 was prepared to generate a standard curve.
RT-qPCR was conducted with the Platinum SYBR Green qPCR SuperMix-UDG by Invitrogen and “QuantiTect” Primers by Qiagen. To measure the expression of the housekeeping genes SDHA and HPRT1, the reaction mix was prepared as follows:

13 µl	Platinum SYBR Green PCR SuperMix UDG (2x)
0.75 µl	forward primer (10 µM)
0.75 µl	reverse primer (10 µM)
2.5 µl	template cDNA
8 µl	H_2Odd

The RT-qPCR reaction mix for genes of interest CDK12 and CDK13 contained:

13 µl	Platinum SYBR Green PCR SuperMix UDG (2x)
2.5 µl	10x QuantiTect Primer
2.5 µl	template cDNA
7 µl	H_2Odd

The RT-qPCR was performed in triplicates in a LightCycler 480 from Roche with cycling conditions as follows:

50 °C	20 s	
95 °C	2 min	
95 °C	15 s	45x
60 °C	30 s	

On the basis of the dilution series' threshold cycles (C_T), a linear equation was determined and used to calculate the expression levels of genes of interest and housekeeping genes. The expression of genes of interest was normalized with HRPT1 and SDHA housekeeping genes.

2.2.2.6 Amplification of CDK12 and CDK13 cDNA

CDK12 and CDK13 cDNA was amplified from purchased plasmids (clone #197093242 from Genomics & Proteomics Core Facility: CDK13 in pENTR223.1; clone GC-E2808 from GeneCopoeia: pShuttleGateway PLUS CDK12 ORF) with the Expand Long Range dNTPack.

9.9 µl	Expand Long Range buffer with $MgCl_2$
2.5 µl	dNTPs
1 µl	primer fw (1 µM) (Table 2.10)
1 µl	primer rev (1 µM)
0.7 µl	Expand Long Range enzyme mix
3 µl	plasmid DNA (33.3 ng/µl)
1 µl	DMSO (final concentration 2%)
30.9 µl	H_2O

92 °C	2 min	
92 °C	10 s	
64 °C	15 s	45x
68 °C	4 min 30 s	
68 °C	7 min	

Reaction conditions were optimized for *CDK13* amplification (6% DMSO). The reaction product was separated on a 1.5% agarose gel, the appropriate band was excised from the gel, purified with the Qiaquick Gel Extraction kit and the cDNA sequence was verified.

2.2.2.7 Introduction of Point Mutations to CDK12 and CDK13 pcDNA5/TO Vector

In order to render the kinase domains of CDK12 and CDK13 inactive, two point mutations were introduced with the Gene Art Site-Directed Mutagenesis Plus kit by Invitrogen according to the manufacturer's instructions. The primers to introduce a K756A and a D877N point mutation in CDK12 were designed using the Thermo Fisher online tool (https://www.thermofisher.com/order/oligoDesigner/mutagenesisplus) and are listed in Table 2.11. The primers to introduce a K734A and a D855N point mutation in CDK13 were designed online on https://www.primergenesis.com. Primer mixes were prepared as follows:

CDK12 mix 1: CDK12_3615_FW + CDK12_3252_RV
CDK12 mix 2: CDK12_3252_FW + CDK12_3615_RV
CDK13 mix 1: CDK13 Mut fw2 + CDK13 Mut rev1
CDK13 mix 2: CDK13 Mut fw1 + CDK13 Mut rev2

24 ng of CDK12 plasmid and 60 ng of CDK13 plasmid were employed. The PCR was conducted with the following standard parameters:

37 °C	18 min	
94 °C	2 min	
94 °C	20 s	17x
57 °C	30 s	
68 °C	4 min 53 s (mix 1) / 11 s (mix 2)	
68 °C	5 min	

The CDK13 mutagenesis PCR was further optimized and conducted with 62 °C annealing temperature (PCR step 4) and 10% DMSO.

2.2.3 Molecular Cloning

Standard methods including gel electrophoresis for the separation of DNA fragments, restriction digestions or cryoconservation of *Escherichia coli (E. coli)* were performed as described in Sambrok and Russel (2002) and are not explained in full detail here.

2.2.3.1 Cloning of CDK12 and CDK13 shRNAs into the pTER+ Vector

Linearizaton of the pTER+ vector was carried out at 37 °C for 3 hours:

3.5 µg	pTER+ plasmid
4.5 µg	Bgl II restriction enzyme
4.5 g	Hind III restriction enzyme
10 µl	Buffer R+
77.5 µl	H_20

The enzymes were inactivated at 60 °C for 20 min. The linearized vector was separated on a 1% agarose gel and the corresponding band was excised from the gel. The vector was purified with the QIAquick Gel Extraction Kit.
In an independent reaction, forward and reverse shRNA were annealed (3 min at 95 °C, 1 h at 37 °C):

1 µl	shRNA fw
1 µl	shRNA rev
5 µl	annealing buffer
43 µl	H_2O

The linearized vector and the annealed oligonucleotides were ligated overnight at 16 °C:

1 µl	annealed shRNA
250 ng	linearized pTER+
1 µl	ligation buffer (10x)
4.5 µl	H_2O

2.2.3.2 Cloning of sgRNA into Addgene Vector #50920

The vector pLKO.1-puro U6 sgRNA BfuAI stuffer was a gift from Rene Maehr and Scot Wolfe (Addgene plasmid # 50920). The sgRNA oligos were phosphorylated and annealed in the following reaction:

1 µl	sgRNA fw
1 µl	sgRNA rev
1 µl	10x T4 ligation buffer
0.5 µl	T4 PNK
6.5 µl	H_2O

37 °C	30 min
95 °C	5 min, allow to cool down to room temperature.

Digestion-ligation reaction:

100 ng	pLKO.1-puro U6 sgRNA BfuAI stuffer (#50920)
2 µl	sgRNA oligo duplex (step 1, 1:250 dilution)
2 µl	Fast digest buffer
2 µl	DTT
2 µl	ATP
1 µl	FastDigest BveI
0.5 µl	T7 DNA ligase
	H_2O to 20 µl

37 °C	5 min	6x
23 °C	5 min	

2 µl of the reaction were used to transform *E.coli* cells.

2.2.3.3 Cloning of CDK12/CDK13 into pcDNA5/TO

The receiving vector pcDNA5/TO and the CDK12/CDK13 cDNAs were each digested to introduce matching restriction overlaps. For CDK12, BamHI and BspTI enzymes were employed in Tango buffer. For CDK13, Xho and BspTI were employed in O buffer. The linearized fragments were ligated in a 1:3 vector to insert ratio with T4 ligase and additional ATPs overnight at 16 °C. The products CDK12 pcDNA5/TO and CDK13 pcDNA5/TO were transformed into *E.coli* bacteria.

2.2.3.4 Transformation of Competent *E.coli* cells

Chemically competent *E.coli* cells were thawed on ice. 2-5 µl plasmid solution (20 – 50 µg DNA) were added, the solution was carefully mixed and incubated on ice for 30 min. The bacteria were heat shocked at 42 °C for 2 min and cooled down on ice for 3 min. 250 µl of pre-warmed super optimal broth with catabolite repression (SOC) medium were added to the suspension and it was incubated for 30 min at 37 °C. Finally, the transfected bacteria were plated onto Lysogeny broth (LB) dishes with the appropriate antibiotics and incubated at 37 °C for at least 14 hours. Single colonies were picked and used to inoculate 4 ml LB medium. The cultures were incubated with agitation for 14 hours (160 rpm, 37 °C). The next day, glycerol stocks were prepared and the remainder of the culture

was used for plasmid isolation. For larger plasmid yields (using Maxi Kit), 4 ml starter cultures were grown only for 6-8 hours, diluted into 300 ml LB medium (1:500) and grown overnight.

2.2.3.5 Isolation and Purification of Plasmid DNA from *E.coli*

Plasmids were isolated from *E.coli* using the QIAPrep Spin Miniprep or QIAGEN Plasmid Maxi Kit according to the manufacturer's protocols. The sequence of the plasmids was confirmed by sequencing using the primers listed in Table 2.9.

2.2.4 Immunoblotting

Cells were harvested after an experiment, pelleted and resuspended in an appropriate amount of lysis buffer and again centrifuged to separate the lysate and cellular debris. The protein concentration was determined with the BioRad Protein Assay (Bradford assay). The protein amount was adjusted to 20-30 ng per sample with lysis buffer and Laemmli sample buffer was added. Proteins were then denaturated for 2 min at 95 °C.

Separation of proteins was performed with pre-cast NU-PAGE Tris-Acetate Midi gels (3-8% PAA gradient) and matching 1x NuPAGE Tris-Acetate SDS Running Buffer in the Criterion BioRad system.

Protein transfer to a 0.45 µm nitrocellulose membrane was achieved by wet blotting. To this end, gel and membrane were assembled into a stack with two Whatman papers on each side. NU-PAGE gels were blotted in NU-PAGE transfer buffer. The blotting took place at 110 V for 1 – 1.5 hours or at 40 V and 4 °C for 16 hours.

The success of the blotting process was confirmed by staining the membrane with Ponceau S solution. After taking a picture, the staining was washed out. The membrane was then blocked for at least 1 hour on a shaker. Incubation with the primary antibody was done overnight at 4 °C at the indicated dilution in blocking solution (Table 2.2). After three washing steps of 5 minutes with TBS-T, the secondary antibody diluted in TBS-T was added for one hour. Finally, the membrane was again washed three times. The protein bands were detected using the Clarity Western ECL Substrate kit and the ChemiSmart system from Vilber Lourmat.

2.2.5 Flow Cytometry

2.2.5.1 Cell Cycle Analysis

Cells were harvested after an experiment, pelleted and the supernatant removed while retaining ~500 µl. The cells were resuspended and 1 ml of citric acid buffer was added for

fixation. The samples were kept at 4 °C for a maximum of one week until time of analysis. For the staining, cells were pelleted, resuspended in 300 µl DAPI solution (0.5 µg/µl in PBS) and incubated for 30 min at RT in the dark.

The samples were analyzed with the MACSQuant VYB flow cytometer. The main cell population was positioned in the lower left quadrant of the dot plot by adjusting the forward scatter (FSC) and side scatter (SSC) voltages. The voltage of laser V1 was adjusted individually for each sample to place the G_1 cell cycle peak at 300. 30,000 events excluding debris and doublets were recorded for each sample. Data analysis was done with the FlowJo cell cycle tool using the Watson pragmatic algorithm. If this was not possible due to strong perturbations of the cell cycle, G_1, S and G_2 phase gates were manually set in the complete experiment.

2.2.5.2 Cell Death Analysis

Cells were harvested after an experiment, pelleted, resuspended in 500 µl PBS and kept on ice. Directly before measurement, 1 µl propidium iodide (PI) / 100µl sample were added to the cell suspension. Samples were acquired as described above. PI was measured in the B2 channel. The gate for the PI-negative population was set in an untreated sample. Where necessary, the gates were adjusted upon visual inspection of the positive and negative population.

2.2.5.3 APO-BrdU TUNEL Assay

To measure apoptosis, the APO-BrdU (Bromdesoxyuridin) TUNEL (Terminal deoxynucleotidyl transferase -mediated dUTP-biotin nick end labeling) kit by Invitrogen was used according to the manufacturer's instructions. Briefly, cells were harvested after an experiment and fixed in 1% formaldehyde in PBS. After two washing steps in PBS, cells were permeabilized in 70% EtOH overnight at -20 °C. Before staining, cells were pelleted, resuspended in PBS and $1x10^6$ cells transferred to a new reaction tube. Incubation in DNA-labeling solution was prolonged to 90 minutes. After staining with the antibody solution and subsequently PI staining buffer, cells were directly analyzed. The BrdU signal was detected in the V2 channel, whereas PI was detected in the B2 channel. Gating of BrdU positive versus negative cells was performed individually for each cell line in untreated samples.

2.2.6 Quantification and Statistical Analyses

2.2.6.1 General Statistics

Differences between mean values were calculated using the Student's t-test for unpaired observations unless specified otherwise. The null hypothesis (differences between tested samples are due to chance) was rejected and differences called significant if the returned p - value was below 0.05. Statistical analysis was performed using Excel (Microsoft).

2.2.6.2 RNA Expression and miRNA Expression Analyses

RNA expression data of the cell cycle synchronization experiments was analyzed by Chunxuan Shao as detailed in Ryl et al. (2017).

For miRNA expression data, the raw reads were trimmed sequentially with cutadapt (Martin, 2011) to remove low quality reads and adapters with the parameters “-q 28 -m 18” and “-O 4 -f fastq -m 18 -a NEBNext=AGATCGGAAGAGCACACGTCT”. Trimmed data were further examined with fqtrim to remove low complexity reads; only reads that were 18 to 25 bps were used in the downstream analysis. Identical reads were collapsed by tally and processed by miRDeep2 for genome alignment, novel miRNA discovery and quantification. The read counts were then normalized with the DESeq2 package in R. Normalization size factors were calculated based on filtered counts (mean counts ≥ 10 reads). Differentially expressed genes were identified with a likelihood ratio test using the DESeq2 with the options ‘‘independentFiltering = FALSE, cooksCutoff = FALSE’’, while the full model and reduced model were specified as “~ Time + Tet_status + Time:Tet_status” and “~ Time”, respectively. Statistical significant miRNA were selected by FDR <= 0.05.

RNA expression data of CDK12/13 shRNA clones and BAY587-treated cells were analyzed by Umut Toprak. Genes with less than one count per million (CPM) were removed and normalization was performed with the trimmed mean of M values (TMM) method (Robinson and Oshlack, 2010). Next, the log-transformed CPM of the normalized values of control and knockdown/treatment samples were used to calculate the fold-change upon knockdown/treatment (mean and trimean) followed by a log2 transformation. Statistical significance was determined by the rank-based Kruskal-Wallis test with no assumption of the underlying distribution (Kruskal and Wallis, 1952).

3.1 The Transcriptional Network of MYCN in Neuroblastoma Cell Lines

As a transcription factor, MYCN regulates large numbers of genes. Effects on proliferation, self-renewal, apoptosis and other cellular processes are well documented (Huang and Weiss, 2013). Yet, many questions remain as to which effects are due to direct regulation of target genes and which to downstream network partners (Lin *et al.*, 2012; Sabo *et al.*, 2014).

3.1.1 MYCN Regulates Transcription of General and Cell Cycle Phase-Specific Drivers of Malignant Phenotype

Previous studies on the regulatory role of MYCN analyzed expression data of bulk cell populations, potentially confounding cell cycle effects with genuine MYCN effects. In order to get a clear picture of the transcriptional effects of MYCN in each cell cycle phase, our group developed a synchronization protocol that allows the observation of cells as they progress through the cell cycle (concept by Emma Bell; Ryl *et al.*, 2017).

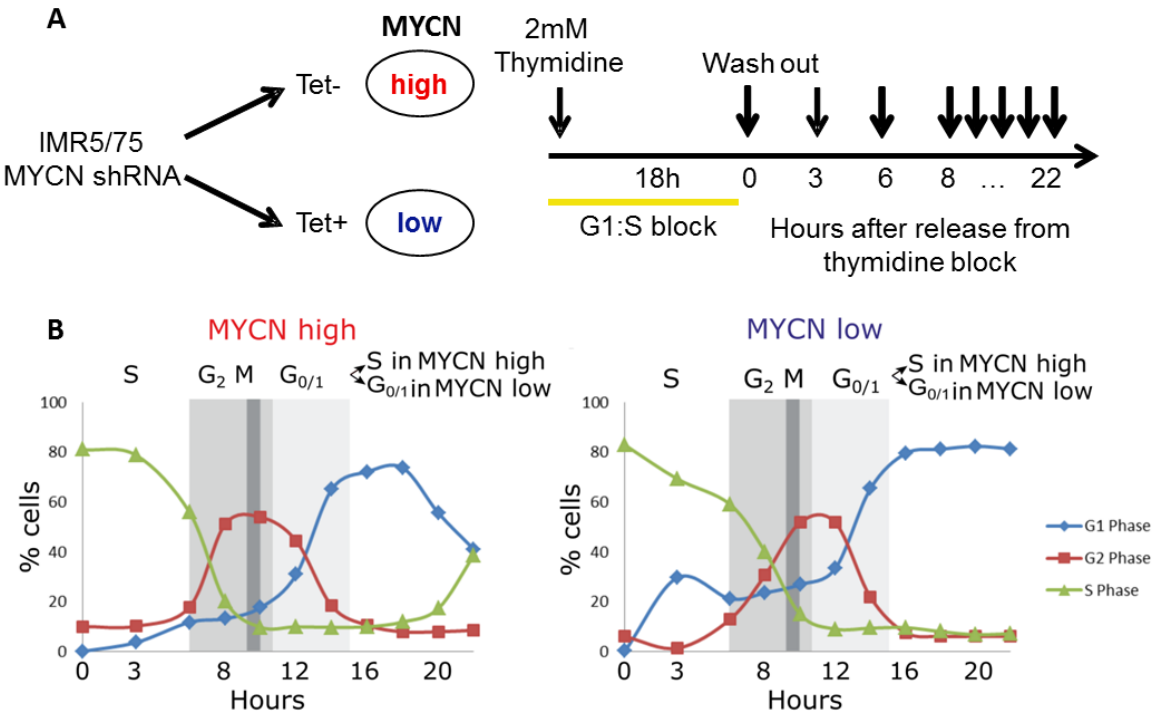

Figure 3: Cell Cycle Distribution after Thymidine Synchronization
(A) IMR-5-75 MYCN shRNA cells with high (red) and low (blue) MYCN protein level were arrested in G1/S phase by thymidine addition and released into the cell cycle 18 h later. Samples were taken and analyzed for cell cycle and gene expression. Adapted from Ryl et al. (2017). **(B)** Cell cycle analysis was performed by DAPI staining and subsequent flow cytometry analysis.

MNA IMR-5-75 cells carrying an shRNA to decrease the endogenous MYCN level were synchronized by thymidine treatment and released into S phase 18 hours later (Figure 3A). Samples were taken after 3, 6 and every two hours for 22 hours, and the synchronization was monitored by cell cycle analysis. Initially, the majority of both MYCN high and MYCN low cells resided in S phase and progressed almost simultaneously through G_2 phase, mitosis and $G_{0/1}$ phase (Figure 3B). MYCN low cells reached G_2 and mitosis slightly later than the faster proliferating MYCN high cells. After 16 to 18 hours a major difference became apparent, since MYCN high cells were able to enter a new cell cycle phase, whereas MYCN low cells remained stalled in $G_{0/1}$ phase.

At every time point, MYCN-induced changes in gene expression were analyzed by RNA sequencing (main experimenter Emma Bell, bioinformatic analysis: Chunxuan Shao). All time points viewed collectively, MYCN significantly upregulated 887 and downregulated 865 genes (Ryl *et al.*, 2017). With few exceptions, the fold changes were moderate and ranged between +/- 2. Unsupervised clustering was performed to detect common patterns of expression changes along the cell cycle. It revealed six distinct clusters (Figure 4). The DAVID functional annotation tool 6.8 was applied separately for each cluster to find significantly enriched gene functions (Huang da *et al.*, 2009a, 2009b). Two of the clusters contained genes that were constitutively up- or downregulated in MYCN high cells throughout the observation period (yellow and green line). In the upregulated cluster, one fifth of gene products were part of the nucleolus and for example involved in ribosomal RNA (rRNA) processing, such as nucleolar protein 56 (NOP56, Figure 5C, Appendix Figure S 1). Also, five snoRNAs were in the constantly upregulated cluster. There was also a significant enrichment of genes involved in DNA replication and G_1/S transition. This included four major players of cell cycle progression, namely CDK4, cyclin D3, cell division cycle 25A (CDC25A) and protein kinase membrane associated tyrosine/threonine 1 (PKMYT1) (Figure 5A). On the other hand, several inhibitors of cell cycle gene *CDK2* were represented in the permanently downregulated cluster (Figure 5A). Genes of this cluster were mostly enriched in the keywords alternative splicing, cell adhesion and synapse (Appendix Figure S 2).

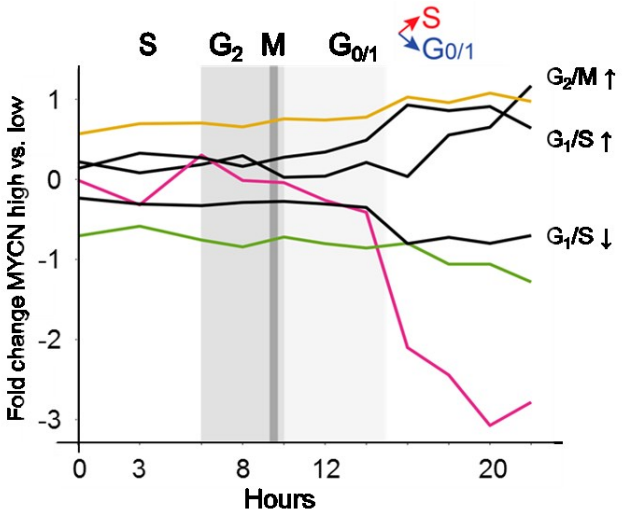

Figure 4: Unsupervised Clustering Reveals Cell Cycle-Resolved Gene Expression Patterns after *MYCN* Knockdown
K-means clustering of differentially expressed genes in RNA expression analysis of synchronized MYCN high and low IMR-5-75 cells. Clusters: "constitutively up" (yellow); "constitutively down" (green), "turbulent" (pink); "G_1/S up"; "G_1/S down"; "G_2/M up". Adapted from Ryl et al. (2017), experiments were conducted jointly with Emma Bell.

Three clusters showed differential expression in particular cell cycle phases (G_1/S up and down, G_2/M up). Indeed, cell cycle phase-specific genes were accumulated in these clusters. For example, a remarkable number of keywords related to mitosis were represented in the G_2/M cluster gene enrichment (Appendix Figure S 5). In the G_1/S up cluster, genes were particularly involved in DNA replication, DNA repair and histones, but also in the cell cycle, more specifically in the G_1/S transition (Figure S 4). In the G_1/S down cluster, genes were solely enriched for alternative splicing (Figure S 3).

Looking at single cell cycle genes confirmed the phases established by flow cytometry (Figure 3). The expression of *CCNE1* was high in both conditions after release from the thymidine block and subsequently dropped strongly (Figure 5B). Only in MYCN high cells, the level rose again, peaking at around 16 hours after release. The expression of *CDK2* followed a very similar pattern. These patterns are in line with the established function of cyclin E together with CDK2 in the transition of cells from G_1 to S phase (see also Introduction, Figure 1). Going further in the cell cycle, the expression of *CCNA2* rose throughout S phase and peaked in G_2, again nicely matching its ascribed role. At 18 to 22 hours, the expression rose again in the MYCN high, but not MYCN low condition, in keeping with the stalling in $G_{0/1}$ that was observed by flow cytometry. *CCNB1* and *B2* expression peaked at 8 – 12 hours, which corresponds to the time of mitosis, when the protein is known to be active. Its partner *CDK1* displayed a very similar expression pattern. Also, the expression peaks of *CCNA2* and *B1* were shifted by up to two hours between MYCN high and low, confirming the slower cycling of MYCN low cells.

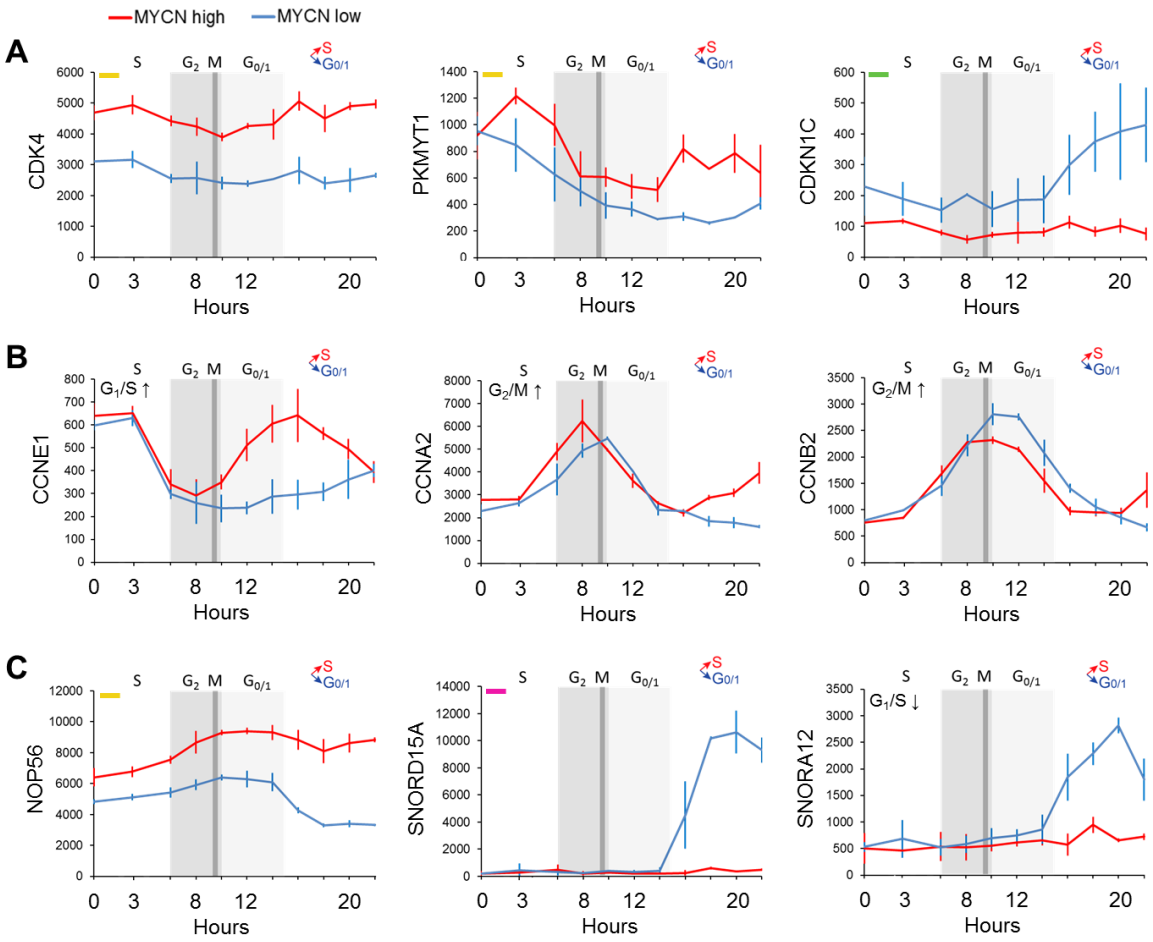

Figure 5: mRNA Expression Profiles of Cell Cycle and Ribosomal Genes
Examples of differentially expressed genes in synchronized MYCN high (red) and low (blue) IMR-5-75 cells. **(A)** Constitutively MYCN-regulated cell cycle genes; **(B)** cell cycle phase-dependently regulated cyclins; **(C)** genes and non-coding RNAs involved in ribosomal processes. Shown are normalized read counts. Affiliation to the clusters "constitutively up" (yellow), "constitutively down" (green), "turbulent" (pink), "G_1/S up"; "G_1/S down"; "G_2/M up" is indicated in the upper left part of the plots. Experiments were conducted jointly with Emma Bell.

The sixth cluster was characterized by a strong increase of transcripts in the MYCN low condition after 14 hours, while they remained constant in MYCN high cells (Figure 4, pink line). Before this time point, read counts in both conditions were typically very low. This small group contained predominantly small nucleolar RNAs (snoRNAs), but also some small nuclear RNAs (snRNAs) and small Cajal body-specific RNAs (scaRNAs). Expression of SNORD15A, for example, reached more than 10,000 reads in MYCN low cells (Figure 5B, middle graph). Eight further snoRNAs were grouped into cluster G_1/S down but had a very similar expression pattern to their counterparts in the pink cluster (Figure 5C, right graph).

Taken together, cell cycle-resolved analysis of gene expression in MYCN high and low cells allowed the differentiation between constitutive MYCN target genes, such as *CDK4* or *NOP56*, and more cell cycle phase-dependent genes, such as *CCNE1* or several snoRNAs.

3.1.2 MYCN-dependent miRNA Expression Changes Reveal an Additional Layer of Gene Regulation

Since MYCN is known to regulate also the expression of miRNAs, changes in miRNA levels in our cell cycle synchronization experiment were analyzed (data analysis: Chunxuan Shao). 164 miRNAs were significantly differentially expressed, 15 of which had previously not been annotated. 55 % of miRNAs were down-regulated, mirroring the balanced distribution of up- and downregulation already observed in the RNA expression data. The list of differentially expressed miRNAs was screened for direct MYCN targets as described by studies of primary NB tumors with our without *MYCN* amplification and of SH-EP cells with inducible *MYCN* overexpression (Megiorni *et al.*, 2017; Mestdagh *et al.*, 2010; Schulte *et al.*, 2008). There was an intersection of ten miRNAs which were consistently higher expressed in the MYCN high situation (Supplementary Table S 1). Only three miRNAs reported to be induced by MYCN contrarily showed downregulation in the present study (miR-16-2-3p, miR-181-5p, let-7b-5p), while six allegedly downregulated miRNAs could be confirmed. Another five miRNAs were downregulated only in parts of the observation period, while a single miRNA showed inverse expression (miR-1908-5p).
A reverse search with TarBase v7.0 revealed that 29 out of 149 differentially expressed miRNAs regulate cell cycle processes, and 78 miRNAs target genes were involved in ribosome biogenesis (Vlachos, Paraskevopoulou*, et al.*, 2015). Among the cell cycle-regulating subgroup were nine miRNAs that are direct MYCN targets (e.g. members of the miR-17-92 cluster). Finally, there were also miRNAs in this dataset which themselves regulate MYCN expression, miR-let-7e-5p and miR-101-3p (Figure 6B) (Buechner *et al.*, 2011).
Next, an unsupervised k-means clustering was performed, which identified five distinct clusters (Figure 6A). Interestingly, the cluster profiles resembled the ones identified in our RNA expression analysis. There were two clusters which were constitutively up- or downregulated by MYCN (yellow and green lines). In two clusters, the expression level diverged in early G_1 or towards the end of the observation period, when MYCN high cells enter S phase while MYCN low cells remain in G_1 phase ("G_1 up" and "G_1/S up" clusters). A rather small cluster exhibited the most prominent fold changes and peaked in G_2 phase ("turbulent", pink line). In G_2/M phase, the expression of MYCN high cells clearly exceeded that of MYCN low cells, whereas it was inversed in G_1/S phase. For each cluster, KEGG (Kyoto Encyclopedia of Genes and Genomes) analysis was performed with the mirPath v.3 algorithm (Figure 7 and Supplementary Figure S 6 – 9) (Vlachos, Zagganas*, et al.*, 2015). Despite the comparable patterns of RNA and miRNA clusters, there was no considerable overlap of significantly enriched processes or cellular components. However, many of the top terms appeared in several of the miRNA clusters.

As an example, the pathway “proteoglycans in cancer” was among the top six results in four clusters. In general, there were many KEGG terms related to cancerous processes or particular entities. Also several signaling pathways linked to tumorigenesis were represented, such as the Hippo and the Transforming Growth Factor ß (TGF-ß) signaling pathways. In addition, several recurrent KEGG terms had to do with synaptic signaling.

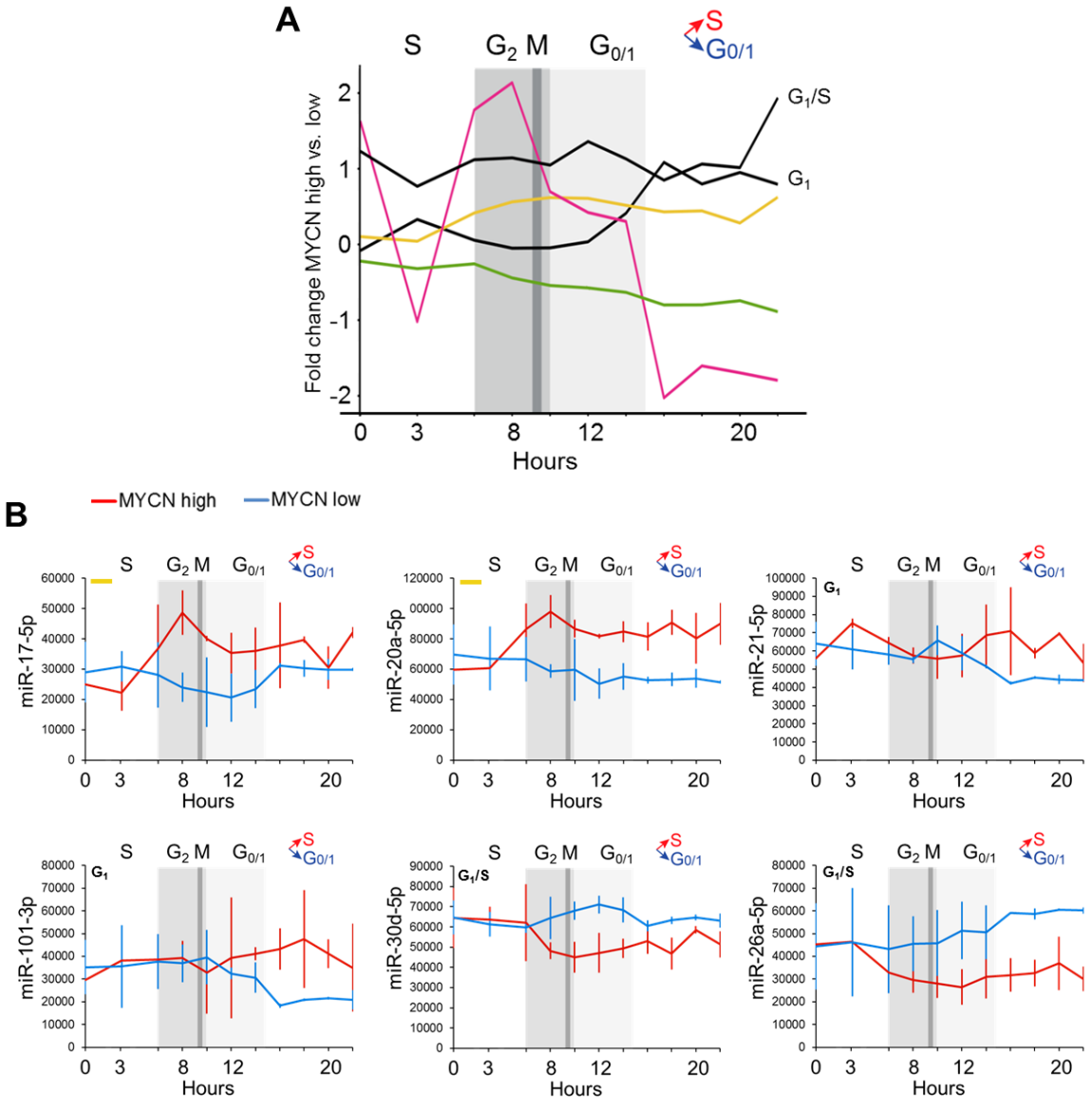

Figure 6: Unsupervised Clustering Reveals Cell Cycle-Resolved miRNA Expression Patterns after MYCN Knockdown
(A) K-means clustering of differentially expressed miRNAs in synchronized MYCN high versus low IMR-5-75 cells. Clusters: “constitutively up” (yellow); “constitutively down” (green), “turbulent” (pink); “G_1/S up”; “G_1 up”. **(B)** Example profiles of highly expressed miRNAs. Affiliation to the clusters is indicated in the upper left part of the plots. Shown are normalized read counts. Experiments were conducted jointly with Emma Bell.

Looking at the read counts of the differentially expressed miRNAs, very strong differences became apparent. More than 35 % of them had read counts of 200 or below. Opposed to that, seven miRNAs had read counts of 50,000 and higher. Reasoning that high read counts mean that the miRNAs in question have a high impact on gene regulation, they were selected for closer inspection (Figure 6B). Two miRNAs, miR-17-5p and miR-20a-5p, were part of the oncogenic cluster miR-17-92 and their expression was increased in MYCN high cells. Congruously, they and also miR-9-5p were among the MYCN-induced targets established above. Additionally, miR-21-5p and miR-101-3p displayed particularly high expression towards the end of the observation period. Opposed to that, miR-26a-5p and miR-30d-5p read counts dropped in MYCN high compared to MYCN low cells.

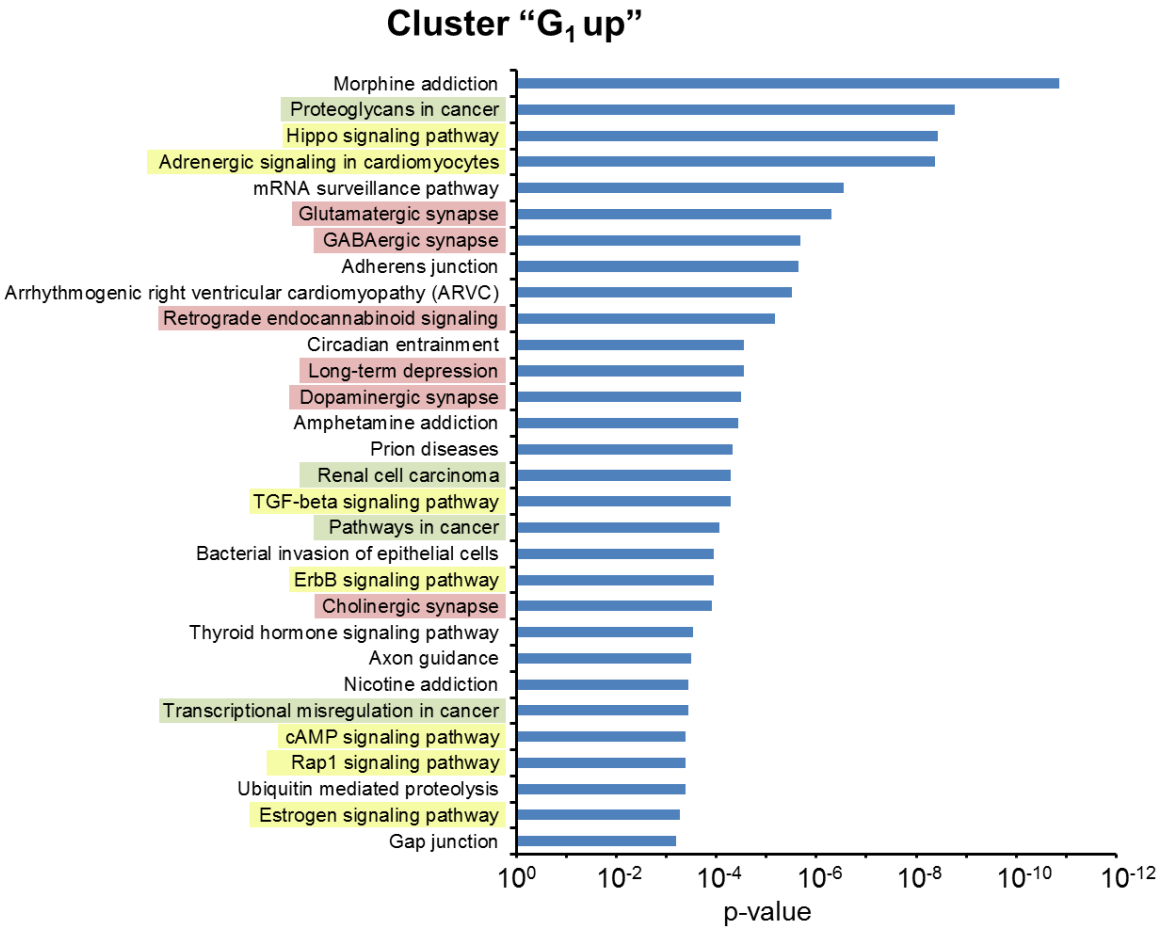

Figure 7: MYCN-Dependent miRNAs Predominantly Regulate Processes Related to Cancer
KEGG analysis of miRNAs grouped together in the G_1 cluster identified cancer- and synapse-related processes (green and red) and several signaling pathways (yellow). List shows the 30 most significant terms with $p \leq 0.05$. Other clusters see Figure S 6 - 9.

In summary, cell cycle-resolved analysis of miRNA expression demonstrated that MYCN regulates the expression level of many miRNAs that play a role in different cancer entities. Cluster-specific gene enrichment analysis showed that different miRNAs fulfill similar functions over the course of the cell cycle.

3.2 CDK13, a Novel Target in *MYCN*-amplified Neuroblastoma

3.2.1 MYCN Synthetic Lethal Screens Identify CDK13 as One of the Top Candidates

MYCN-amplified tumor cells depend on the transcriptional deregulation caused by aberrant MYCN levels as described in the first part of this study. After all, many oncogenic processes are sustained by MYCN and its downstream interaction partners, for example proliferation, angiogenesis or inhibition of differentiation (Westermann *et al.*, 2008). Since MYC(N) itself is considered to be largely undruggable, new strategies aim at identifying those downstream interaction partners that are indispensable for the survival of MYCN-driven tumors (Kaelin, 2005). In this context, a high-throughput druggable genome synthetic lethal screen in NB cells with regulatable MYCN was performed in a joint project of our group (Sina Gogolin) and Bayer AG. The model system used in the screen was MNA IMR-5-75 cells with an inducible *MYCN* shRNA that allows reduction of MYCN protein by approximately 65 % (Muth *et al.*, 2010; Ryl *et al.*, 2017).

The screen covered more than 10,000 druggable genes with three siRNAs per gene. Cell numbers were counted as a read-out 96 h after transfection. Candidates were identified based on a strong reduction in viability induced in the MYCN high condition and a strong effect of MYCN (i.e. a large difference between the viability of MYCN low – MYCN high, Figure 8). In addition, these putative MYCN synthetic lethal candidates were subjected to a gene ontology analysis, which revealed an enrichment of CDKs and cyclins among the best-scoring candidates. It pinpointed some well-established players in neuroblastoma biology, such as CDK2, 4 and 7. Also among these candidates was the transcriptional kinase CDK13, which has so far mostly lacked attention of the cancer research community.

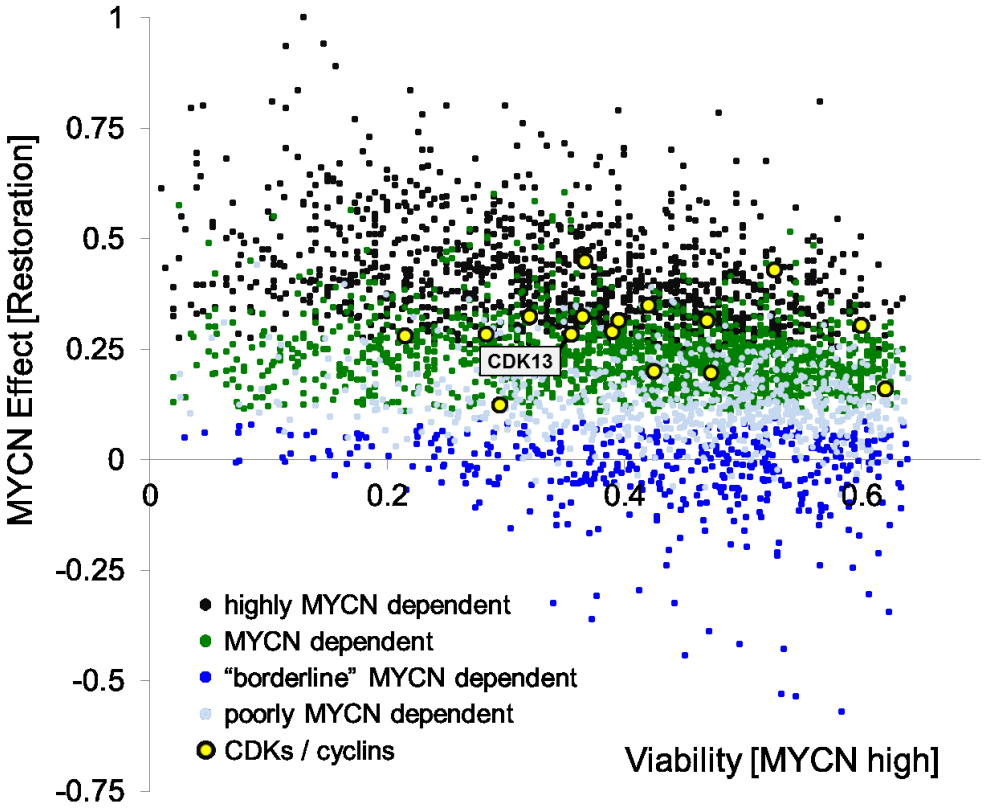

Figure 8: Identification of Cell Cycle Genes as Synthetic Lethal Candidates
IMR-5-75 cells were transfected with 3 siRNAs per gene and incubated for 96 h. Viability was determined by counting Hoechst-stained nuclei. MYCN effect was calculated by subtracting viability of the MYCN high from that of MYCN low cells. Highlighted in yellow are synthetic lethal CDKs and cyclins. Experiments were performed by Sina Gogolin and colleagues at Bayer AG.

A second, independent synthetic lethal screen was performed by collaboration partners in Finland. Here, SH-SY-5Y cells with inducible MYCN overexpression were used as a model system. They were transfected with a pool of four siRNAs per gene, an approach that reduces potential off-target effects. The read-out of this screen was a CellTiter Glo assay measuring metabolic activity of the cells. Cyclin K, the partner cyclin of CDK13, was among the 52 proliferation-reducing hits of this screen, thus fortifying our interest into the kinase as a potential candidate (Figure 9).

CDK13 was therefore picked for further validation next to three other potentially interesting candidates, which formed the intersection of both synthetic lethal screens. The analysis of the additional candidates has been pursued in separate projects and will not be discussed here.

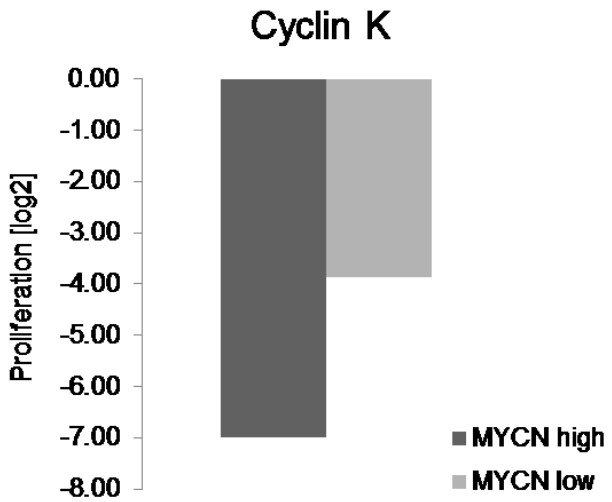

Figure 9: Cyclin K Is among the Top Hits of a Synthetic Lethal Screen in *MYCN*-Overexpressing SH-SY-5Y Cells
Cells were seeded and *MYCN* expression was induced by tetracycline addition for one day. Cells were transfected with an siRNA pool (four siRNAs per gene) and incubated for 72 h. Cell viability was measured by CellTiter Glo. Shown are normalized, loess fitted viability data points divided by the median of negative controls. Experiments were performed by Saija Haapa-Paananen and colleagues (VTT Technical Research Centre of Finland).

3.2.2 Evaluation of CDK13 and CDK12 as Potential Therapeutic Candidates

It was decided to include CDK12 next to CDK13 into all further analyses. First of all, it is highly homologous to CDK13 and interacts with the same partner cyclin, namely cyclin K. Differences and similarities in their cellular function have not been fully elucidated until now. Second, *CDK12* is mutated or amplified in several cancer entities, including ovarian and breast cancer (Natrajan *et al.*, 2014; Popova *et al.*, 2016). Thus, interest into CDK12 as a potential new target has increased strongly during the last years.

Validation of CDK13 repression in additional neuroblastoma cell lines. As a next step, the effects of knocking down *CDK13* or *CDK12* were analyzed in a larger panel of cell lines. Viability of the cells after knockdown was analyzed by two methods, first assessment of confluence as a measure of growth and second Cell Titer Blue (CTB) assay as a measure of metabolic activity. Cells treated with negative control siRNAs or with transfection reagent only served as controls. In addition, success of the transfection was controlled by knocking down *polo-like kinase 1* (*PLK1*), which is indispensable in NB cells, leading to strong cell death.
For *CDK13*, four siRNAs were tested. Of these, in general only siRNA1 and 3 proved effective, while siRNA2 and 4 only had minor effects in one of the cell lines (Figure 10). Of the nine tested neuroblastoma cell lines, SK-N-BE(2)c, NB-69, CHP-134, SK-N-AS and SH-EP cells responded strongly to knockdown of *CDK13*. In addition, the cell lines

KELLY, LS and IMR-32 responded partly. IMR-5-75 cells responded strongly to siRNA1 and in part to siRNA3. They also showed a slight response to knockdown of *CDK12* by siRNA1, but not 3. The same was true for SK-N-BE(2)c. In addition, *CDK12* knockdown modestly decreased viability of SH-EP cells. Also two lung and two colon cancer cell lines were tested (shown here: strong responder HCT116). Of these, only one lung cancer cell line did not respond to *CDK13* repression. Non-transformed fibroblast cells (NHDF) were not at all affected by knockdown of *CDK12* or *CDK13*.

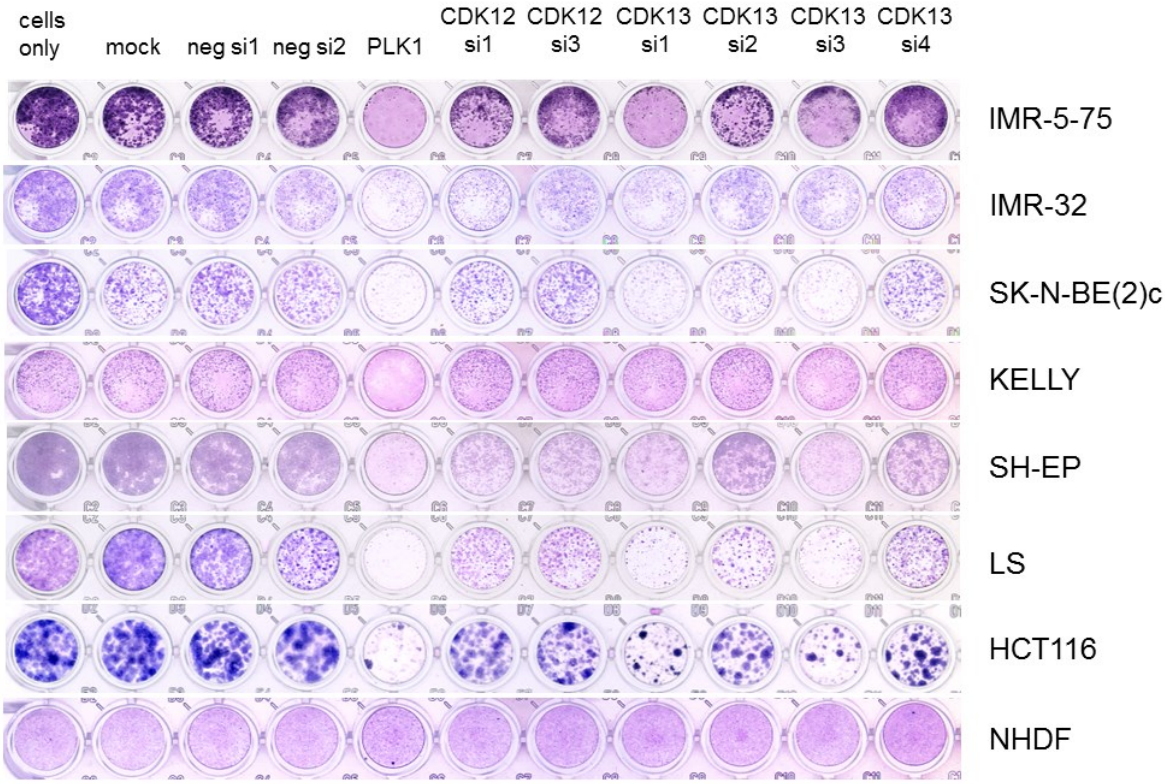

Figure 10: *CDK13* Repression Reduces Confluence in Most NB Cell Lines
Cells were treated with indicated siRNAs for 96 h, fixed and confluence was evaluated by Giemsa staining. Experiments were performed by Sina Gogolin.

Expression pattern of CDK12, 13 and CCNK during the cell cycle. Looking at the RNA levels of our candidates in the cell cycle synchronization experiment revealed that neither *CDK13* nor *CDK12* or *CCNK* were differentially expressed in MYCN high and low cells. Expression of *CDK12* peaked in late S phase / early G_2 phase (Figure 11). Opposed to this, *CDK13* expression went up at mitosis and remained constant throughout G_1 and early S phase. *CCNK* levels were constant throughout the observation period and read counts much lower than those of the CDKs.

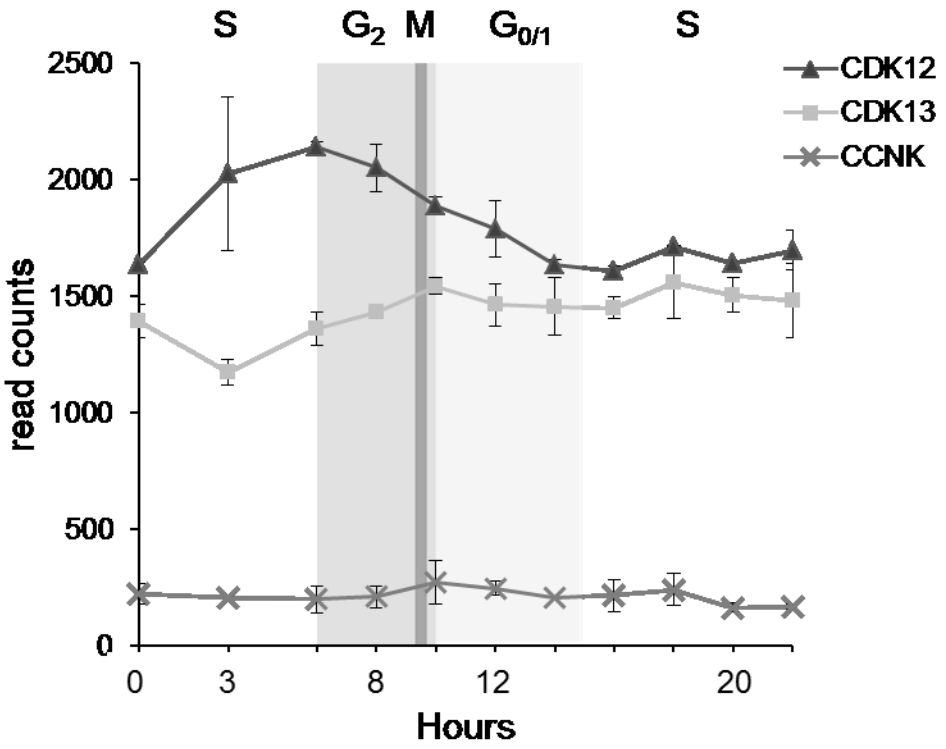

Figure 11: Expression Profiles of *CDK12, 13* and *CCNK*.
IMR-5-75 cells were synchronized as described in chapter 3.1.1 and RNA sequencing performed at the indicated time points. Shown are read counts of *CDK12, 13* and *CCNK* in MYCN high cells. Experiments were conducted jointly with Emma Bell.

Role of CDK12, 13 and cyclin K in primary tumors. When comparing the proteome of MNA tumors with that of low risk tumors by mass spectrometry, we found that the cyclin K level was strongly decreased ($p < 0.001$, experiments performed by Michal Nadler-Holly, Figure 12A). Also CDK13 and CDK12 were significantly decreased ($p < 0.01$).

This finding was confirmed by looking at *CDK13* RNA expression in a publicly available cohort of 498 primary NBs, which was significantly lower in MNA tumors ($p = 7.3\ e^{-10}$, Figure 12B).

Low expression levels of *CDK13* also significantly correlated with poor overall survival ($p = 0.034$, Bonferroni-corrected for multiple testing). While *CDK13*-high cases had a survival probability of roughly 80 %, it was below 50 % in *CDK13*-low cases (Figure 12C). For *CDK12*, the opposite trend was observed, however it was not significant after multiple testing correction (data not shown).

Taken together, data from NB cell lines and primary tumors both indicated an important role of CDK13 in NB biology and thus supported further investigation of CDK13 as a potential therapeutic target.

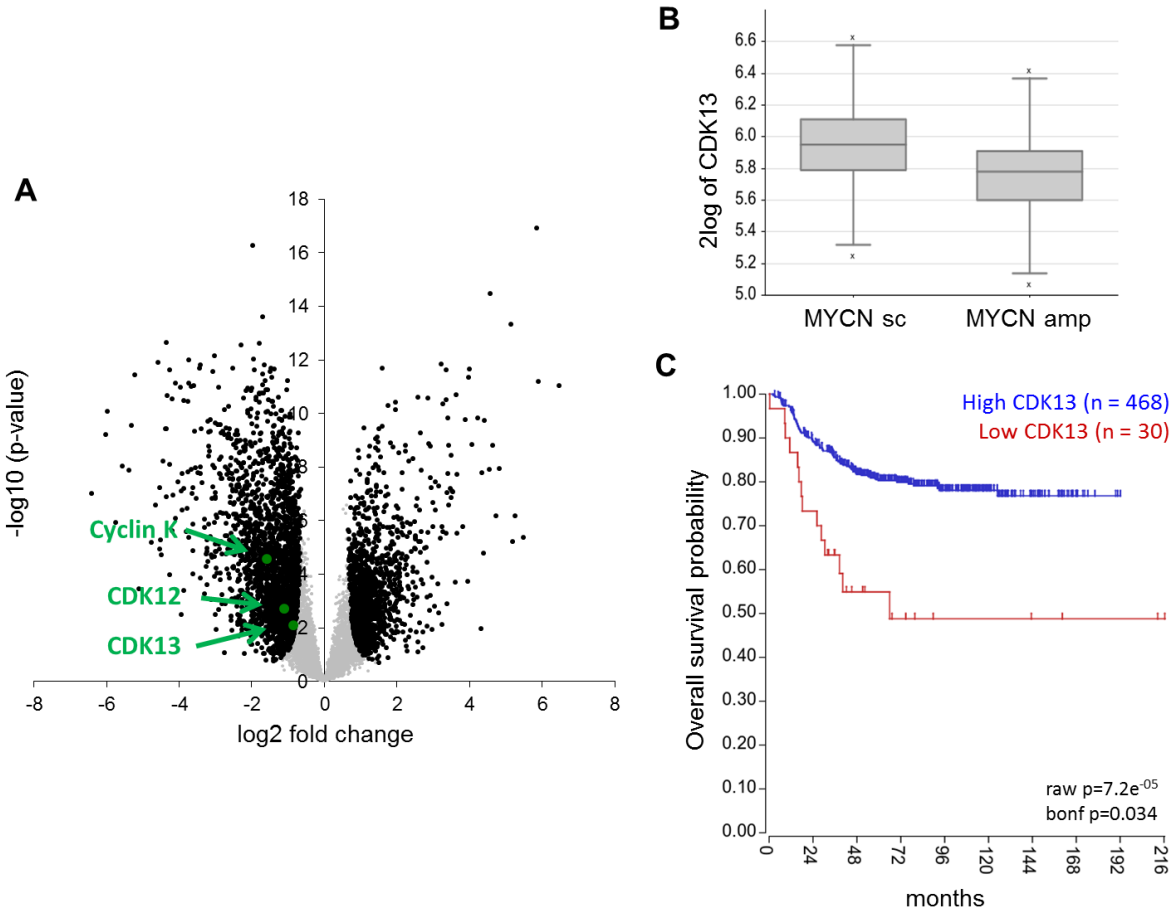

Figure 12: CDK13 Is Reduced in *MYCN*-Amplified Neuroblastoma Tumors
(A) Mass spectrometry; proteome of primary neuroblastoma samples with *MYCN*-amplification compared to single copy status. Experiments were performed by Michal Nadler-Holly (Max Delbrück Center for Molecular Medicine, Berlin). **(B)** *CDK13* RNA expression analysis in primary tumors; sc = single copy, amp = amplified. **(C)** Kaplan Meier plot showing overall survival for high versus low *CDK13* expression. **(B), (C)**: created with R2 Genomics Analysis and Visualization Platform.

3.2.3 Characterization of CDK13 Dependency in *MYCN*-regulatable Neuroblastoma Cells

Next, cellular models with regulatable MYCN level were employed to learn more about its role regarding sensitivity of neuroblastoma cell lines towards knockdown of *CDK13*.

Inducible MYCN knockdown. First, IMR-32 and IMR-5-75 cells with an inducible *MYCN* shRNA were used. One day after repression of *MYCN*, *CDK12* or *CDK13* were additionally knocked down by siRNA. Knockdown of both kinases induced between 10 - 30 % cell death as determined by uptake of PI due to damaged cell membrane (Figure 13; data for IMR-5-75 *MYCN* shRNA not shown). *CDK13* knockdown tended to induce more cell death than that of *CDK12*. However, the extent of cell death was irrespective of the MYCN level. With regard to the cell cycle distribution upon *CDK13*

knockdown, there was a trend towards an accumulation of cells in G_1 phase accompanied by reductions in S and G_2 phase (Figure 13C). Knockdown of *CDK12* similarly led to slightly increased cell numbers in G_1 and reduced numbers in S phase in the MYCN low condition (Figure 13B).

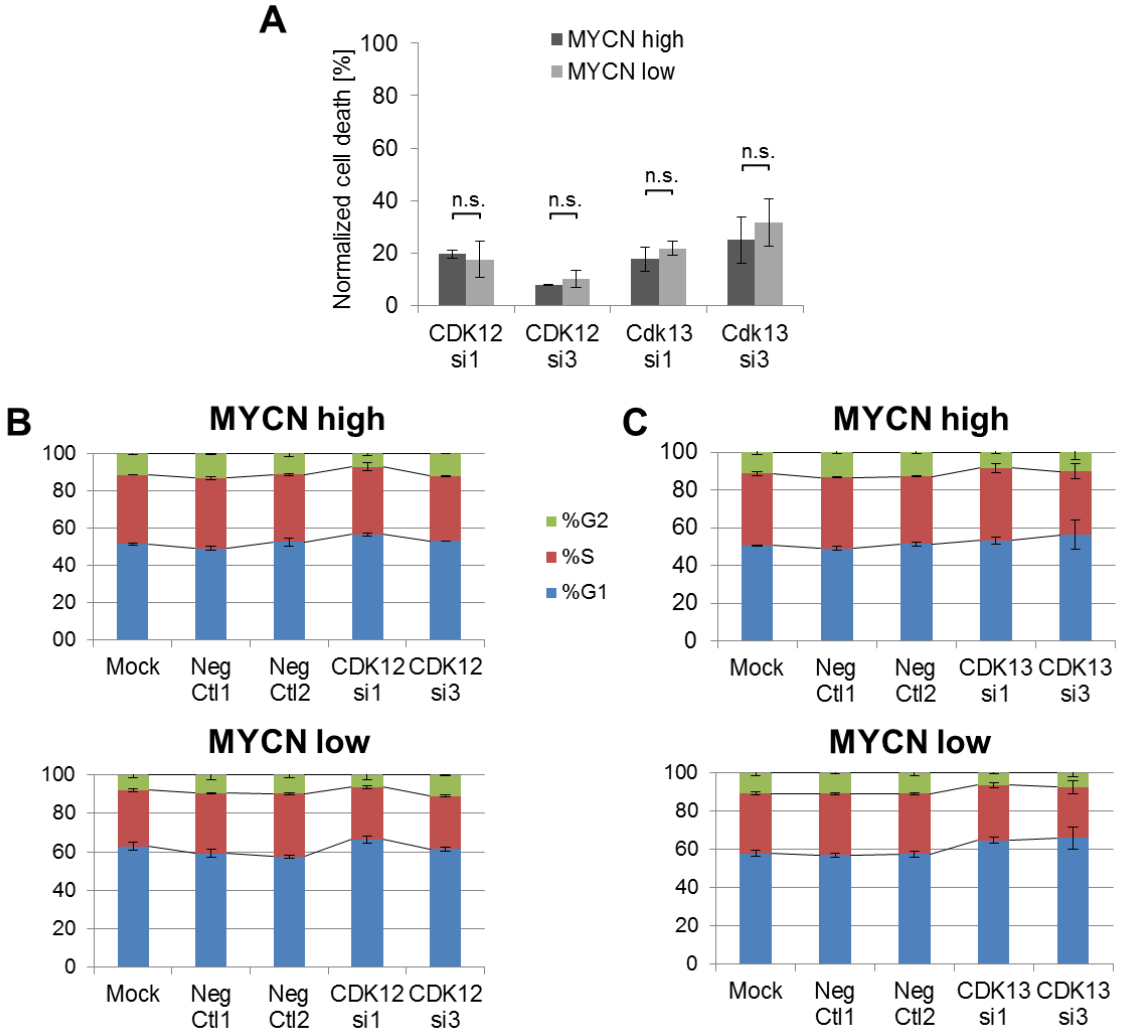

Figure 13: Knockdown of *CDK12* or *CDK13* in IMR-32 Induces Moderate Cell Death Irrespective of MYCN Level.
MYCN knockdown was induced in IMR-32 *MYCN* shRNA cells and after 24 h, cells were transfected with siRNAs against *CDK12* or *CDK13* or treated with transfection agent only (mock). After 96 h, floating and adherent cells were harvested. **(A)** Cell death; cells were stained with PI and directly analyzed by flow cytometry. Amount of positive cells was normalized to negative controls 1 and 2; mean ± SEM, n = 2/3. **(B), (C)** Cell cycle; cells were fixed in citric acid buffer, stained with DAPI and analyzed by flow cytometry; mean ± SEM, n = 2/3.
n.s. = not significant

Inducible MYCN overexpression. SH-EP cells have very low levels of endogenous MYCN, but the stable subclone TET21N allows conditional overexpression of MYCN (Lutz *et al.*, 1996). In general, high MYCN led to an increase of S and G_2 phase cells. In this model, knockdown of *CDK12* induced moderate cell death in the MYCN overexpression condition (siRNA 1: 20 %, siRNA 3: 10 %, $p < 0.05$, Figure 14A). In addition, there was a

trend towards more cells residing in G_1 phase compared to one out of two non-targeting controls and mock transfection (Figure 14B). siRNA3 targeting *CDK13* induced 76 % cell death in MYCN high cells, but only 18 % in MYCN low ($p < 0.001$, Figure 14A). Cell cycle analysis revealed less cells in G_1 accompanied by an increase of S and G_2 phase cells in the MYCN low and high condition (Figure 14C). Opposed to that, CDK13 siRNA1 did not induce any cell death at all; instead, cells seemed to be arrested in G_1. Apparently, *CDK12* and *CDK13* repression elicited arrest in different phases of the cell cycle.

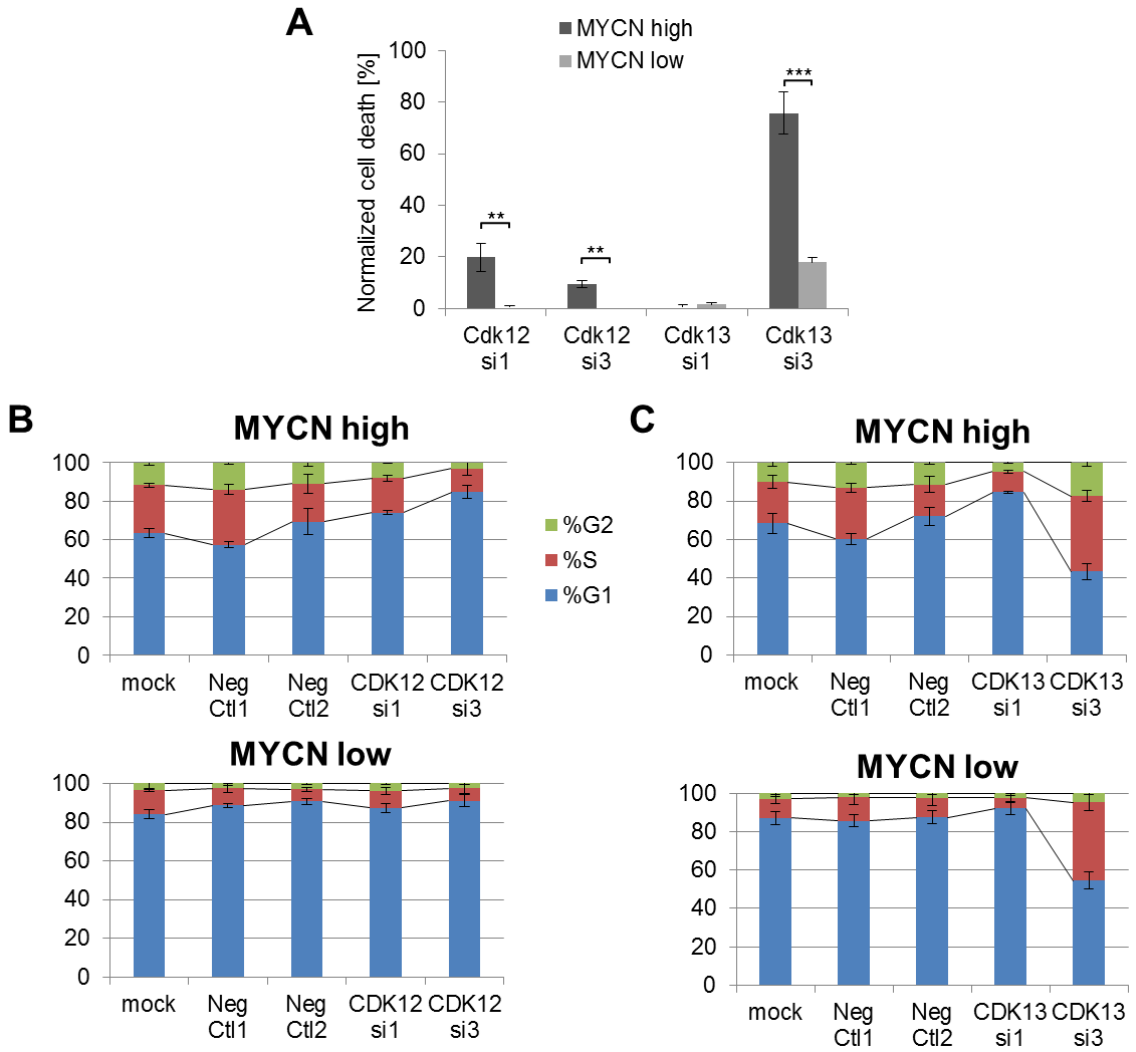

Figure 14: Knockdown of *CDK13* Induces Strong Cell Death in MYCN-High SH-EP TET21N Cells
Overexpression of MYCN was induced in SH-EP TET21N cells and after 24 h, cells were transfected with siRNAs against *CDK12* or *CDK13* or treated with transfection agent only (mock). After 96 h, floating and adherent cells were harvested. **(A)** Cell death; cells were stained with PI and directly analyzed by flow cytometry. Amount of positive cells was normalized to negative controls 1 and 2; mean ± SEM, n = 2/3. **(B), (C)** Cell cycle; cells were fixed in citric acid buffer, stained with DAPI and analyzed by flow cytometry; mean ± SEM, n = 2/3.
*** $p < 0.001$, ** $p < 0.01$

3.2.4 Conditional *CDK12/13* Knockdown in Neuroblastoma Cells

In order to further explore the effects of *CDK13* knockdown in neuroblastoma cells, stable cell lines with vectors containing shRNAs against *CDK12* or *CDK13* were generated. For the creation of the short hairpins, the sequence of the siRNAs was used (CDK12 si1+3, CDK13 si1+3).

Knockdown efficiency of shRNA clones. After transfection of IMR-5-75 with the shRNAs, single clone cultures were raised and the extent of the knockdown was determined by immunoblotting. The cell clones with the best knockdown results, which were used in all further analyses, were A8 (CDK13 sh1), L3 (CDK13 sh3), B5 (CDK12 sh1), G1 (CDK12 sh3) and 2C (scramble sh / scr sh). Upon induction of the shRNA, protein was reduced by 70 – 85 % (CDK13 sh1), 45 – 88 % (CDK13 sh3), 35 – 60 % (CDK12 sh1) and 85-98 % (CDK12 sh3) on average (Figure 15). The induction of scramble shRNA did not lead to a reduction in CDK12 or CDK13 level; if anything, the levels were moderately increased.

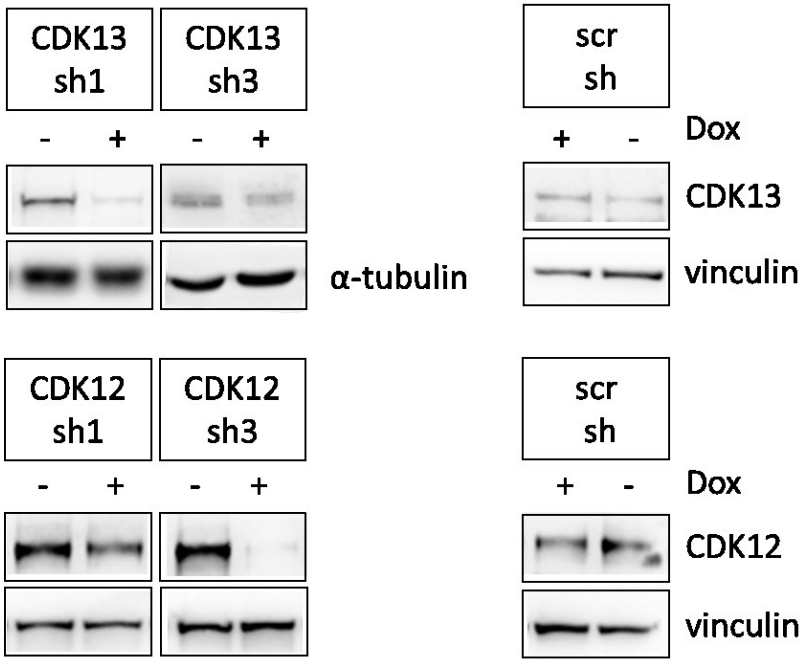

Figure 15: Doxycycline-Induced shRNA Targeting CDK13 or CDK12 Results in Decreased Protein Levels.
Expression of *CDK12*, *CDK13* or *scramble* (scr) shRNA was induced by doxycycline (Dox) addition. After 72 h, floating and adherent cells were harvested and lysed for immunoblotting. Vinculin or α-tubulin were used as loading controls. Representative replicate out of n ≥ 3.

Modest reductions in cell viability and colony formation. All described experiments were conducted with 72 h and 96 h time windows with concordant results (96 h data not shown). The viability of the cells after knockdown was analyzed by CTB and growth assay. Confluence was reduced by 25 % on average in the CDK13 sh1 clone, and only slightly or not at all reduced in the other clones when compared to the scramble control (Figure 16A). The effect on metabolic activity of the cells was even less pronounced (data not shown). A colony formation assay demonstrated decreased ability to form colonies from single cells upon *CDK13* knockdown (Figure 16B). The results varied strongly between 10 and 90%, with a mean reduction of 41 % for CDK13 sh1. For CDK13 sh3, colony formation was reduced by approximately 70 % in four out of five biological replicates ($p < 0.001$ in each of these replicates). Effects of *CDK12* knockdown were less variable with the two CDK12 shRNA clones significantly reducing colony formation by 39 % and 98 % on average ($p < 0.01$ in every biological replicate). Also induction of scramble shRNA led to an average reduction of colony formation by 47 % ($p < 0.01$).

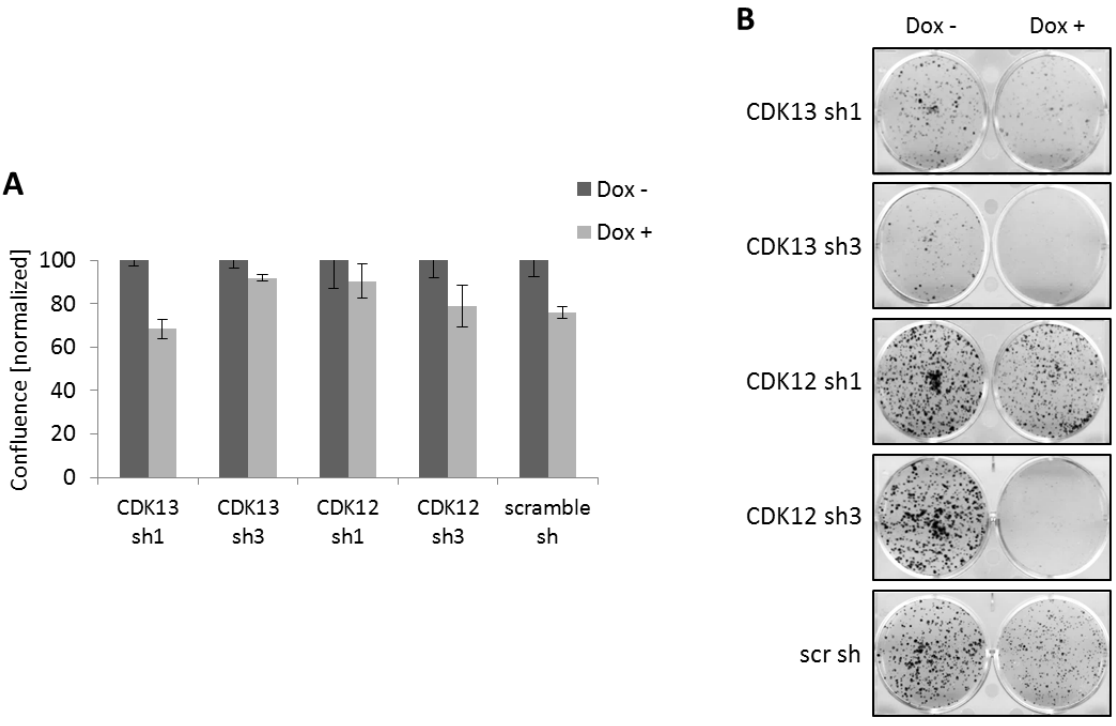

Figure 16: Knockdown of *CDK13* in Stable IMR-5-75 Clones Modestly Impacts on Cell Viability and Colony Formation Capacity
Expression of *CDK12*, *CDK13* or *scramble (*scr) shRNA was induced by doxycycline addition. At the given endpoint, cells were fixed and confluence was evaluated by Giemsa staining. **(A)** Growth assay; cells were seeded at high density and incubated for 72h; technical replicate's mean ± SEM. **(B)** Colony formation assay; cells were seeded at low density and incubated for 7-10 days before fixation and Giemsa staining. Representative biological replicates out of n ≥ 3.

No effects on cell death or cell cycle distribution observed. The experiments on viability were complemented by PI stainings to analyze cell death. Neither *CDK13* nor *CDK12* knockdown did increase the amount of cell death in the cell clones (Figure 17A).

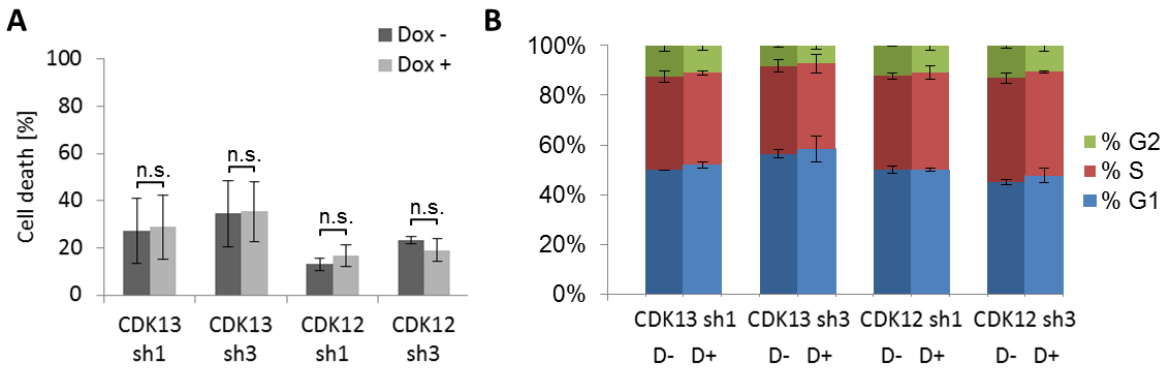

Figure 17: Knockdown of *CDK13* in Stable IMR-5-75 Clones Does Not Induce Cell Death or Alter Cell Cycle
Expression of *CDK12* or *CDK13* shRNA was induced by doxycycline addition for 72 h. **(A)** Cell death; cells were harvested, stained with PI and directly analyzed by flow cytometry; mean ± SEM, n = 2. **(B)** Cell cycle; cells were fixed in citric acid buffer, stained with DAPI and analyzed by flow cytometry; mean ± SEM, n = 2.
n.s. = not significant

Next, the effect of *CDK13* and *CDK12* knockdown on the cell cycle tested, but the distribution was not altered (Figure 17B).

RNA expression analysis. In order to better understand the differences between CDK13 and CDK12 function, RNA expression of IMR-5-75 clones 96 h after induction of shRNA was analyzed. Differentially expressed genes (DEGs) were defined as having the same direction of regulation (thus the same sign of the fold change) for both shRNAs and with > 2-fold change in at least one out of two (normalization and bioinformatic analysis: Umut Toprak). Generally speaking, the number of DEGs was very low. Knockdown of *CDK13* induced more downregulation than upregulation of genes (66 versus five genes). Knockdown of *CDK12* induced upregulation of eight genes, and downregulation of three genes. None of the DEGs overlapped between CDK12 and CDK13. But it was noticeable that all gene lists included a relatively large proportion of transcripts for non-coding RNAs, mainly miRNAs or pseudogenes. Among the most strongly increased transcripts after *CDK12* knockdown were five miRNAs. Upon knockdown of *CDK13*, miRNAs constituted three of the five most upregulated transcripts and eight of the ten most downregulated transcripts. PKIA, a protein kinase inhibitor, was among the most strongly downregulated transcripts after *CDK13* knockdown.

CRISPRi-induced knockdown of CDK13. Since some of the shRNA clones only achieved moderate knockdown efficiencies, a different technique promising higher efficiency was employed next. Clustered regularly interspaced short palindromic repeats interference (CRISPRi) works by steric inhibition of Pol II by a deactivated Cas9 (dCas)

enzyme, thus preventing transcription of the targeted gene. In this approach, dCas was integrated into the AAVS1 (Adeno-Associated Virus Integration Site 1) locus by a TALEN (Transcription activator-like effector nuclease)-assisted gene trap. The necessary vectors were a gift of Mandegar and colleagues, who reported consistent knockdown efficiencies of 95 % and more in their hands (Mandegar *et al.*, 2016). IMR-5-75 cells were transfected with AAVS1 TALEN F and R and the doxycycline-inducible vector pAAVS1-NDi-CRISPRi with dCas-KRAB (Krüppel associated box) fused to an mCherry construct ("dCas", step 1). A single clone with even mCherry expression was selected, expanded and again transfected with one of three different sgRNAs against *CDK13* and two non-targeting control vectors (sgRNA 6, 8, 10, scr 2 + 3, step 2). Single clones were raised from the polyclonal cultures and the knockdown efficiency was determined by immunoblotting. The protein level of CDK13 was indeed reduced by 50 to 90 % in the clones chosen for further analysis, while the scramble controls did not alter CDK13 protein level (Figure 18A). In addition, viability and confluence of the cell clones was reduced by around 40 % upon doxycycline addition to induce sgRNA expression (Figure 18C). However, this effect also occurred in dCas9 cell clones of step 1, which did not yet contain the sgRNA vector.

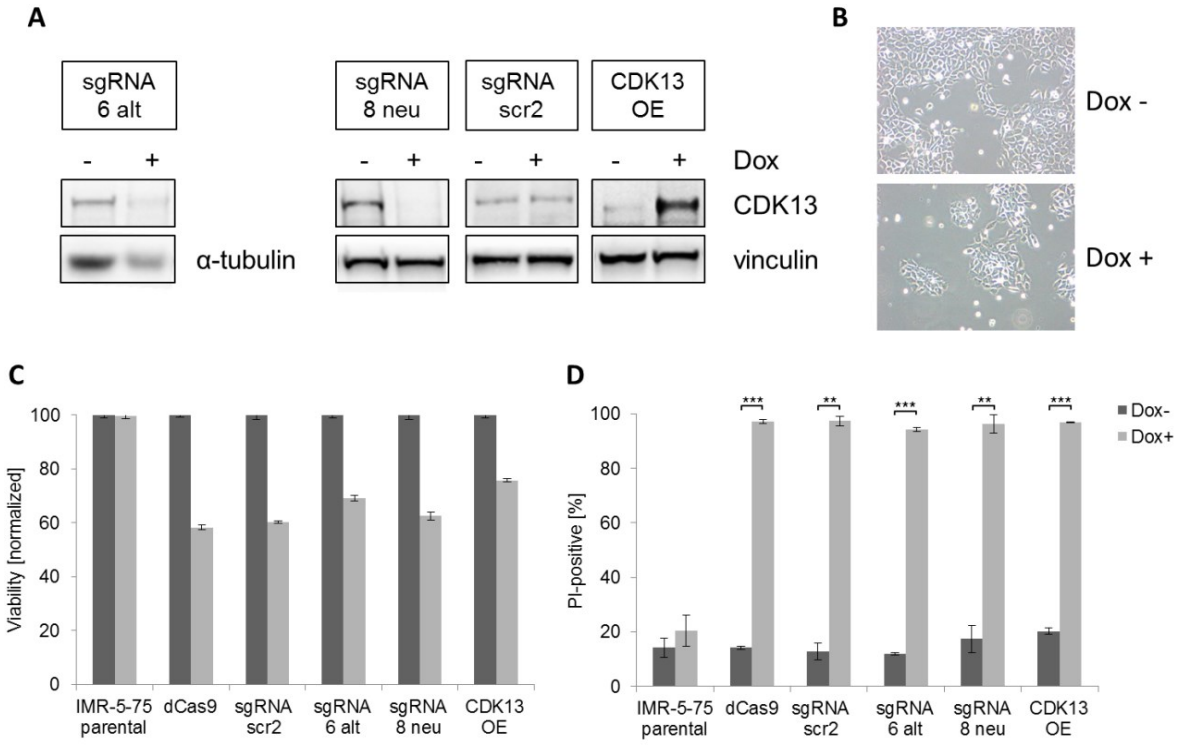

Figure 18: Induction of dCas9 Vector Negatively Affects Viability in IMR-5-75 Cells
Expression of sgRNA and OE vector was induced by doxycycline addition. **(A)** After 96 h, floating and adherent cells were harvested and lysed for immunoblotting. Vinculin or α-tubulin were used as loading controls. **(B)** Representative light microscopy image of sgRNA 6 clone. Magnification 10x. **(C)** Viability was assessed by CTB after 96 h. Representative biological replicates out of n = 4. **(D)** Cell death; cells were harvested, stained with PI and directly analyzed by flow cytometry; mean ± SEM, n = 3.
*** $p < 0.001$, ** $p < 0.01$

A live/dead cell exclusion staining to determine the amount of cell death revealed that upon induction by doxycycline, more than 90 % cells stained positive for PI in sgRNA 6, dCas9 and sgRNA scr ($p < 0.002$, Figure 18D). Yet, no change in morphology characteristical of cell death could be observed (Figure 18B). In addition, a cytotox membrane integrity assay did not confirm that induction of the dCas vector should cause a damaged cell membrane (data not shown).
Due to the general loss of viability, further in-depth characterization of these cell clones is not shown here. In order to see whether the effect on viability could be rescued, overexpression (OE) plasmids were introduced into the sgRNA 6 alt clone (*CDK12* OE*, CDK13* OE and kinase-dead mutants *CDK12* KDM and *CDK13* KDM). Induction of *CDK13* knockdown and simultaneous ectopic overexpression of *CDK12* or *CDK13* did not improve viability (Figure 18 C and D).

Taken together, partial knockdown of *CDK13* was enough to elicit a moderate decrease in NB cell viability and colony formation capacity, while response to CDK12 repression was less pronounced in most cases.

3.2.5 CRISPR-induced *CDK12/13* Knockout in Neuroblastoma Cells

A CRISPR knockout of CDK12 and CDK13 was performed in IMR-5-75 cells with the aim of reducing CDK12 or 13 protein to a level close to zero. To this end, the cells were transduced lentivirally with a lentiCRISPRv.2-706 vector containing Cas9, a sgRNA and a GFP reporter (green fluorescent protein). sgRNAs were designed to target *CDK12* (#2b), *CDK13* (#I1) or were a non-targeting control (scr 8.2). The experiments were performed in collaboration with the Friederike Herbst / Hanno Glimm group at the National Center for Tumor Diseases, who kindly provided the necessary viral particles and vectors and had verified the functionality of the sgRNAs in primary colon carcinoma cultures.
Two days after transfection, microscopic survey revealed that the majority of cells had died in the wells transfected with sgRNAs CDK12 and CDK13, while in the scr 8.2 condition cell death was less pronounced. sgRNA CDK12 and CDK13 cells continued to die at day five post transduction despite an additional exchange of culture media (Figure 19). However, a fraction of cells survived and was expanded. The percentage of GFP-positive cells was determined by flow cytometry and ranged between 30-60 %. Positive cells were sorted to obtain a more pure polyclonal culture. Re-analysis of sorted cells confirmed that in all three conditions more than 98 % of the cells were GFP-positive (Appendix, Figure S 10). These cells were used for all experiments described in the following. By then, the polyclonal cultures had recovered from transduction and grew at a proliferation rate reminiscent of the parental cell line.

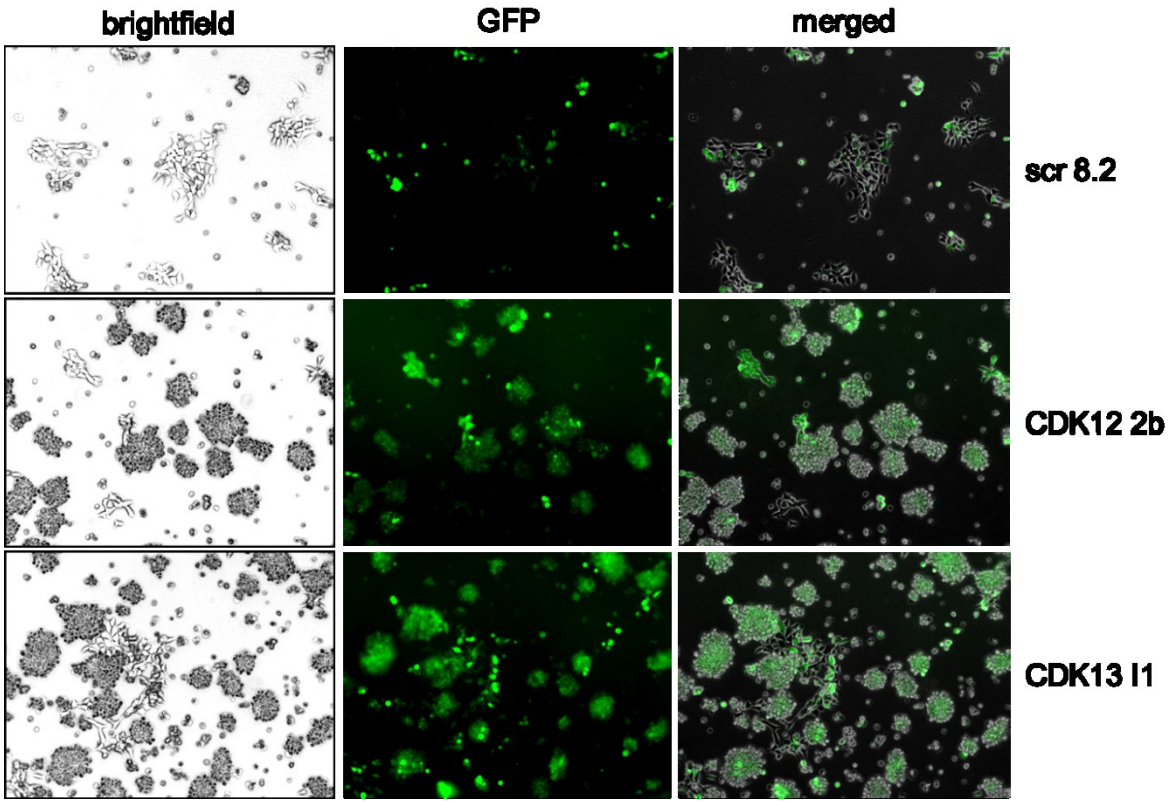

Figure 19: High Amount of Cell Death upon Transduction with CRISPR CDK12 and CDK13 Vectors
IMR-5-75 cells were lentivirally transduced with CRISPR vectors containing Cas9, sgRNAs against CDK12, 13 or scrambled and a GFP construct. Microscopic images were acquired five days post transduction and show aggregates of dead, GFP-positive cells predominantly in the CDK12 and 13 knockout condition. Magnification 10x.

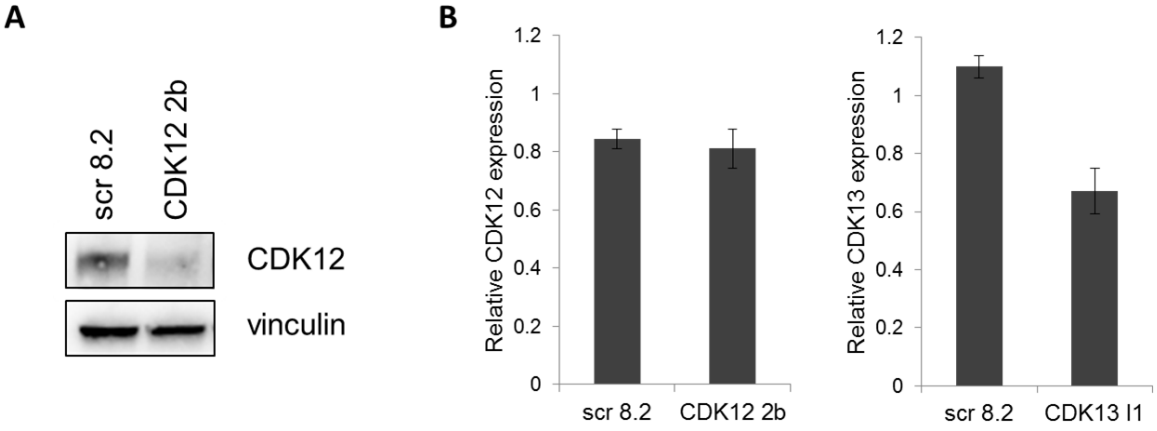

Figure 20: Protein and mRNA Expression Analysis of CRISPR Knockout Cells
IMR-5-75 CRISPR polyclonal cells expressing GFP were enriched by fluorescence-activated cell sorting and expanded in culture. 72 h after seeding, floating and adherent cells were harvested and lysed. **(A)** Immunoblotting; vinculin was used as loading control. **(B)** RT-qPCR.
Representative biological replicates out of n = 3.

The effect of CRISPR on the protein level was examined by immunoblotting, which revealed a reduction of CDK12 by 40 – 60 % (Figure 20A). Due to the lack of a good antibody, immunoblotting of CDK13 was not successful. In addition, mRNA expression of *CDK12* and *CDK13* was determined by RT-qPCR. CDK12 was not reduced on the mRNA level; while *CDK13* was reduced by 35 % on average (Figure 20B).

Next, viability of the CRISPR knockout clones was determined by a CTB assay. It revealed that viability of CDK12 CRISPR clones was not reduced, whereas a trend towards decreased viability was observed in CDK13 CRISPR clones (87 % of scramble control, p = 0.06, Figure 21A).

In addition, the cell cycle distribution was examined by flow cytometry. There were more cells in the G_1 phase in CDK13 CRISPR cells compared to scramble controls, even though the increase was not large (Figure 21B).

In conclusion, CRISPR –mediated gene knockout did not lead to the anticipated extensive loss of target protein and mRNA. Therefore, the impact on viability and cell cycle was limited.

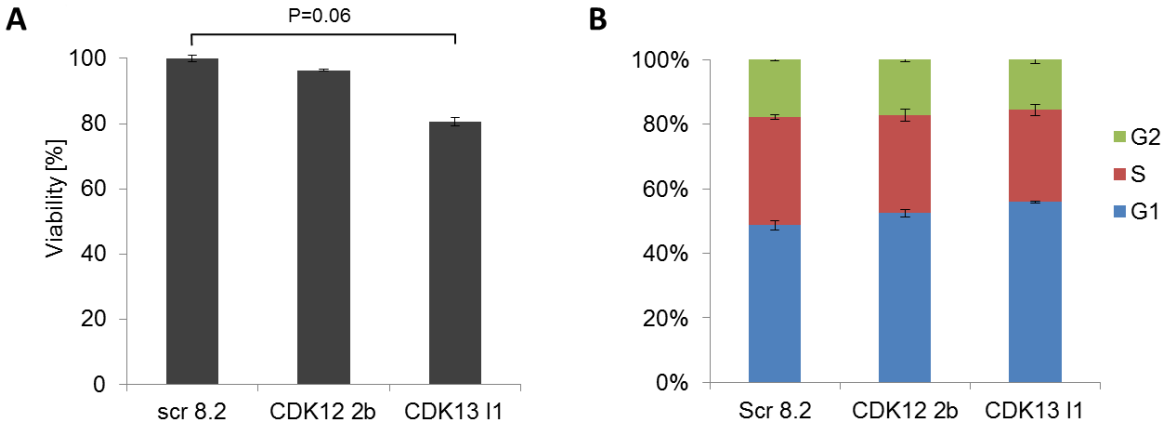

Figure 21: Modest Reductions of Viability and G_1 Arrest in CDK13 CRISPR Knockout Clones
IMR-5-75 CRISPR polyclonal cells expressing GFP were enriched by fluorescence-activated cell sorting and expanded in culture. 72 h after seeding, floating and adherent cells were harvested and lysed. **(A)** Viability was assessed by CTB; shown are technical replicates' mean ± SEM of a representative biological replicate (n = 3). **(B)** Cell cycle analysis; cells were fixed in citric acid buffer, stained with DAPI and analyzed by flow cytometry; mean ± SEM, n = 3.

3.2.6 CDK12/13 Inhibition by Tool Compound BAY-587

Within the scope of our joint project with Bayer AG, our collaboration partner Gerhard Siemeister provided us with a novel tool compound named BAY-587, an ATP competitive inhibitor of CDK12 and CDK13. In a kinase assay, its half-maximal inhibitory concentration (IC50) was 29 nM for CDK12 and 35 nM for CDK13 (Bayer AG, personal communication). At higher concentrations, BAY-587 also inhibits CDK5 / p25 (86 nM), CDK3 (73 nM) and CDK2 / cyclin E (150 nM).

The CTB assay was used to determine metabolic IC50 values for BAY587 and the commercially available, covalent CDK12/13 inhibitor THZ531 in eight different NB cell lines and one colon carcinoma cell line (Figure S 11). IC50 values for BAY-587 ranged from 61 to 174 nM in NB cell lines and 245 nM in colon carcinoma cells HCT-116 (Table 3.1). Sensitivity to BAY-587 did not correlate with sensitivity to THZ531, which was generally less pronounced.

The response to BAY-587 was subject to considerable biological variation between the biological replicates. Phenotypical analysis was therefore also performed with concentrations above and below the calculated IC50 of each cell line.

Table 3.1: Summary of IC50 Values of CDK12/13 Inhibitors BAY-587 and THZ531 in NB Cell Lines and Colon Carcinoma Cell Line HCT116, as Well as Effects on Cell Death and Colony Formation Capacity upon BAY-587 Treatment

	MYC/MYCN status	Additional aberrations	IC50 BAY-587 [nM]	IC50 THZ531 [nM]	BAY-587 induced cell death [%]	BAY-587 induced colony formation inhibition
SK-N-DZ	amp		61	1956	57	very strong
IMR-32	amp		62	110	53	complete
CHP-134	amp		67	1555	62	very strong
IMR-5-75	amp		108	224	73	very strong
SK-N-BE(2)c	amp	TP53 mut, NF1 del	113	3709	32	strong
NB-69	MYC act transl		143	2607	47	complete
TR-14	amp	MDM2, CDK4 amp	170	5931	36	very strong
SH-EP	MYC act transl	ALK mut	174	584	81	complete
HCT116	normal / RAS mut		245	205	47	complete

amp = amplified; act. transl = activating translocation; mut = mutant

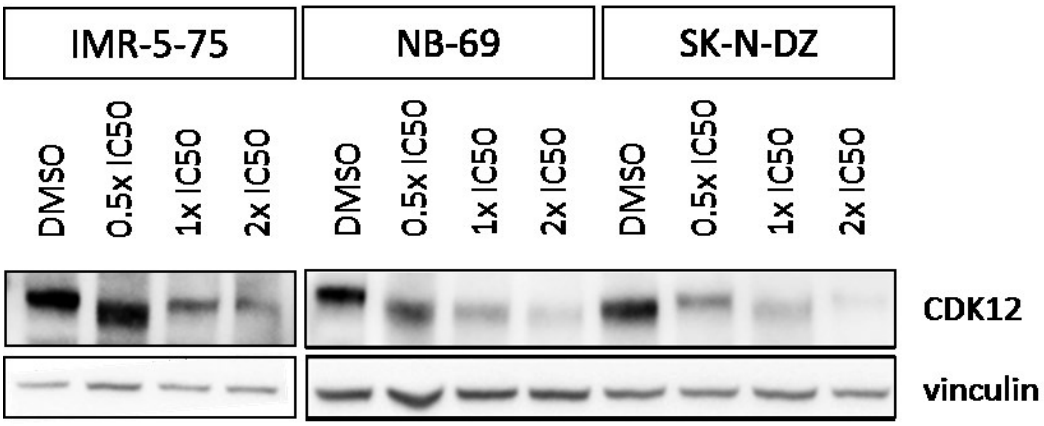

Figure 22: Treatment with CDK12/13 Inhibitor BAY-587 Reduces the Level of CDK12
Cells were treated with multiples of their individual IC50 value or DMSO as a control. After 8 h, cells were harvested and lysed for immunoblotting. ; vinculin was used as loading control. Representative image out of n = 2.

BAY-587 reduced the protein level of CDK12. Immunoblotting of NB-69, SK-N-DZ, SH-EP and IMR-5-75 cells treated with BAY-587 revealed that the CDK12 level was reduced in a dose-dependent manner already 8 h after treatment and remained down until the end of the observation period (96 h, Figure 22). Treatment with a concentration equivalent to the individual IC50 reduced CDK12 level by 70 % in NB-69, by 75 - 85 % in SK-N-DZ and by 90 – 95 % in IMR-5-75. The examination of CDK13 levels was hampered by the lack of a good antibody. A single replicate in IMR-5-75 cells indicated that CDK13 protein might increase inversely to CDK12 decline (data not shown).

Colony formation capacity is dramatically reduced. Single cells were seeded at very low density to test their capacity to form colonies upon treatment with either of the two inhibitors. Colony formation was significantly reduced by BAY-587 treatment at IC50 concentrations in all tested cell lines ($p < 0.05$). In general, BAY-587 had a more profound effect on colony formation capacity than THZ531. In four cell lines, no colonies grew at all after BAY-587 treatment (IMR-32, NB-69, SH-EP, HCT116, Figure 23, left panel). In IMR-5-75, SK-N-DZ, CHP-134, TR-14 and SK-N-BE(2)c, colony formation was also severely compromised (right panel). SK-N-BE(2)c cells were least affected but BAY-587 still led to a 89 % reduction of the area covered with colonies when compared to DMSO controls. Treatment with BAY-587 at a concentration of 25 % below IC50 was still very effective in reducing colony formation capacity to a minimum (data not shown). When treated with THZ531, colonies were significantly reduced by more than 95 % in the three cell lines IMR-5-75, SH-EP and HCT116 ($p < 0.05$). In the other cell lines, the difference between cells treated with THZ531 and controls was not statistically significant; all the same, colonies were reduced by more than 80 % (Figure 23).

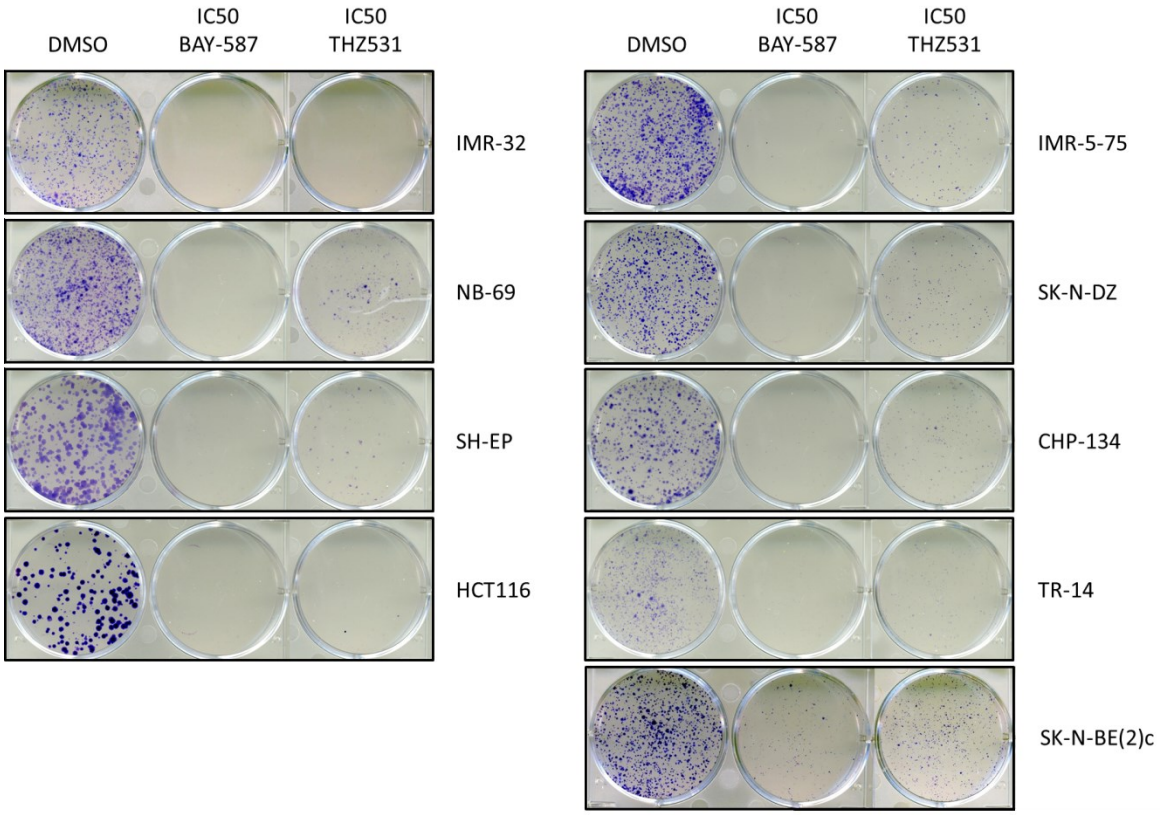

Figure 23: CDK12/13 Inhibition Impacts on Colony Formation Capacity
Colony formation assay; cells were seeded at low density, treated with BAY-587 or THZ531 on the following day and incubated for 7 - 10 days before fixation and Giemsa staining. Representative biological replicates out of n ≥ 3.

Cell cycle distribution is strongly disturbed. Next, changes in the cell cycle were analyzed after 96 h. Upon treatment with IC50 + 25 % of the inhibitors, the fraction of cells in sub-G_1 increased dramatically and the typical cell cycle distribution was frequently lost, making assignment to the phases difficult. At BAY-587 IC50 concentration, the number of cells in G_1 phase decreased in cell lines NB-69, SK-N-DZ, CHP-134, TR-14 and HCT116 (Figure 24). This change was accompanied by modest increases in the other cell cycle phases, for example S phase in NB-69 and CHP-134 cells. Opposed to that, in IMR-32, the amount of cells in G_1 phase was increased, while it was reduced in S and G_2 phase. In IMR-5-75 cells, no changes were apparent. In SH-EP cells, cells from every phase seemed to move towards the sub-G_1 fraction with increasing concentrations. Upon treatment with THZ531, G_1 phase fractions significantly decreased and S-phase fractions increased in IMR-5-75, SHEP, HCT116 and CHP-134 cells (Figure 24).

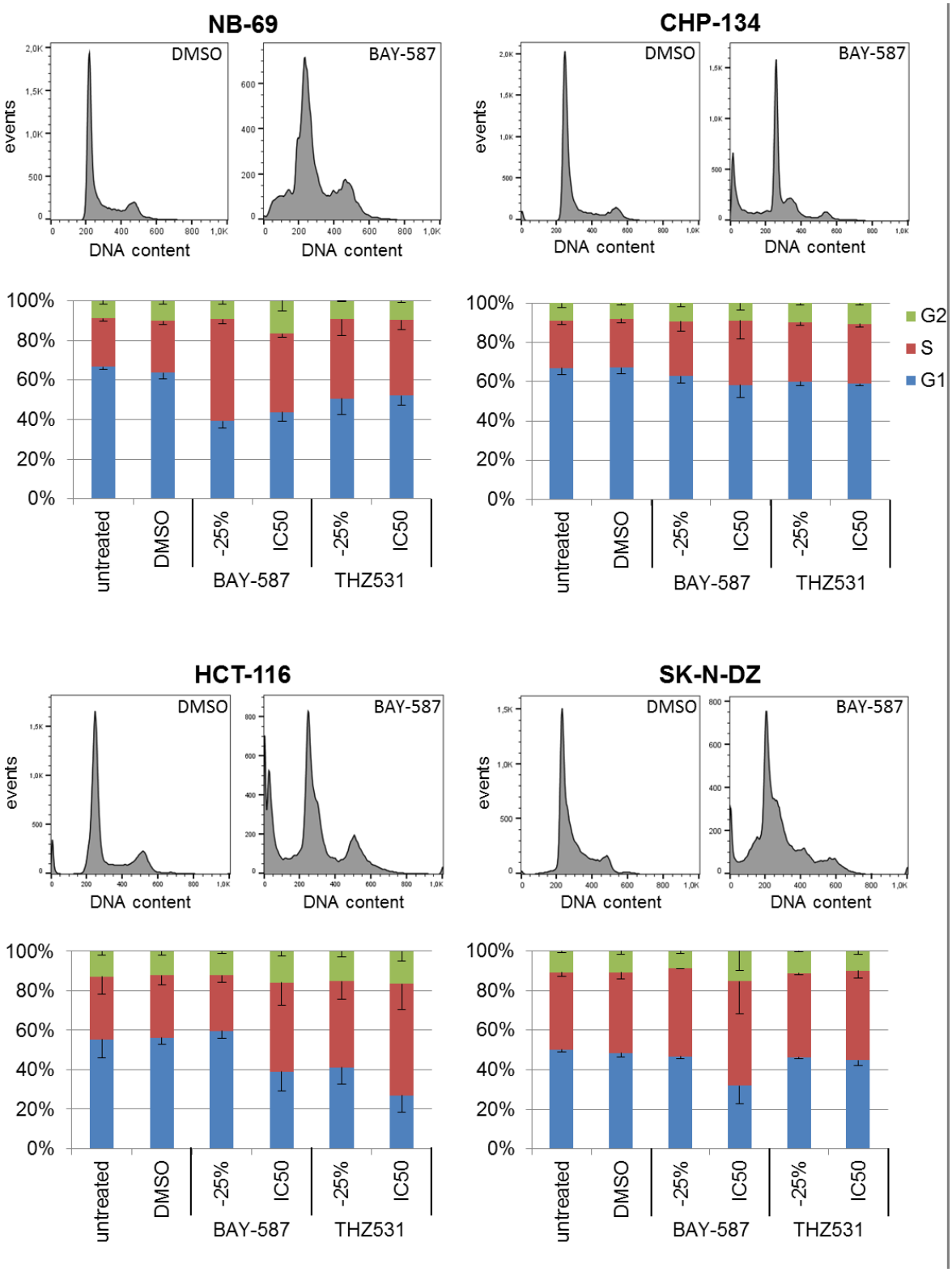

Figure 24: CDK12/13 Inhibition Induces Cell Cycle Distribution Changes
Cells were treated with inhibitors, grown for 96 h and harvested. For cell cycle analysis, cells were fixed in citric acid buffer, stained with DAPI and analyzed by flow cytometry. Shown are representative histograms comparing DMSO controls with cells treated with IC50 of BAY-587 (upper panel) and average cell cycle distribution (lower panel). Sub-G_1 fraction omitted for better comparability; mean - SEM, n ≥ 3.

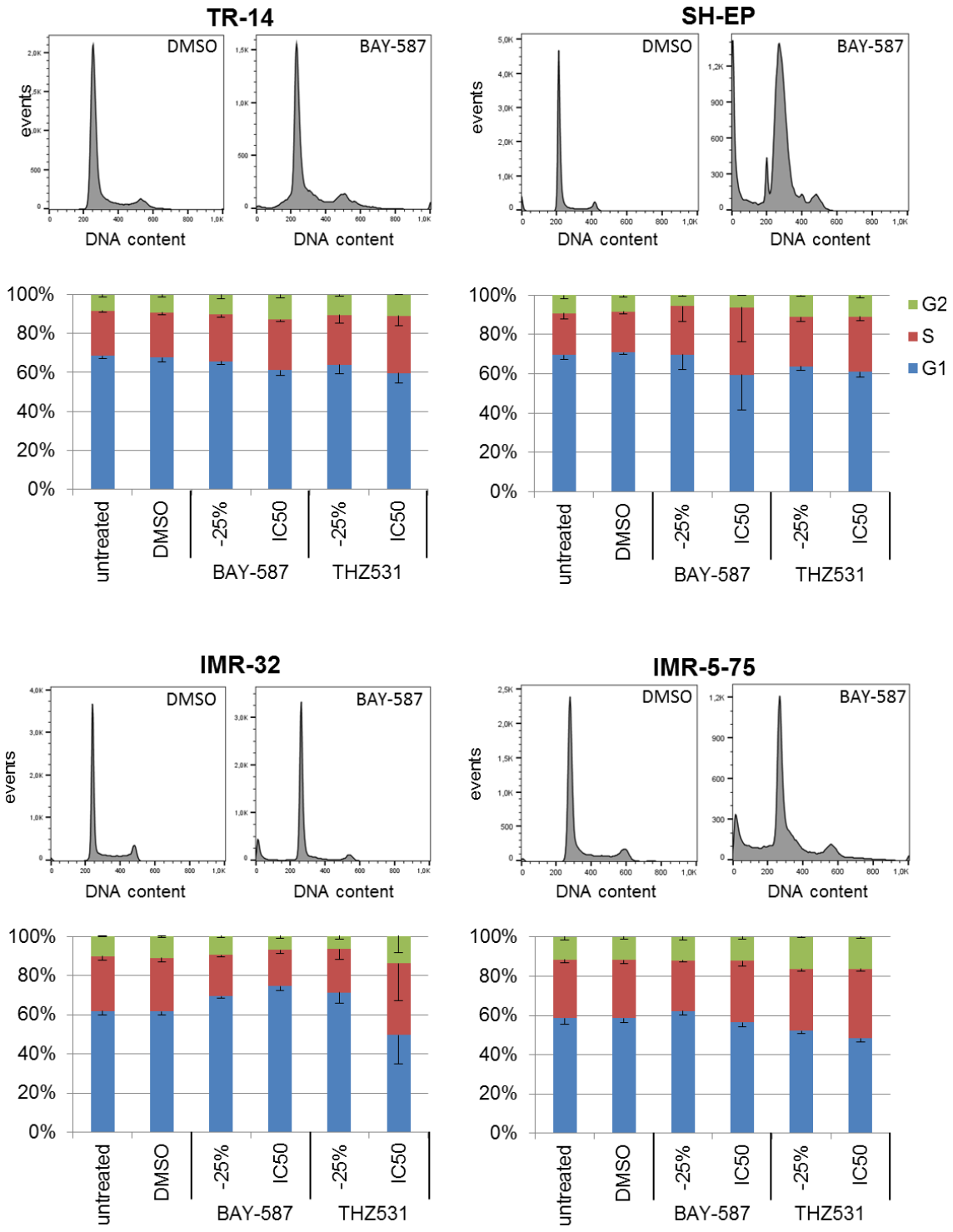

Figure 24, continued.

Strong induction of cell death. The amount of cell death induced by both compounds was examined by performing a live/dead cell exclusion staining after 96 h. At IC50 concentrations, BAY-587 induced cell death between 30 – 80 % without any correlation to the cell lines' sensitivity to the inhibitor (Table 3.1). The amount of induced cell death increased with dose (Figure 25). However, the intensity of PI staining was variable. IMR-5-75, IMR-32 and SK-N-DZ cells stained strongly after inhibitor treatment. Opposed to that, most cells accumulated in an intermediate population with a lower PI signal in SH-EP cells. This population could be separated from live and healthy cells by the forward scatter. Microscopic inspection of the cells did not indicate an increase in floating and thus dead cells. NB-69, TR-14, SK-N-BE(2)c and HCT116 cells had similar PI staining profiles, but in these cases microscopic inspection revealed dead cells floating in the medium. SH-EP cells were treated with BAY-587 and incubated for a prolonged period of seven days. Still, the amount of floating cells did not increase, showing that the onset of cell death was not just delayed in these cells (data not shown).

Four cell lines were selected for further experiments to elucidate the response to BAY-587 treatment. IMR-5-75 and SK-N-DZ represent MNA cell lines with intermediate and sensitive response to BAY-587, respectively. Additionally, NB-69 and SH-EP both harbor a MYC activating translocation and showed an intermediate and weak response to BAY-587, respectively.

To identify the mode of cell death, it was attempted to rescue the selected cell lines from BAY-587-induced cell death. Cells were treated with BAY-587 in combination with inhibitor of ferroptosis Ferrostatin-1, inhibitor of necroptosis Necrostatin-1, inhibitor of apoptosis zVAD or inhibitor of autophagy Bafilomycin A1. For this assay, a new batch of BAY-587 was used and the concentrations were adapted to mitigate its impact and thereby enable potential rescue mechanisms (SK-N-DZ: 47 nM, IMR-5-75: 70 nM, NB-69 and SH-EP: 93 nM). However, no rescue could be achieved with any of the used inhibitors (Figure 26).

Next, an Apo-BrdU TUNEL assay was performed 24 h after treatment for the detection of apoptotic cells with DNA strand breaks. In IMR-5-75 and SH-EP cells, an additional 4.7 and 3.4 % of total cells had DNA strand breaks when compared to DMSO controls (Figure 27B). DNA staining by PI revealed that cells with DNA strand breaks stemmed from all phases of the cell cycle (Figure 27A). In SK-N-DZ cells, an extra 14.7 % of cells had DNA strand breaks with a slight prevalence of cells from the S phase. Most DNA strand breaks occurred in NB-69 cells (additional 20.6 % of total cells).

In addition to the TUNEL assay, an assay detecting active Caspase 3/7 was performed also 24 h after treatment (Figure 27C). Active Caspase3/7 was mostly present in NB-69 and SK-N-DZ cells with fivefold and 3.4-fold induction, respectively. A less than twofold induction was detected in IMR-5-75.

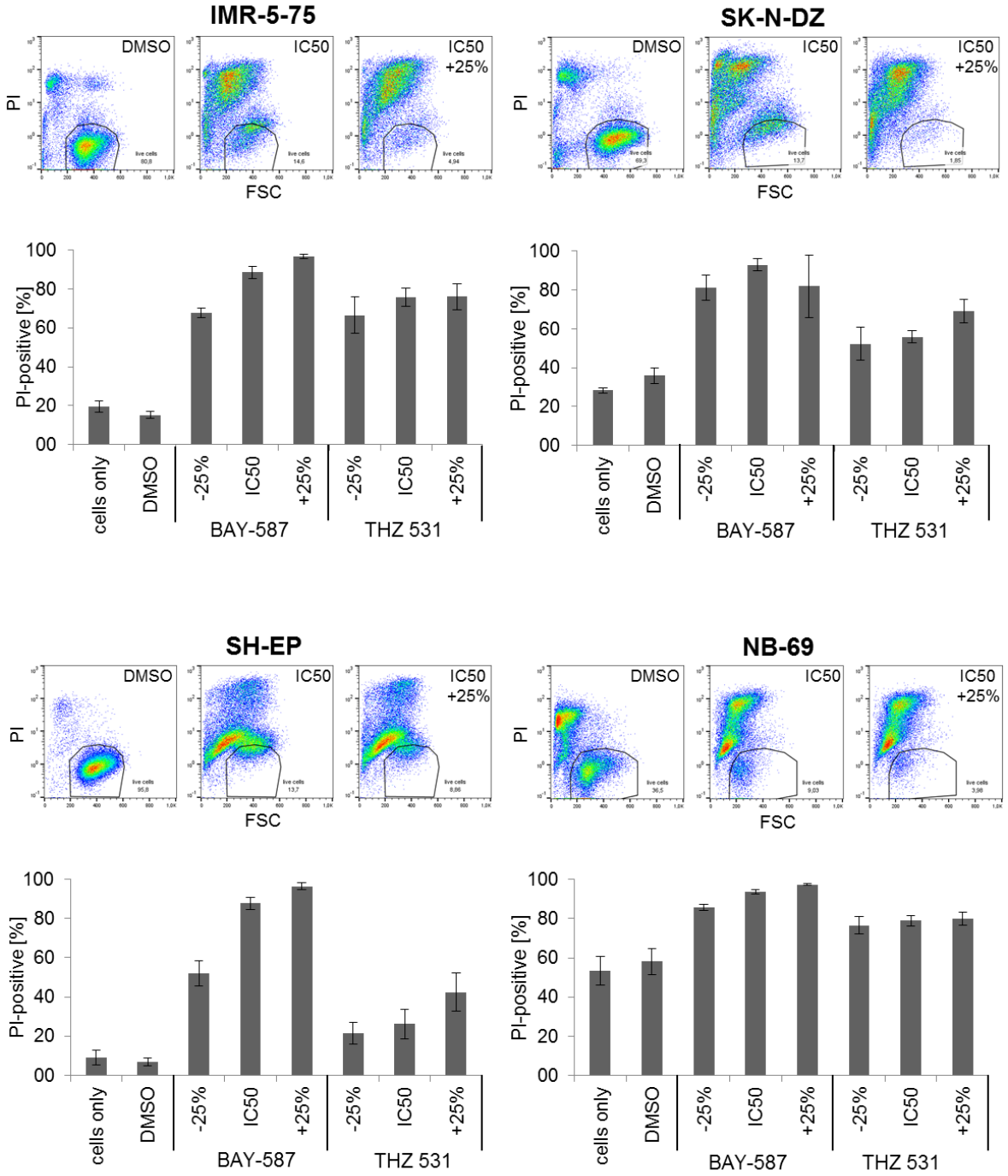

Figure 25: CDK12/13 Inhibition Induces Dose-Dependent Cell Death in All Cell Lines Tested
Cell death; cells were treated with BAY-587, THZ531 or DMSO as a control. After 96 h, cells were harvested, stained with PI and directly analyzed by flow cytometry. Shown are representative dot plots with gates indicating live cells (upper panels) and bar charts with the average proportion of PI-positive cells (lower panels; mean ± SEM, n ≥ 3).

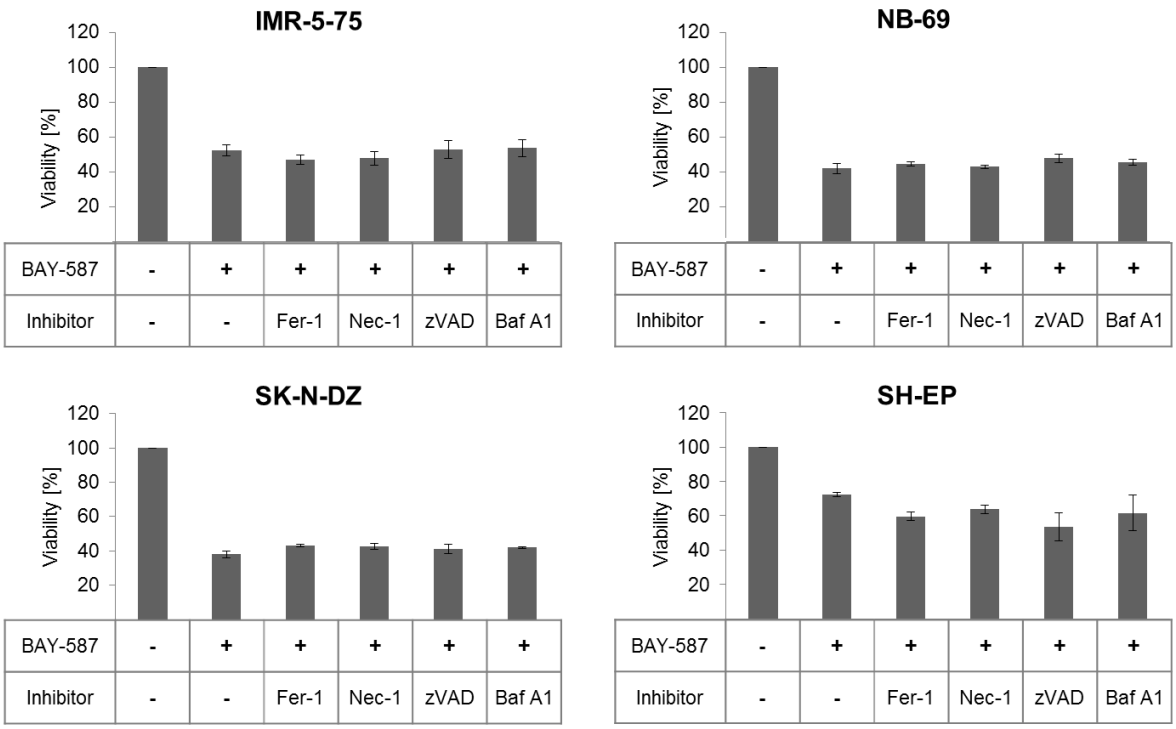

Figure 26: BAY-587-Induced Cell Death Cannot Be Rescued
Cells were treated with BAY-587 and inhibitors of specific cell death types. Viability was assessed by CTB after 96 h. Fer-1 = Ferrostatin-1 (ferroptosis); Nec-1 = Necrostatin-1 (necroptosis); zVAD = zVAD(OMe)-FMK (apoptosis); Baf A1 = Bafilomycin A1 (autophagy). mean ± SEM, n = 3

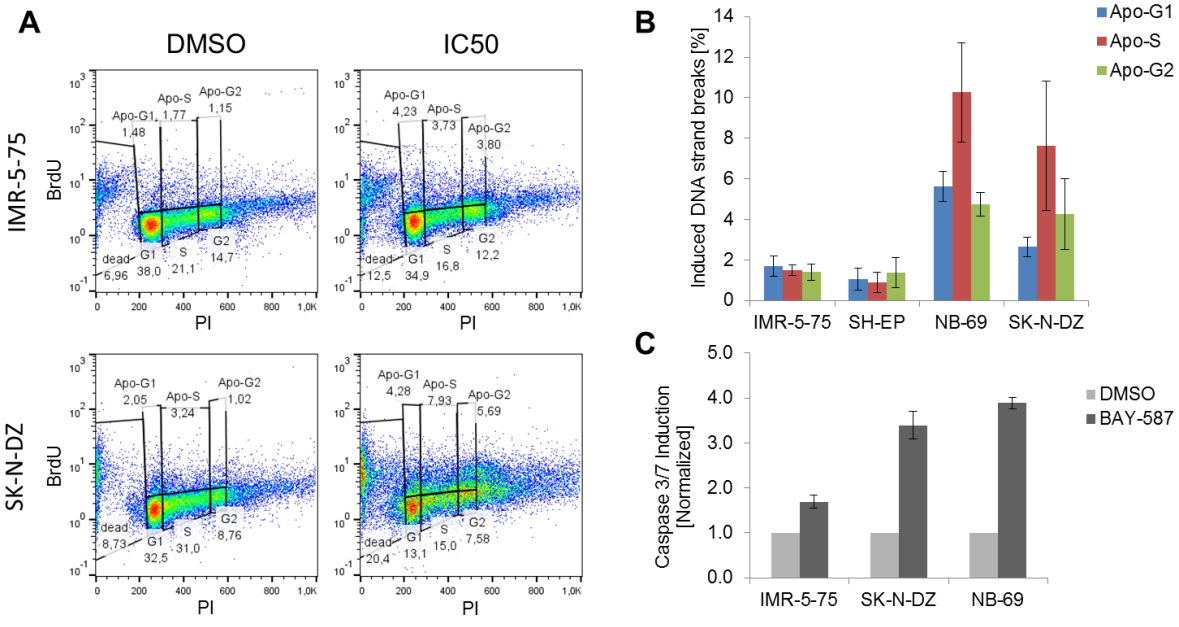

Figure 27: Cells from All Phases of the Cell Cycle Enter Apoptosis upon BAY-587 Treatment.
Cells were treated with BAY-587 for 24 h. **(A, B)** TUNEL assay; cells were harvested, stained with Apo-BrdU and PI and analyzed by flow cytometry. **(A)** Representative replicates illustrating gating strategy. **(B)** Induced DNA strand breaks per cell cycle phase (percentage of BrdU-positive cells in DMSO controls was subtracted from that of treated cells); mean ± SEM, n = 4. **(C)** Caspase-Glo 3/7 assay; luminescence was measured with a Tecan Spark reader; mean ± SEM, n = 3.

RNA expression analysis. Since both CDK13 and CDK12 are transcriptional CDKs, their inhibition likely influences gene expression. Therefore RNA expression was examined in IMR-5-75, SK-N-DZ, NB-69 and SH-EP cells after BAY-587 treatment. First, the time window after treatment was determined when no morphological changes indicating cell death had occurred yet (eight hours). Three different concentrations of the inhibitor were used: 0.5 x IC50, 1 x IC50 and 2 x IC50 of BAY-587. Genes with a fold change of larger than two were regarded as differentially expressed (normalization and bioinformatic analysis: Umut Toprak).

The number of significantly DEGs correlated with the concentration of the inhibitor in all cell lines. For example, at 0.5 x IC50, there were 1401 DEGs in SK-N-DZ cells (Figure 28A, sum of down- and upregulated genes). Of these, approximately 90 % were also differentially regulated at higher concentrations. At IC50, there were already 3108 DEGs and at 2 x IC50, there were 4442 DEGs. Approximately two to three times more genes were down- than upregulated in all four cell lines. However, there were large differences between the cell lines regarding the number of DEGs. In SH-EP cells, almost no genes were differentially regulated at 0.5 x IC50. The number was slightly higher in IMR-5-75. Differential gene expression was highest in SK-N-DZ and NB-69 cells.

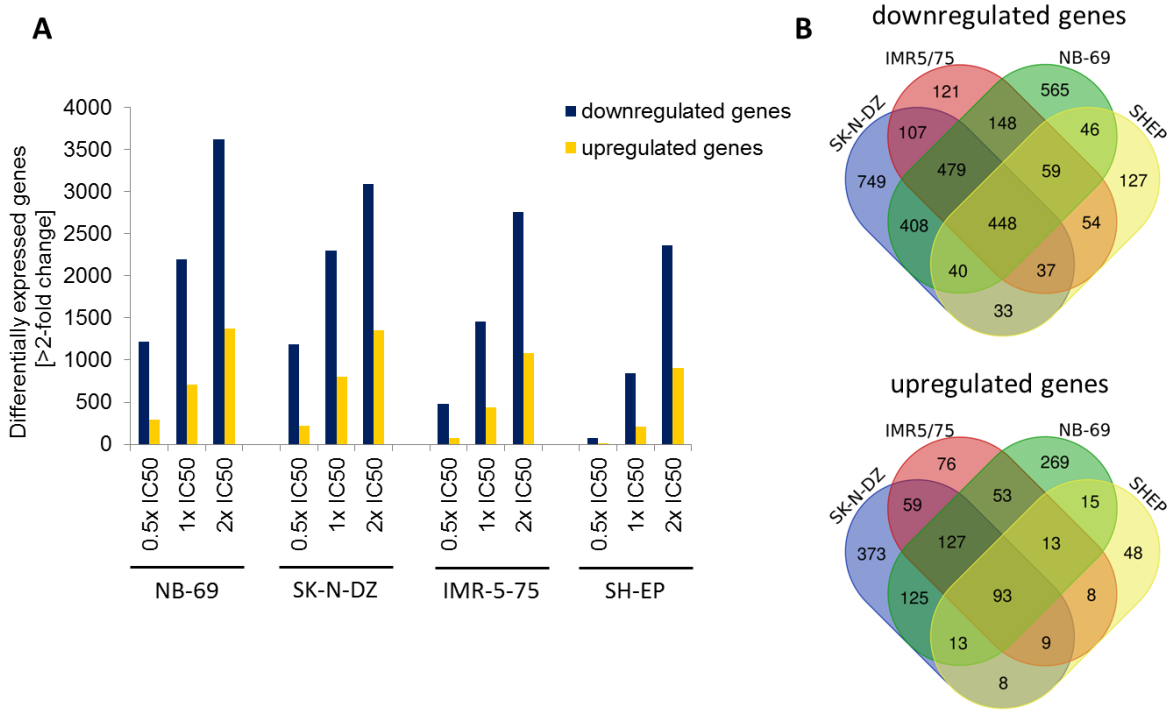

Figure 28: The Extent of Gene Expression Regulation by BAY-587 Treatment Varies between Cell Lines

RNA expression analysis; cells were treated with BAY-587 and harvested after 8 h for RNA extraction and subsequent library preparation. **(A)** Number of differentially regulated genes in dependence on cell line and inhibitor concentration. **(B)** Overlap of DEGs between cell lines at 1 x IC50 of BAY-587.

There was considerable overlap of the genes which were differentially expressed in the four cell lines. For example, there were 448 commonly downregulated genes in the 1 x IC50 condition, corresponding to approximately 20 % of downregulated genes in NB-69 and SK-N-DZ and more than 50 % in SH-EP (Figure 28B). In addition, another 615 downregulated genes were shared in three of the four cell lines. 93 genes were commonly upregulated, making up 10 – 45 % of all DEGs in the different cell lines. A total of 162 upregulated genes were shared between three of four cell lines. When comparing SK-N-DZ and NB-69, the two cell lines with the strongest differential expression, the overlap amounted to roughly 35 % and 50 % of downregulated and upregulated genes, respectively.

The DAVID functional annotation tool 6.8 was employed to search for gene enrichments (Huang da *et al.*, 2009a, 2009b). Regardless of fold-change, the top 500 down- or upregulated genes with significant p-value < 0.05 were included to attain enough genes for this analysis. Only gene ontology (GO) term_direct categories were selected in the interest of clarity. Genes downregulated at concentrations of 0.5 x and 1 x IC50 in SK-N-DZ were significantly enriched in processes related to the cilium and its assembly (Figure 29). Genes downregulated at 1 x and 2 x IC50 concentrations were enriched in the DNA repair mechanisms homologous recombination and nucleotide-excision. Genes with elevated expression at all tested concentrations of the inhibitor were related to the cellular component nucleus. In addition, at IC50, several categories related to transcription were among the results.

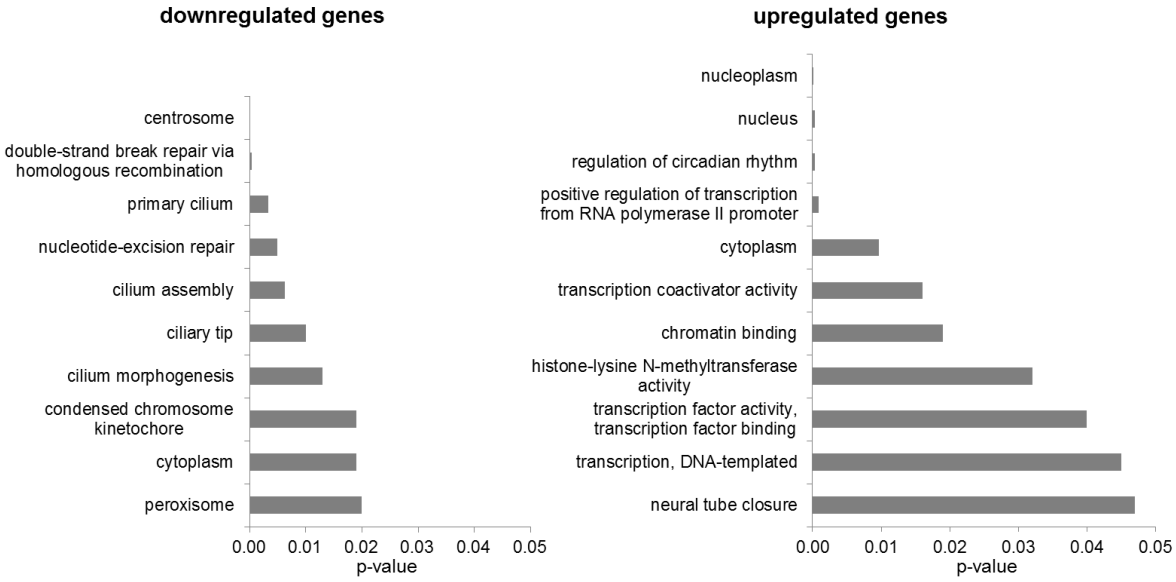

Figure 29: CDK12/13 Inhibition Leads to Downregulation of DNA Repair Genes and Upregulation of DNA Transcription Genes
Functional annotation analysis of top 500 DEGs in SK-N-DZ after BAY-587 treatment at IC50 using DAVID; p-values are Benjamini-Hochberg adjusted.

Table 3.2: Intersection of Functional Annotation Terms Enriched in Genes Downregulated upon BAY-587 Treatment

Cell lines	Functional Annotations
all cell lines	alternative splicing
SK-N-DZ, IMR-5-75, SH-EP	DNA repair, DNA damage
IMR-5-75, SK-N-DZ, NB-69	splice variant

Table 3.3: Intersection of Functional Annotation Terms Enriched in Genes Upregulated upon BAY-587 Treatment

Cell lines	Functional Annotations
all cell lines	nucleoplasm, nucleus, isopeptide bond, activator, repressor, transcription, cytoplasm, Ubl conjugation, biological rhythms, compositionally biased region:Ser-rich, transcription regulation, phosphoprotein
SK-N-DZ, IMR-5-75, SH-EP	coiled coil, compositionally biased region:Gln-rich, compositionally biased region:Poly-Ser, splice variant, transferase, chromatin regulator, alternative splicing, methylation, SH3 domain, compositionally biased region:Pro-rich, chromosomal rearrangement
IMR-5-75, SH-EP, NB-69	protein binding

Many of the above-mentioned categories were also present in the gene enrichment sets of IMR-5-75, NB-69 and SH-EP. In order to determine the intersection of categories between the cell lines, enrichment analyses with all DAVID default annotation categories were performed for DEGs at IC50. Alternative splicing was the only common functional annotation of downregulated gene sets of all cell lines (Table 3.2). Furthermore, DNA repair and DNA damage were common annotations of downregulated genes in SK-N-DZ, IMR-5-75 and SH-EP cells. There were 12 annotations common to upregulated genes of all cell lines, including nucleus, transcription regulation, phosphoproteins and biological rhythms (Table 3.3). SK-N-DZ, IMR-5-75 and SH-EP cells additionally shared annotations related to alternative splicing and chromatin modifications.

In summary, the effects of BAY-587 induced inhibition of CDK12 and CDK13 in NB cell lines included induction of cell death, abolishment of colony formation and profound gene expression changes. The compound was more effective than the commercially available THZ531.

4.1 The Transcriptional Network of MYCN in Neuroblastoma Cell Lines

Elucidating the transcriptional impact of high MYCN levels in NB cells in a cell cycle-resolved analysis was the central task of the first part of this thesis. A better understanding of direct and secondary transcriptional effects of MYCN can help to devise desperately needed new therapeutic approaches for patients with high-risk tumors with *MYCN* amplification. It can also advise on the timing of drug administration particularly in combination therapies (Ryl *et al.*, 2017).

4.1.1 MYCN Regulates Transcription of General and Cell Cycle Phase-Specific Drivers of Malignant Phenotype

In order to compare gene regulation in MYCN high versus low cells in a cell cycle-resolved fashion, the cells were synchronized at the G_1:S transition. Gene expression was analyzed every two hours, while the cells went largely synchronously through S, G_2, M and $G_{0/1}$ phase. At this point, MYCN high cells progressed into S phase, whereas MYCN low cells remained in G_1 phase. Overall, equal numbers of genes were up- and downregulated in MYCN high cells. This finding is in contrast to previous reports claiming that MYC acts as a transcriptional amplifier by binding promoters of already actively transcribed genes (Lin *et al.*, 2012; Nie *et al.*, 2012). While this discrepancy might be explained by differences between c-MYC and MYCN function and different entities surveyed (lymphocytes, embryonic stem cells), there are also conflicting studies in the field of NB. Zeid and colleagues found that transcription is globally downregulated upon loss of MYCN (2018). However, mechanistic studies have uncovered multiple ways of MYCN-mediated transcriptional repression (Gherardi *et al.*, 2013). Hence, balanced up- and downregulation of gene expression is likely the consequence of a number of distinct mechanisms.

In this respect, the time course experiment revealed gene sets that were constantly up- and downregulated and can therefore be considered as primary targets of MYCN. Gene enrichment analysis of the constantly upregulated gene set identified the processes G_1/S transition and DNA replication. It seems that high MYCN constitutively induces expression of cell cycle drivers like *CDK4* or *PKMYT1*. In addition, MYCN constitutively downregulates certain inhibitors of the cell cycle, such as *CDKN1A*. Regulation of these direct MYCN targets entails the fast proliferation characteristic of MYCN high cells.

Other cyclins and CDKs were expressed differentially only towards the end of the observation period, when MYCN high and low cells diverged in their behavior (e.g. *CCNE1, CCNA2, CCNB*). It is conceivable that these differences arise from MYCN-induced faster progression through the cell cycle.

Next to cell cycle genes, the upregulated gene set was enriched in the interconnected keywords nucleolus, rRNA processing and snoRNAs. Ribosomes translate mRNA into proteins and consist of rRNA and ribosomal proteins. Processing of rRNA predominantly takes place in the nucleolus and involves chemical modifications that are guided by snoRNAs (Pelletier *et al.*, 2018). Increased ribosome biogenesis allowing more protein synthesis is essential for the accelerated proliferation of malignant cells. In particular, it has been linked to MYC-driven cancers (Barna *et al.*, 2008; Wahlstrom and Henriksson, 2015). Also snoRNA expression is often increased in cancer tissue (Gong *et al.*, 2017). Schramm and colleagues reported that snoRNA levels were upregulated by MYCN (Schramm *et al.*, 2013). Contrary to these findings, only five snoRNAs were constantly upregulated in the present study. Interestingly, the transcript level of 36 further snoRNAs rose dramatically in MYCN low cells at the time when they remained stalled in $G_{0/1}$ phase, indicating that they must have an important function. Possibly, the cells try to overcome the arrest by fueling protein synthesis. Next to taking part in the processing of rRNA for the genesis of ribosomes, a number of non-canonical functions for snoRNAs have been established recently. These include regulation of splicing and chromatin structure as well as serving as precursors of miRNAs (Dupuis-Sandoval *et al.*, 2015). Thus, it remains to be clarified what the role and consequences of snoRNA upregulation in MYCN low cells are.

Among the keywords identified in the constantly downregulated cluster was cell adhesion, which is again concordant with a more aggressive phenotype capable of metastasizing (Seyfried and Huysentruyt, 2013). Genes enriched in this cluster were also associated with alternative splicing and the synapse.

Summed up, MYCN induced and repressed a similar number of genes in this cellular model. This included constitutively regulated genes, many of which are essential for the maintenance of a pro-proliferative phenotype with high biosynthetic activity. In addition, many cell cycle genes were differentially regulated in specific cell cycle phases as a consequence of accelerated cell cycle progression.

4.1.2 MYCN-dependent miRNA Expression Changes Reveal an Additional Layer of Gene Regulation

Understanding of the transcriptional impact of MYCN in NB is not complete without considering the regulation of miRNAs. Consequentially, the expression of miRNAs was analyzed in our MYCN-regulatable cell cycle model. Of all miRNAs detected, 156 or

roughly 27 % were differentially expressed in MYCN high versus low cells. This number is slightly higher than in a study comparing MNA tumors with non-amplified ones (20 %) (Megiorni *et al.*, 2017). Approximately the same number of miRNAs was up- and downregulated in MYCN high cells. The direction of MYCN-induced expression changes has previously been debated between different studies. Schulte and colleagues found only upregulated miRNAs by comparing expression in primary MNA tumors with an *in vitro* model of ectopic *MYCN* overexpression (2008). Opposed to that, Chen and Stallings reported up- and downregulated miRNAs in MNA tumors and cell lines treated with retinoic acid to induce differentiation and downregulation of MYCN (2007). The two studies agreed on the upregulation of four miRNAs by MYCN, let-7b, miR-92, miR-181a, miR-181b. The comparison of such previously reported MYCN targets in NB with results of this study revealed a good degree of overlap. However, four miRNAs did not coincide with the reported direction of regulation.

Among the results were many miRNAs regulating genes belonging to processes identified in the mRNA expression analysis. For instance, the list included 29 miRNAs known to regulate the cell cycle and more than half of the miRNAs were ascribed to be involved in ribosome biogenesis, even though this process did not appear in the functional annotation enrichment analysis. Instead, cluster-wise KEGG analysis showed that the pathways and processes identified for the five clusters strongly resembled each other. Recurrent keywords were different cancer types as well as signaling pathways which are defective in cancer. This suggests that there is a general motif of MYCN-dependent miRNA regulation, which is active throughout all cell cycle phases and serves to drive NB malignancy for example by accelerated cell cycle progression, aberrant signaling pathways and increased biosynthesis of proteins and mRNA. Another recurrent theme was synaptic signaling, which had also been identified in the constantly downregulated genes cluster. This implies that expression of corresponding genes may be repressed by miRNAs.

The notion that miRNAs heavily contribute to the oncogenic effects exerted by MYCN was supported by studying particularly highly expressed miRNAs. Among these were two miRNAs from the miR-17-92 cluster, which were consistently high during the cell cycle in MYCN high cells (miR-20a-5p and miR-17-5p). miRNAs from these clusters have been attributed an oncogenic role in various hematopoietic and solid cancers like leukemia, colon, pancreatic and breast cancer (Mogilyansky and Rigoutsos, 2013). Overexpression of miRNAs from the miR-17-92 cluster was also detected in NB cells overexpressing *MYCN* and tumors with *MYCN* amplification (Schulte *et al.*, 2008). What is more, inhibition of this cluster in MNA neuroblastomas increases the expression of CDK2 inhibitor *p21* and causes cell cycle arrest and apoptosis (Fontana *et al.*, 2008). However, the regulatory impact of these miRNAs is extremely complex. A target gene study demonstrated that

miR-20a and miR-17 inhibit a whole range of both pro-proliferative and anti-proliferative genes, such as *CCND, E2F1, CDKN1A* or *PTEN*, which in summary mediates a pro-proliferative phenotype (Trompeter *et al.*, 2011). Further, in the present study miR-21-5p expression was increased in MYCN high cells starting from G_1 phase. This miRNA has been found to drive bladder, lung and gastric cancer and Hodgkin lymphoma (Gu *et al.*, 2018; Z. Liu *et al.*, 2018; Xu *et al.*, 2014; Yuan *et al.*, 2018). Little is known about the role of miR-21-5p in NB except for a report that inhibition induces apoptosis in NB cell line SK-N-SH (Wang *et al.*, 2017).

Inconsistently, miR-101-3p was also upregulated in MYCN high cells, despite having a tumor suppressive role in endometrial, lung, pancreatic and other cancers and being associated with better survival prognosis (Hu *et al.*, 2017; S. Zhang *et al.*, 2017). Similarly, miR-101-3p was shown to inhibit proliferation and colony formation capacity in a MNA neuroblastoma cell line. Despite these discrepancies, it is quite possible that effects may differ between tumor types or cell lines of the same entity. The role of miR-26a-5p, for example, is still under debate and seems to vary between tumor entities. It is frequently downregulated in hepatocellular carcinoma and prostate cancer tissue and adopts tumor suppressive functions in breast, bladder and gastric cancer (Guo *et al.*, 2016; L. Liang *et al.*, 2017). Opposed to that, it promotes tumor growth in lung cancer and ovarian cancer (B. Liu *et al.*, 2012; Shen *et al.*, 2014). In the present study, miR-26a-5p was downregulated in MYCN high cells, arguing for a rather inhibitory role in MNA neuroblastoma cells. This is in line with a study that found low expression of miR-26a-5p to be correlated with poor outcome and MYCN expression in a mouse model as well as in the same cell model used in this study (Beckers *et al.*, 2015). Finally, in this study miR-30d-5p was also expressed less in the MYCN high condition. In the literature, it is described as a tumor suppressive miRNA by some studies, for example in colon, lung and prostate cancer (Song *et al.*, 2018; Y. Wu *et al.*, 2017; R. Zhang *et al.*, 2017). There is no data available yet regarding the role of miR-30d in neuroblastoma. The expression pattern in the present study suggests that it might be inhibited in more aggressive MNA tumors.

In summary, in this study a number of potentially oncogenic miRNAs were increased in MYCN high cells, while potentially tumor-suppressive miRNAs were decreased. Therefore, it can be concluded that in neuroblastoma, MYCN uses miRNAs as an additional layer of gene regulation promoting hallmarks of malignancy like proliferation, metabolism and metastasis. Each miRNA usually has several target genes, and inversely each gene has multiple binding sites for different miRNAs. This leads to a very complex, delicate system of redundancies, additive effects and feedback loops responsible for the fine-tuning of processes like cell cycle progression (Trompeter *et al.*, 2011).

Also, the study provides first evidence for the activity and effect of miR-30d-5p in neuroblastoma. However, in order to gain an understanding of the role of specific miRNAs, more experiments would need to be conducted, for example phenotypical analysis of knockdowns, bioinformatic target predictions and expression analysis in primary tumors.

4.2 CDK13, a Novel Target in *MYCN*-amplified Neuroblastoma

4.2.1 MYCN Synthetic Lethal Screens Identify CDK13 as One of the Top Candidates

The aim of the second part of this study was to identify and characterize a novel potential target for the treatment of high-risk neuroblastomas. To this end, synthetic lethal relationships in MYCN-driven tumors were sought. Synthetic lethal genes constitute promising new therapeutic targets, since their inhibition would selectively affect MYCN-driven cancer cells, but not healthy tissue (Cermelli *et al.*, 2014). At the same time, understanding of a synthetic lethal relationship may help to elucidate processes and pathways that are essential for malignant behavior. Several other groups have performed synthetic lethal screens with aberrant *MYCN* or *c-MYC* expression in the past. However, work published on this subject so far mostly employed *MYCN*-normal cells with ectopic overexpression of the protein or compared several cell lines with different genetic background (Chayka *et al.*, 2015; Toyoshima *et al.*, 2012). In this respect, the present approach to screen an isogenic cell line with pre-existing MYCN dependency more closely reflects the actual tumor situation. Not surprisingly, it emerged that CDKs and cyclins were particularly strongly represented among the synthetic lethal candidates identified in the screen.

Work in our own group and by others has established the essential role of CDKs in NB biology. MNA cells depend on high levels of CDK4 to evade drug-induced DNA damage due to a weakened G_1 checkpoint (Gogolin *et al.*, 2013). A dual inhibitor of CDK4 and CDK6 was shown to induce cell cycle arrest and senescence preferentially in MNA neuroblastoma cell lines (Rader *et al.*, 2013). Also treatment with CDK2, CDK7/9 or pan-CDK inhibitors is able to impede NB cell growth (Chipumuro *et al.*, 2014; Dolman *et al.*, 2015; Loschmann *et al.*, 2013).

Toyoshima and colleagues performed a synthetic lethal screen with human foreskin fibroblasts ectopically overexpressing *c-MYC*. They reported hits related to the transcriptional machinery, DNA repair and mitotic control, among others (Toyoshima *et al.*,

2012). In particular, *CDK2* and *CCNK* were among the synthetic lethal genes. The relevance of *CDK2* as a synthetic lethal candidate in NB has also been demonstrated in a study of Molenaar and colleagues. They reported induction of apoptosis after *CDK2* knockdown by different RNA interference techniques exclusively in cell lines with *MYCN*-amplification (Molenaar *et al.*, 2009).

Chayka and colleagues implemented an shRNA drop out screen in NB cells that ectopically overexpress *MYCN* (2015). They infected their cells with pools of shRNAs and determined which genes had been depleted after the incubation time of two weeks due to synthetic lethality in high MYCN. This approach identified genes involved in the cell cycle and proliferation, but also in cell death, cellular movement and DNA replication. One of the final candidates was PKMYT1*,* which is responsible for the inactivation of CDK1 and thus progression of the cell cycle.

Another siRNA screen comparing MNA and *MYCN*-single copy cells identified the transcriptional kinase CDK9 as a potential candidate (Cermelli *et al.*, 2014).

Taken together, there exists ample evidence to support our interest in CDKs and cyclins as candidates for a synthetic lethal relationship with MYCN. At the same time, the above-mentioned kinases have already been thoroughly studied by us and others. Therefore, this thesis focuses on a less well-known family member, CDK13. Its relevance is confirmed by the fact that its partner cyclin K was among the top candidates in the second synthetic lethal screen performed in SY5Y cells with ectopic *MYCN* overexpression.

4.2.2 Evaluation of CDK12/13 as Potential Therapeutic Candidates

The evaluation of CDK13 in additional neuroblastoma cell lines revealed that while half of the tested cell lines responded strongly to the knockdown, there were also several intermediate responders, such as IMR-32 and IMR-5-75. However, this does not necessarily have to be a disadvantage. For the validation, siRNA-dependent knockdown was used, which never achieves complete gene inhibition and is applied only transitory. As a consequence, “weak” candidates may be underestimated (Cermelli *et al.*, 2014). A complete inhibition or gene knockout for a prolonged time may lead to more detrimental effects in the cells studied. In addition, inhibition of very strong candidates might induce toxicity also in non-transformed cells.

CDK12 knockdown was effective to some degree in three of nine tested NB cell lines. There was no unifying characteristic in the genetic background of these cell lines. In summary, presence of CDK13 protein is vital in most, if not all NB cell lines, whereas CDK12 seems to be dispensable in many of the tested cell lines. Also the additionally tested lung cancer cells with *c-MYC* amplification and colon cancer cells with *c-MYC* overexpression responded to knockdown of *CDK13*. Findings of the present study

performed in our MNA neuroblastoma cells may therefore be transferrable to other entities, thereby considerably increasing its applicability.

A temporal pattern of transcript abundance characterized the expression of *CDK12* and *CDK13* in synchronized MNA IMR-5-75 cells. *CDK12* mRNA levels were highest before mitosis, which is well in line with its reported function. Greifenberg et al. found that CDK12 positively regulates genes involved in DNA metabolic processes, DNA replication and DNA repair (2016). All of these processes are necessary for the cell to prepare for mitosis. CDK13, on the other hand, is highly expressed when CDK12 levels go down, suggesting that they might have overlapping functions.

Data from primary neuroblastoma showed that protein levels of CDK13 together with CDK12 and cyclin K are decreased in MNA tumors. This is in contrast to many of the cell cycle CDKs and cyclins, which are elevated in these tumors (Ryl *et al.*, 2017). It is conceivable that MYCN upregulates drivers of the cell cycle to ensure rapid proliferation while neglecting transcriptional CDKs. Consequently, any further reduction of the latter might be difficult to tolerate.

4.2.3 Characterization of CDK13 Dependency in MYCN-regulatable Neuroblastoma Cells

We used *MYCN*-regulatable cell models to confirm the synthetic lethal relationship between CDK13 and high MYCN levels. However, upon siRNA-mediated *CDK13* knockdown, a differential induction of cell death was only observed in SH-EP cells with inducible *MYCN* overexpression, but not in IMR cells with inducible *MYCN* knockdown. Analysis of the effects of *CDK13* knockdown on cell cycle distribution was complicated by the changes already induced by differential *MYCN* expression. In the MYCN high condition, there are more cells in S and G_2 phase, concordant with their faster proliferation rates (Gogolin *et al.*, 2013). This said, observations diverged between the two models. While *CDK13* knockdown led to an increase in G_1 phase in IMR cells, an S phase arrest was observed in SH-EP cells. In addition, *CDK12* knockdown induced a G_1 arrest in the SH-EP and, less pronounced, in the IMR-32 model.

The described differences in response to *CDK12* and *CDK13* knockdown can be attributed to the fact that the three cell lines have a different genetic background. IMR-5-75 and IMR-32 are accustomed and dependent on aberrant *MYCN* expression. In addition, shRNA-mediated knockdown is not capable of completely eliminate MYCN. Opposed to this, *MYCN* overexpression is new to SH-EP cells, which have to cope with the concomitant changes in transcription and proliferation, only to name a few.

4.2.4 Conditional *CDK12/13* Knockdown in Neuroblastoma Cells

As a next step in the characterization of MNA neuroblastoma vulnerability to *CDK12/13* knockdown, IMR-5-75 clones with shRNAs against *CDK12* and *CDK13* were generated. In comparison to the siRNA technique, shRNAs produce less off-target effects and offer the possibility to select single clones instead of analyzing the bulk population, which includes an unknown proportion of non-transfected cells (Rao *et al.*, 2009).

The selection of suitable single clones with strong knockdown on the protein level was complicated by the lack of good antibodies against CDK12 and CDK13. In the course of this study, antibodies by four different companies were tested. All had high unspecific background staining and weak specific staining. Therefore, accurate protein quantification was very challenging. The protein knockdown was most consistent in CDK13 sh1 and CDK12 sh3 clones. CDK13 sh1 was also the cell clone where knockdown reduced viability most strongly. In line with this, IMR-5-75 cells had also responded most strongly to CDK13 siRNA1, from which the shRNA sequence was adopted. In contrast, knockdown by CDK13sh3 predominantly induced loss of colony formation capacity. Even though knockdown of CDK12 by shRNA3 did not impact on viability, it almost completely abolished colony formation. The lack of a more prominent phenotype upon loss of CDK13 may in part also be explained by leakiness of the shRNA vector. This means that also in the absence of doxycycline, the target gene might be repressed to a certain degree which could already negatively impact on the cells. Given that the knockdown efficiency achieved upon induction of the shRNA was still incomplete, it can be concluded that IMR-5-75 are able to cope reasonably well with minimal residual CDK12 or CDK13 protein. Likely, the two proteins can at least in part compensate the loss of each other due to overlapping functions. However, the extent of overlap is currently still unclear. Two different RNA expression studies claimed that the overlap of CDK13- with CDK12-regulated genes amounted to 25 versus 75 %, respectively. Therefore, RNA expression was studied upon shRNA-induced knockdown of *CDK12* and *CDK13*. However, only a small number of DEGs was identified, and no overlap between genes regulated by CDK12 and CDK13 was detected. miRNAs and pseudogenes were strikingly often represented in the results. Size selection during the library preparation process diminishes smaller RNA species; therefore it is conceivable that the actual number of deregulated miRNAs could be much higher. A specialized small RNA sequencing approach could shed light on this question.

4.2.5 CRISPR-induced *CDK12/13* Knockout in Neuroblastoma Cells

Going further, an inducible CRISPR interference model was set up to achieve stronger protein knockdown. The employed vectors were designed by Mandegar and colleagues (2016). They had reported high knockdown efficiencies of up to 99 %, and observed no cell death or changes in proliferation or morphology upon expression of the *dCas9-KRAB* gene alone. Three different guide RNAs against *CDK13* were tested which achieved variable knockdown efficiencies between 50 – 90 %. Moreover, the effect of inducing expression of only the dCas vector without presence of the guide RNA vector was tested. Both alternatives reduced viability and confluence in our neuroblastoma cells. Apparently, the dCas9-KRAB fusion protein itself has a detrimental effect on them, even though most publications using dCas9-KRAB report little to no off-target effects. Many more studies have dealt with the specificity of functional Cas9, but results varied depending on the cell line and species used (X. Wu *et al.*, 2014). Since Mandegar and colleagues worked with human induced pluripotent stem cells, this might explain the differences observed.
Thakore and colleagues specifically compared the effects of dCas9-KRAB to untransduced controls and observed 29 differentially expressed genes (2015). In addition, a ChIP Seq study found more than 2000 peaks where dCas9 without guide RNAs bound to the genome (X. Wu *et al.*, 2014). Conceivably, dCas9 scans the DNA for possible PAM sequences, which are an essential recognition motif for dCas9 binding (Sternberg *et al.*, 2014). Likely, the same happened in the present case, so that dCas-KRAB randomly inhibited parts of the genome.

4.2.6 CDK12/13 Inhibition by Tool Compound BAY-587

Analysis of the IC50 values of CDK12/13 inhibitors BAY-587 and THZ531 in several neuroblastoma cell lines with diverse genetic backgrounds revealed that BAY-587 was active at lower concentrations than THZ531. However, sensitivity of the cell lines to BAY-587 did not predict the extent of sensitivity to THZ531. The same observation was made by our collaboration partners working with primary colon carcinoma cultures (Friederike Herbst, personal communication). This discrepancy probably occurs due to the differing mode of action. MNA cell lines tended to be more sensitive to BAY-587 than those with *MYC*-activating translocation. However, since only eight cell lines were analyzed in this study, a statistical evaluation was not yet possible.
Treatment with BAY-587 decreased the level of CDK12 protein in a dose-dependent manner. Previous studies demonstrated that cyclin K stabilizes CDK12, but not CDK13 (Blazek *et al.*, 2011). It seems that BAY-587 leads to a degradation of CDK12. Based on

the study by Blazek and colleagues, one explanation might be that binding of cyclin K is prevented.

In general, the effects of CDK12/13 inhibition in NB cells were very promising. BAY-587 treatment at IC50 concentration completely or almost completely abolished colony formation capacity in all studied cell lines. In addition, it compromised cell cycle progression. The sub-G_1 fraction increased dose-dependently, suggesting an increase of cell death. This is in line with results of a study analyzing THZ531 effect in Jurkat cells, a model of acute T cell leukemia (Zhang *et al.*, 2016). They also reported an increasing sub-G_1 fraction, albeit only at concentrations four times the IC50 and above. This indicates that neuroblastoma have a higher vulnerability towards inhibition of CDK12 and CDK13.

Interestingly, different cell cycle arrest phenotypes occurred in different cell lines. In the majority of cell lines analyzed, cells tended to accumulate in S phase, only in IMR-32, there was an increase in G_1 phase cells upon BAY-587 treatment. It seems that the cellular response towards CDK12/13 inhibition differs between different NB cell lines.

The induction of cell death by CDK12/13 inhibition was confirmed by a live/dead exclusion staining with PI. In SH-EP cells, a population with intermediate PI staining and decreased FSC signal formed with increasing concentrations of BAY-587. This was despite a lack of morphological changes of the cell culture. Since cell death goes along with shrinkage of the cell manifested through low FSC, it could be possible that this population is just beginning to die, but their membrane is not yet completely disrupted preventing heavy uptake of PI (Healy *et al.*, 1998). To explore this possibility, incubation of SH-EP cells treated with BAY-587 was prolonged to seven days and afterwards their morphology was assessed. Still, no increase in cells swimming in the medium could be observed. Possibly, the cells went into senescence, which could be assayed by β-galactosidase staining. Alternatively, it might be conceivable that the cells become smaller without losing viability because CDK12/13 inhibition preferentially leads to downregulation of transcription, eventually leading to a general decrease of protein content. This hypothesis could be tested by live-cell imaging.

The next step was to identify the type of cell death occurring in our cell lines. Neither the addition of apoptosis, necrosis, ferroptosis nor autophagy inhibitors prevented cell death. However, two independent assays detected the presences of DNA strand breaks characteristic of late apoptosis and of active Caspases 3 and 7, which indicate early apoptosis. Therefore, the observed phenotype most likely is a consequence of apoptotic cell death.

Gene expression analysis upon BAY-587 treatment revealed that the extent of differential expression mirrored the sensitivity of the cell lines to the inhibitor. The number of up- and downregulated genes was highest in cell lines with strong induction of cell death (NB-69,

SK-N-DZ). Contrarily, SH-EP cells, which had low levels of apoptosis, also lacked large changes in gene expression. Despite this difference, the intersection of DEGs was remarkably large. It accounted for half of the downregulated genes in SH-EP cells and was especially high between NB-69 and SK-N-DZ cells. This suggested that inhibition of CDK12/13 affected similar pathways in our neuroblastoma cells despite their different genetic background and differences in the observed phenotype upon inhibition.

To find out more about the biological implications, a gene enrichment analysis was performed. Downregulated genes were enriched in the cellular component nucleus across increasing concentrations, as was exemplified by SK-N-DZ. As CDK12 and CDK13 are localized in nuclear speckles, this result was in line with expectations (H. H. Chen *et al.*, 2007; Ko *et al.*, 2001). Low concentrations of the inhibitor also led to a decrease in genes belonging to cilia and their formation. The primary cilium is a protuberance from the cell, which is involved in cell signaling, but also the control of cell growth / proliferation. Consequently, loss or decrease of the primary cilium have been attributed to several cancer types (Khan *et al.*, 2016). The downregulation of primary cilium genes seems therefore counterintuitive at first glance and merits further investigation. Higher concentrations of the inhibitor led to reductions in the expression of DNA repair genes.

Next, the functional categories enriched in DEGs of all or three out of four cell lines were determined. There were two recurrent categories of downregulated genes, alternative splicing and DNA damage / repair. Liang and colleagues previously reported the regulation of RNA processing upon both *CDK12* and *CDK13* knockdown (2015). Earlier functional studies found that overexpression of *CDK13* and *CDK12* altered splicing (H. H. Chen *et al.*, 2007). Interestingly, alternative splicing was also among the categories downregulated in MYCN high cells in the first part of this thesis. This might be an explanation for the synthetic lethal relationship between MYCN and CDK13. If genes involved in alternative splicing are already downregulated in MYCN high cells, any further reduction mediated by loss of CDK13 might be difficult to tolerate. DNA repair, on the other hand, has previously been linked to CDK12 (K. Liang *et al.*, 2015). In addition, Zhang *et al.* saw an enrichment of DNA damage repair genes after treatment with THZ531 (2016). In this study, upregulated genes of all cell lines were enriched in terms centered around the nucleus, transcription and its regulation, phosphoprotein and biological rhythms. The first three annotation groups can be explained by the role of CDK12 and 13 in phosphorylating the CTD of RNA Pol II, thereby regulating transcription elongation (Greenleaf, 2018). Further, CDK12/13 seem to preferentially regulate genes with regions rich in particular amino acids (serine, proline). Also, upregulated genes were enriched in alternative splicing mechanisms. Finally, chromatin regulators were upregulated in three of our cell lines. A study performed in *C. elegans* found that knockdown of CDK12

reduces the level of histone 3 lysine 36 trimethylations (Bowman *et al.*, 2013). These histone marks serve to recruit DNA damage repair gene RAD51 to the DNA (Aymard *et al.*, 2014). Hence, this could be one mechanism how CDK12 regulates DNA damage repair.

Taken together, it can be concluded that the observed effects on gene regulation are fully in agreement with the reported roles of CDK12 and CDK13. This may serve as a confirmation of the specificity of the inhibitor. In addition, novel target gene categories could be identified. However, differences and common functions of the two kinases cannot be elucidated by this approach.

The inhibition of CDK12 and CDK13 by BAY-587 induced strong cell death also in those cell lines identified as intermediate responders (IMR-5-75, IMR-32). This can likely be explained by two reasons. First, the inhibitor is active against all CDK12/13 proteins in the cells. Opposed to that, a knockdown induced by siRNA or in the shRNA cell clones is never complete, so that the cells are left with a certain amount of residual active protein. Second, the inhibitor is active against both kinases and therefore redundant functions cannot be fulfilled by the remaining kinase as is the case in the knockdown setting.

4.3 Conclusion and Perspective

This thesis contributes to the understanding of MYCN addiction in NB by examining cell cycle-resolved transcriptional changes in MYCN low and high cells. It distinguished constitutively activated and repressed genes that fuel malignant behavior of MYCN high cells from secondary transcriptional effects arising through this behavior. It showed that MYCN furthermore partly relies on miRNAs to implement and amplify these transcriptional changes. Consequences of high MYCN levels included the acceleration of the cell cycle and increased ribosome biogenesis and protein translation, which is in line with published data. Moreover, a potential role of snoRNAs was discovered, which were heavily upregulated in MYCN low cells towards the end of the observation period. Not much is known about the role of this non-coding RNA species in NB. It would therefore be interesting to functionally investigate the role of selected candidates in NB for example by inducing degradation through antisense oligonucleotides or by overexpression studies.

The second part of this thesis examines CDK13 as a potential new therapeutic target in NB. *CDK13* repression using different technical approaches resulted in decreased viability and colony formation capacity as well as altered cell cycle distribution despite residual protein. The highly homologous family member CDK12 seems to be less vital in the NB setting, which is in contrast to other cancer entities. Combined inhibition of CDK13 and

CDK12 by the novel compound BAY-587 elicited impressive effects including a strong induction of cell death, cell cycle arrest mostly in S phase and far reaching changes in gene expression.

Work on CDK13 continues in the context of a joint project with Bayer AG. In order to achieve complete or at least extensive reduction of CDK12 and CDK13, CRISPR knockout single clones will be established and biallelic editing confirmed by sequencing. Should it prove that clones with homozygous knockout of *CDK12* or *CDK13* are not viable, an inducible system will need to be implemented. In addition to the kinases, the role of their partner cyclin K will also be investigated by corresponding knockout studies. Next to IMR-5-75 cells, which were predominantly used in this thesis, additional cell lines will be selected based on high sensitivity to siRNA-mediated *CDK13* knockdown and BAY-587 treatment. Moreover, the analysis of CDK12/13 inhibition suggests that a combined knockout of *CDK12* and *CDK13* could be more effective than single knockouts. All knockout models will be phenotypically characterized with a particular focus on gene expression and proteome analysis. This will identify common and specific downstream targets of CDK12 and CDK13, thereby adding to the knowledge on general CDK12/13-mediated transcriptional regulation gathered in BAY-587-treated cells.

Going further, ectopical overexpression of *CDK12* and *CDK13* in the knockout clones will clarify in how far the two proteins may take over each other's function and thus rescue the observed phenotype. This will be complemented by overexpression of mutant genes with non-functional kinase domains to evaluate the relevance of the enzymatic activity for the knockout phenotype.

Sensitivity to the inhibitor BAY-587 will be examined in a larger panel of NB cell lines to determine the role of *MYCN* amplification and other genetic aberrations for the response. The most sensitive and least sensitive cell lines will be selected to analyze the effect of BAY-587, hoping to elucidate its mode of action. To verify that BAY-587 induces apoptosis as suggested by the present study, additional experiments should be conducted, for example annexin stainings.

Given that DNA damage repair genes were downregulated upon BAY-587 treatment in all four cell lines examined, it is conceivable that vulnerability towards DNA damage is increased upon inhibition of CDK12/13. It would thus be very interesting to combine the inhibitor with DNA damaging agents, such as doxorubicin, or with irradiation.

In conclusion, this thesis sheds light on the transcriptional consequences of MYCN addiction and establishes CDK13 as a promising drug target in neuroblastoma.

5 REFERENCES

Aleem, E., & Arceci, R. J. (2015). *"Targeting cell cycle regulators in hematologic malignancies"*. Front Cell Dev Biol, 3, 16. doi: 10.3389/fcell.2015.00016

Ayer, D. E., Kretzner, L., & Eisenman, R. N. (1993). *"Mad: a heterodimeric partner for Max that antagonizes Myc transcriptional activity"*. Cell, 72(2), 211-222.

Aymard, F., Bugler, B., Schmidt, C. K., Guillou, E., Caron, P., Briois, S., Iacovoni, J. S., Daburon, V., Miller, K. M., Jackson, S. P., & Legube, G. (2014). *"Transcriptionally active chromatin recruits homologous recombination at DNA double-strand breaks"*. Nat Struct Mol Biol, 21(4), 366-374. doi: 10.1038/nsmb.2796

Barna, M., Pusic, A., Zollo, O., Costa, M., Kondrashov, N., Rego, E., Rao, P. H., & Ruggero, D. (2008). *"Suppression of Myc oncogenic activity by ribosomal protein haploinsufficiency"*. Nature, 456(7224), 971-975. doi: 10.1038/nature07449

Bartkowiak, B., & Greenleaf, A. L. (2015). *"Expression, purification, and identification of associated proteins of the full-length hCDK12/CyclinK complex"*. J Biol Chem, 290(3), 1786-1795. doi: 10.1074/jbc.M114.612226

Bartkowiak, B., Liu, P., Phatnani, H. P., Fuda, N. J., Cooper, J. J., Price, D. H., Adelman, K., Lis, J. T., & Greenleaf, A. L. (2010). *"CDK12 is a transcription elongation-associated CTD kinase, the metazoan ortholog of yeast Ctk1"*. Genes Dev, 24(20), 2303-2316. doi: 10.1101/gad.1968210

Baudino, T. A., McKay, C., Pendeville-Samain, H., Nilsson, J. A., Maclean, K. H., White, E. L., Davis, A. C., Ihle, J. N., & Cleveland, J. L. (2002). *"c-Myc is essential for vasculogenesis and angiogenesis during development and tumor progression"*. Genes Dev, 16(19), 2530-2543. doi: 10.1101/gad.1024602

Beckers, A., Van Peer, G., Carter, D. R., Gartlgruber, M., Herrmann, C., Agarwal, S., Helsmoortel, H. H., Althoff, K., Molenaar, J. J., Cheung, B. B., Schulte, J. H., Benoit, Y., Shohet, J. M., Westermann, F., Marshall, G. M., Vandesompele, J., De Preter, K., & Speleman, F. (2015). *"MYCN-driven regulatory mechanisms controlling LIN28B in neuroblastoma"*. Cancer Lett, 366(1), 123-132. doi: 10.1016/j.canlet.2015.06.015

Bell, E., Premkumar, R., Carr, J., Lu, X., Lovat, P. E., Kees, U. R., Lunec, J., & Tweddle, D. A. (2006). *"The role of MYCN in the failure of MYCN amplified neuroblastoma cell lines to G1 arrest after DNA damage"*. Cell Cycle, 5(22), 2639-2647. doi: 10.4161/cc.5.22.3443

Biedler, J. L., & Spengler, B. A. (1976). *"A novel chromosome abnormality in human neuroblastoma and antifolate-resistant Chinese hamster cell lives in culture"*. J Natl Cancer Inst, 57(3), 683-695.

Blackwood, E. M., & Eisenman, R. N. (1991). *"Max: a helix-loop-helix zipper protein that forms a sequence-specific DNA-binding complex with Myc"*. Science, 251(4998), 1211-1217.

Blazek, D., Kohoutek, J., Bartholomeeusen, K., Johansen, E., Hulinkova, P., Luo, Z., Cimermancic, P., Ule, J., & Peterlin, B. M. (2011). *"The Cyclin K/Cdk12 complex maintains genomic stability via regulation of expression of DNA damage response genes"*. Genes Dev, 25(20), 2158-2172. doi: 10.1101/gad.16962311

Bosken, C. A., Farnung, L., Hintermair, C., Merzel Schachter, M., Vogel-Bachmayr, K., Blazek, D., Anand, K., Fisher, R. P., Eick, D., & Geyer, M. (2014). *"The structure and substrate specificity of human Cdk12/Cyclin K"*. Nat Commun, 5, 3505. doi: 10.1038/ncomms4505

Bowman, E. A., Bowman, C. R., Ahn, J. H., & Kelly, W. G. (2013). *"Phosphorylation of RNA polymerase II is independent of P-TEFb in the C. elegans germline"*. Development, 140(17), 3703-3713. doi: 10.1242/dev.095778

Brattain, M. G., Fine, W. D., Khaled, F. M., Thompson, J., & Brattain, D. E. (1981). *"Heterogeneity of malignant cells from a human colonic carcinoma"*. Cancer Res, 41(5), 1751-1756.

Brodeur, G. M., Seeger, R. C., Schwab, M., Varmus, H. E., & Bishop, J. M. (1984). *"Amplification of N-myc in untreated human neuroblastomas correlates with advanced disease stage"*. Science, 224(4653), 1121-1124.

Brodeur, G. M., Sekhon, G., & Goldstein, M. N. (1977). *"Chromosomal aberrations in human neuroblastomas"*. Cancer, 40(5), 2256-2263.

Buechner, J., Tomte, E., Haug, B. H., Henriksen, J. R., Lokke, C., Flaegstad, T., & Einvik, C. (2011). *"Tumour-suppressor microRNAs let-7 and mir-101 target the proto-oncogene MYCN and inhibit cell proliferation in MYCN-amplified neuroblastoma"*. Br J Cancer, 105(2), 296-303. doi: 10.1038/bjc.2011.220

Burkhart, C. A., Cheng, A. J., Madafiglio, J., Kavallaris, M., Mili, M., Marshall, G. M., Weiss, W. A., Khachigian, L. M., Norris, M. D., & Haber, M. (2003). *"Effects of MYCN antisense oligonucleotide administration on tumorigenesis in a murine model of neuroblastoma"*. J Natl Cancer Inst, 95(18), 1394-1403.

Carr-Wilkinson, J., O'Toole, K., Wood, K. M., Challen, C. C., Baker, A. G., Board, J. R., Evans, L., Cole, M., Cheung, N. K., Boos, J., Kohler, G., Leuschner, I., Pearson, A. D., Lunec, J., & Tweddle, D. A. (2010). *"High Frequency of p53/MDM2/p14ARF Pathway Abnormalities in Relapsed Neuroblastoma"*. Clin Cancer Res, 16(4), 1108-1118. doi: 10.1158/1078-0432.CCR-09-1865

Cermelli, S., Jang, I. S., Bernard, B., & Grandori, C. (2014). *"Synthetic lethal screens as a means to understand and treat MYC-driven cancers"*. Cold Spring Harb Perspect Med, 4(3). doi: 10.1101/cshperspect.a014209

Chang, T. C., Yu, D., Lee, Y. S., Wentzel, E. A., Arking, D. E., West, K. M., Dang, C. V., Thomas-Tikhonenko, A., & Mendell, J. T. (2008). *"Widespread microRNA repression by Myc contributes to tumorigenesis"*. Nat Genet, 40(1), 43-50. doi: 10.1038/ng.2007.30

Chayka, O., D'Acunto, C. W., Middleton, O., Arab, M., & Sala, A. (2015). *"Identification and pharmacological inactivation of the MYCN gene network as a therapeutic strategy for neuroblastic tumor cells"*. J Biol Chem, 290(4), 2198-2212. doi: 10.1074/jbc.M114.624056

Chen, H. H., Wang, Y. C., & Fann, M. J. (2006). *"Identification and characterization of the CDK12/cyclin L1 complex involved in alternative splicing regulation"*. Mol Cell Biol, 26(7), 2736-2745. doi: 10.1128/MCB.26.7.2736-2745.2006

Chen, H. H., Wong, Y. H., Geneviere, A. M., & Fann, M. J. (2007). *"CDK13/CDC2L5 interacts with L-type cyclins and regulates alternative splicing"*. Biochem Biophys Res Commun, 354(3), 735-740. doi: 10.1016/j.bbrc.2007.01.049

Chen, H. R., Lin, G. T., Huang, C. K., & Fann, M. J. (2014). *"Cdk12 and Cdk13 regulate axonal elongation through a common signaling pathway that modulates Cdk5 expression"*. Exp Neurol, 261, 10-21. doi: 10.1016/j.expneurol.2014.06.024

Chen, Y., & Stallings, R. L. (2007). *"Differential patterns of microRNA expression in neuroblastoma are correlated with prognosis, differentiation, and apoptosis"*. Cancer Res, 67(3), 976-983. doi: 10.1158/0008-5472.CAN-06-3667

Chen, Y., Takita, J., Choi, Y. L., Kato, M., Ohira, M., Sanada, M., Wang, L., Soda, M., Kikuchi, A., Igarashi, T., Nakagawara, A., Hayashi, Y., Mano, H., & Ogawa, S. (2008). *"Oncogenic mutations of ALK kinase in neuroblastoma"*. Nature, 455(7215), 971-974. doi: 10.1038/nature07399

Cheung, N. K., Zhang, J., Lu, C., Parker, M., Bahrami, A., Tickoo, S. K., Heguy, A., Pappo, A. S., Federico, S., Dalton, J., Cheung, I. Y., Ding, L., Fulton, R., Wang, J., Chen, X., Becksfort, J., Wu, J., Billups, C. A., Ellison, D., Mardis, E. R., Wilson, R. K., Downing, J. R., Dyer, M. A., & St Jude Children's Research Hospital-Washington University Pediatric Cancer Genome, P. (2012). *"Association of age at diagnosis and genetic mutations in patients with neuroblastoma"*. JAMA, 307(10), 1062-1071. doi: 10.1001/jama.2012.228

Chila, R., Guffanti, F., & Damia, G. (2016). *"Role and therapeutic potential of CDK12 in human cancers"*. Cancer Treat Rev, 50, 83-88. doi: 10.1016/j.ctrv.2016.09.003

Chipumuro, E., Marco, E., Christensen, C. L., Kwiatkowski, N., Zhang, T., Hatheway, C. M., Abraham, B. J., Sharma, B., Yeung, C., Altabef, A., Perez-Atayde, A., Wong,

K. K., Yuan, G. C., Gray, N. S., Young, R. A., & George, R. E. (2014). *"CDK7 inhibition suppresses super-enhancer-linked oncogenic transcription in MYCN-driven cancer"*. Cell, 159(5), 1126-1139. doi: 10.1016/j.cell.2014.10.024

Cohn, S. L., Pearson, A. D., London, W. B., Monclair, T., Ambros, P. F., Brodeur, G. M., Faldum, A., Hero, B., Iehara, T., Machin, D., Mosseri, V., Simon, T., Garaventa, A., Castel, V., Matthay, K. K., & Force, I. T. (2009). *"The International Neuroblastoma Risk Group (INRG) classification system: an INRG Task Force report"*. J Clin Oncol, 27(2), 289-297. doi: 10.1200/JCO.2008.16.6785

Cooper, M. A. (2000). "*The Cell: A Molecular Approach"*.

Cowell, J. K., & Rupniak, H. T. (1983). *"Chromosome analysis of human neuroblastoma cell line TR14 showing double minutes and an aberration involving chromosome 1"*. Cancer Genet Cytogenet, 9(3), 273-280.

Croce, C. M. (2008). *"Oncogenes and cancer"*. N Engl J Med, 358(5), 502-511. doi: 10.1056/NEJMra072367

Dai, Q., Lei, T., Zhao, C., Zhong, J., Tang, Y. Z., Chen, B., Yang, J., Li, C., Wang, S., Song, X., Li, L., & Li, Q. (2012). *"Cyclin K-containing kinase complexes maintain self-renewal in murine embryonic stem cells"*. J Biol Chem, 287(30), 25344-25352. doi: 10.1074/jbc.M111.321760

Davidson, G., Shen, J., Huang, Y. L., Su, Y., Karaulanov, E., Bartscherer, K., Hassler, C., Stannek, P., Boutros, M., & Niehrs, C. (2009). *"Cell cycle control of wnt receptor activation"*. Dev Cell, 17(6), 788-799. doi: 10.1016/j.devcel.2009.11.006

Davidson, L., Muniz, L., & West, S. (2014). *"3' end formation of pre-mRNA and phosphorylation of Ser2 on the RNA polymerase II CTD are reciprocally coupled in human cells"*. Genes Dev, 28(4), 342-356. doi: 10.1101/gad.231274.113

Delmore, J. E., Issa, G. C., Lemieux, M. E., Rahl, P. B., Shi, J., Jacobs, H. M., Kastritis, E., Gilpatrick, T., Paranal, R. M., Qi, J., Chesi, M., Schinzel, A. C., McKeown, M. R., Heffernan, T. P., Vakoc, C. R., Bergsagel, P. L., Ghobrial, I. M., Richardson, P. G., Young, R. A., Hahn, W. C., Anderson, K. C., Kung, A. L., Bradner, J. E., & Mitsiades, C. S. (2011). *"BET bromodomain inhibition as a therapeutic strategy to target c-Myc"*. Cell, 146(6), 904-917. doi: 10.1016/j.cell.2011.08.017

Diaz-Padilla, I., Siu, L. L., & Duran, I. (2009). *"Cyclin-dependent kinase inhibitors as potential targeted anticancer agents"*. Invest New Drugs, 27(6), 586-594. doi: 10.1007/s10637-009-9236-6

Dolman, M. E., Poon, E., Ebus, M. E., den Hartog, I. J., van Noesel, C. J., Jamin, Y., Hallsworth, A., Robinson, S. P., Petrie, K., Sparidans, R. W., Kok, R. J., Versteeg, R., Caron, H. N., Chesler, L., & Molenaar, J. J. (2015). *"Cyclin-Dependent Kinase Inhibitor AT7519 as a Potential Drug for MYCN-Dependent Neuroblastoma"*. Clin Cancer Res, 21(22), 5100-5109. doi: 10.1158/1078-0432.CCR-15-0313

Duffy, D. J., Krstic, A., Halasz, M., Schwarzl, T., Fey, D., Iljin, K., Mehta, J. P., Killick, K., Whilde, J., Turriziani, B., Haapa-Paananen, S., Fey, V., Fischer, M., Westermann, F., Henrich, K. O., Bannert, S., Higgins, D. G., & Kolch, W. (2015). *"Integrative omics reveals MYCN as a global suppressor of cellular signalling and enables network-based therapeutic target discovery in neuroblastoma"*. Oncotarget, 6(41), 43182-43201. doi: 10.18632/oncotarget.6568

Dupuis-Sandoval, F., Poirier, M., & Scott, M. S. (2015). *"The emerging landscape of small nucleolar RNAs in cell biology"*. Wiley Interdiscip Rev RNA, 6(4), 381-397. doi: 10.1002/wrna.1284

Ekumi, K. M., Paculova, H., Lenasi, T., Pospichalova, V., Bosken, C. A., Rybarikova, J., Bryja, V., Geyer, M., Blazek, D., & Barboric, M. (2015). *"Ovarian carcinoma CDK12 mutations misregulate expression of DNA repair genes via deficient formation and function of the Cdk12/CycK complex"*. Nucleic Acids Res, 43(5), 2575-2589. doi: 10.1093/nar/gkv101

Even, Y., Escande, M. L., Fayet, C., & Geneviere, A. M. (2016). *"CDK13, a Kinase Involved in Pre-mRNA Splicing, Is a Component of the Perinucleolar Compartment"*. PLoS One, 11(2), e0149184. doi: 10.1371/journal.pone.0149184

Felsher, D. W., & Bishop, J. M. (1999). *"Transient excess of MYC activity can elicit genomic instability and tumorigenesis"*. Proc Natl Acad Sci U S A, 96(7), 3940-3944.

Fernandez, P. C., Frank, S. R., Wang, L., Schroeder, M., Liu, S., Greene, J., Cocito, A., & Amati, B. (2003). *"Genomic targets of the human c-Myc protein"*. Genes Dev, 17(9), 1115-1129. doi: 10.1101/gad.1067003

Firestein, R., Bass, A. J., Kim, S. Y., Dunn, I. F., Silver, S. J., Guney, I., Freed, E., Ligon, A. H., Vena, N., Ogino, S., Chheda, M. G., Tamayo, P., Finn, S., Shrestha, Y., Boehm, J. S., Jain, S., Bojarski, E., Mermel, C., Barretina, J., Chan, J. A., Baselga, J., Tabernero, J., Root, D. E., Fuchs, C. S., Loda, M., Shivdasani, R. A., Meyerson, M., & Hahn, W. C. (2008). *"CDK8 is a colorectal cancer oncogene that regulates beta-catenin activity"*. Nature, 455(7212), 547-551. doi: 10.1038/nature07179

Fisher, R. P. (2017). *"CDK regulation of transcription by RNAP II: Not over 'til it's over?"*. Transcription, 8(2), 81-90. doi: 10.1080/21541264.2016.1268244

Fontana, L., Fiori, M. E., Albini, S., Cifaldi, L., Giovinazzi, S., Forloni, M., Boldrini, R., Donfrancesco, A., Federici, V., Giacomini, P., Peschle, C., & Fruci, D. (2008). *"Antagomir-17-5p Abolishes the Growth of Therapy-Resistant Neuroblastoma through p21 and BIM"*. PLoS One, 3(5). doi: ARTN e2236

10.1371/journal.pone.0002236

Frank, S. R., Parisi, T., Taubert, S., Fernandez, P., Fuchs, M., Chan, H. M., Livingston, D. M., & Amati, B. (2003). *"MYC recruits the TIP60 histone acetyltransferase complex to chromatin"*. EMBO Rep, 4(6), 575-580. doi: 10.1038/sj.embor.embor861

Freytag, S. O., & Geddes, T. J. (1992). *"Reciprocal regulation of adipogenesis by Myc and C/EBP alpha"*. Science, 256(5055), 379-382.

Fulda, S., Lutz, W., Schwab, M., & Debatin, K. M. (1999). *"MycN sensitizes neuroblastoma cells for drug-induced apoptosis"*. Oncogene, 18(7), 1479-1486. doi: 10.1038/sj.onc.1202435

Gartel, A. L., Ye, X., Goufman, E., Shianov, P., Hay, N., Najmabadi, F., & Tyner, A. L. (2001). *"Myc represses the p21(WAF1/CIP1) promoter and interacts with Sp1/Sp3"*. Proc Natl Acad Sci U S A, 98(8), 4510-4515. doi: 10.1073/pnas.081074898

Geoerger, B., Bourdeaut, F., DuBois, S. G., Fischer, M., Geller, J. I., Gottardo, N. G., Marabelle, A., Pearson, A. D. J., Modak, S., Cash, T., Robinson, G. W., Motta, M., Matano, A., Bhansali, S. G., Dobson, J. R., Parasuraman, S., & Chi, S. N. (2017). *"A Phase I Study of the CDK4/6 Inhibitor Ribociclib (LEE011) in Pediatric Patients with Malignant Rhabdoid Tumors, Neuroblastoma, and Other Solid Tumors"*. Clin Cancer Res, 23(10), 2433-2441. doi: 10.1158/1078-0432.CCR-16-2898

Gherardi, S., Valli, E., Erriquez, D., & Perini, G. (2013). *"MYCN-mediated transcriptional repression in neuroblastoma: the other side of the coin"*. Front Oncol, 3, 42. doi: 10.3389/fonc.2013.00042

Gogolin, S., Ehemann, V., Becker, G., Brueckner, L. M., Dreidax, D., Bannert, S., Nolte, I., Savelyeva, L., Bell, E., & Westermann, F. (2013). *"CDK4 inhibition restores G(1)-S arrest in MYCN-amplified neuroblastoma cells in the context of doxorubicin-induced DNA damage"*. Cell Cycle, 12(7), 1091-1104. doi: 10.4161/cc.24091

Gong, J., Li, Y., Liu, C. J., Xiang, Y., Li, C., Ye, Y., Zhang, Z., Hawke, D. H., Park, P. K., Diao, L., Putkey, J. A., Yang, L., Guo, A. Y., Lin, C., & Han, L. (2017). *"A Pan-cancer Analysis of the Expression and Clinical Relevance of Small Nucleolar RNAs in Human Cancer"*. Cell Rep, 21(7), 1968-1981. doi: 10.1016/j.celrep.2017.10.070

Gopinathan, L., Ratnacaram, C. K., & Kaldis, P. (2011). *"Established and novel Cdk/cyclin complexes regulating the cell cycle and development"*. Results Probl Cell Differ, 53, 365-389. doi: 10.1007/978-3-642-19065-0_16

Greenleaf, A. L. (2018). *"Human CDK12 and CDK13, multi-tasking CTD kinases for the new millennium"*. Transcription, 1-20. doi: 10.1080/21541264.2018.1535211

Greifenberg, A. K., Honig, D., Pilarova, K., Duster, R., Bartholomeeusen, K., Bosken, C. A., Anand, K., Blazek, D., & Geyer, M. (2016). *"Structural and Functional Analysis of the Cdk13/Cyclin K Complex"*. Cell Rep, 14(2), 320-331. doi: 10.1016/j.celrep.2015.12.025

Gu, J. B., Bao, X. B., & Ma, Z. (2018). *"Effects of miR-21 on proliferation and apoptosis in human gastric adenocarcinoma cells"*. Oncol Lett, 15(1), 618-622. doi: 10.3892/ol.2017.6171

Guo, K., Zheng, S., Xu, Y., Xu, A., Chen, B., & Wen, Y. (2016). *"Loss of miR-26a-5p promotes proliferation, migration, and invasion in prostate cancer through negatively regulating SERBP1"*. Tumour Biol, 37(9), 12843-12854. doi: 10.1007/s13277-016-5158-z

Hanahan, D., & Weinberg, R. A. (2000). *"The hallmarks of cancer"*. Cell, 100(1), 57-70.

Hanahan, D., & Weinberg, R. A. (2011). *"Hallmarks of cancer: the next generation"*. Cell, 144(5), 646-674. doi: 10.1016/j.cell.2011.02.013

Harper, J. V., & Brooks, G. (2005). *"The mammalian cell cycle: an overview"*. Methods Mol Biol, 296, 113-153.

Healy, E., Dempsey, M., Lally, C., & Ryan, M. P. (1998). *"Apoptosis and necrosis: mechanisms of cell death induced by cyclosporine A in a renal proximal tubular cell line"*. Kidney Int, 54(6), 1955-1966. doi: 10.1046/j.1523-1755.1998.00202.x

Hertwig, F., Peifer, M., & Fischer, M. (2016). *"Telomere maintenance is pivotal for high-risk neuroblastoma"*. Cell Cycle, 15(3), 311-312. doi: 10.1080/15384101.2015.1125243

Hu, J., Wu, C., Zhao, X., & Liu, C. (2017). *"The prognostic value of decreased miR-101 in various cancers: a meta-analysis of 12 studies"*. Onco Targets Ther, 10, 3709-3718. doi: 10.2147/OTT.S141652

Huang da, W., Sherman, B. T., & Lempicki, R. A. (2009a). *"Bioinformatics enrichment tools: paths toward the comprehensive functional analysis of large gene lists"*. Nucleic Acids Res, 37(1), 1-13. doi: 10.1093/nar/gkn923

Huang da, W., Sherman, B. T., & Lempicki, R. A. (2009b). *"Systematic and integrative analysis of large gene lists using DAVID bioinformatics resources"*. Nat Protoc, 4(1), 44-57. doi: 10.1038/nprot.2008.211

Huang, M., & Weiss, W. A. (2013). *"Neuroblastoma and MYCN"*. Cold Spring Harb Perspect Med, 3(10), a014415. doi: 10.1101/cshperspect.a014415

Iraci, N., Diolaiti, D., Papa, A., Porro, A., Valli, E., Gherardi, S., Herold, S., Eilers, M., Bernardoni, R., Della Valle, G., & Perini, G. (2011). *"A SP1/MIZ1/MYCN repression complex recruits HDAC1 at the TRKA and p75NTR promoters and affects neuroblastoma malignancy by inhibiting the cell response to NGF"*. Cancer Res, 71(2), 404-412. doi: 10.1158/0008-5472.CAN-10-2627

Jain, M., Arvanitis, C., Chu, K., Dewey, W., Leonhardt, E., Trinh, M., Sundberg, C. D., Bishop, J. M., & Felsher, D. W. (2002). *"Sustained loss of a neoplastic phenotype by brief inactivation of MYC"*. Science, 297(5578), 102-104. doi: 10.1126/science.1071489

Janoueix-Lerosey, I., Lequin, D., Brugieres, L., Ribeiro, A., de Pontual, L., Combaret, V., Raynal, V., Puisieux, A., Schleiermacher, G., Pierron, G., Valteau-Couanet, D., Frebourg, T., Michon, J., Lyonnet, S., Amiel, J., & Delattre, O. (2008). *"Somatic and germline activating mutations of the ALK kinase receptor in neuroblastoma"*. Nature, 455(7215), 967-970. doi: 10.1038/nature07398

Kaelin, W. G., Jr. (2005). *"The concept of synthetic lethality in the context of anticancer therapy"*. Nat Rev Cancer, 5(9), 689-698. doi: 10.1038/nrc1691

Kaldis, P. (1999). *"The cdk-activating kinase (CAK): from yeast to mammals"*. Cell Mol Life Sci, 55(2), 284-296. doi: 10.1007/s000180050290

Kasten, M., & Giordano, A. (2001). *"Cdk10, a Cdc2-related kinase, associates with the Ets2 transcription factor and modulates its transactivation activity"*. Oncogene, 20(15), 1832-1838. doi: 10.1038/sj.onc.1204295

Kaur, M., & Cole, M. D. (2013). *"MYC acts via the PTEN tumor suppressor to elicit autoregulation and genome-wide gene repression by activation of the Ezh2*

methyltransferase". Cancer Res, 73(2), 695-705. doi: 10.1158/0008-5472.CAN-12-2522

Kearns, N. A., Genga, R. M., Enuameh, M. S., Garber, M., Wolfe, S. A., & Maehr, R. (2014). *"Cas9 effector-mediated regulation of transcription and differentiation in human pluripotent stem cells"*. Development, 141(1), 219-223. doi: 10.1242/dev.103341

Khan, N. A., Willemarck, N., Talebi, A., Marchand, A., Binda, M. M., Dehairs, J., Rueda-Rincon, N., Daniels, V. W., Bagadi, M., Thimiri Govinda Raj, D. B., Vanderhoydonc, F., Munck, S., Chaltin, P., & Swinnen, J. V. (2016). *"Identification of drugs that restore primary cilium expression in cancer cells"*. Oncotarget, 7(9), 9975-9992. doi: 10.18632/oncotarget.7198

Kim, H. E., Kim, D. G., Lee, K. J., Son, J. G., Song, M. Y., Park, Y. M., Kim, J. J., Cho, S. W., Chi, S. G., Cheong, H. S., Shin, H. D., Lee, S. W., & Lee, J. K. (2012). *"Frequent amplification of CENPF, GMNN and CDK13 genes in hepatocellular carcinomas"*. PLoS One, 7(8), e43223. doi: 10.1371/journal.pone.0043223

Kime, L., & Wright, S. C. (2003). *"Mad4 is regulated by a transcriptional repressor complex that contains Miz-1 and c-Myc"*. Biochem J, 370(Pt 1), 291-298. doi: 10.1042/BJ20021679

Knoepfler, P. S., Cheng, P. F., & Eisenman, R. N. (2002). *"N-myc is essential during neurogenesis for the rapid expansion of progenitor cell populations and the inhibition of neuronal differentiation"*. Genes Dev, 16(20), 2699-2712. doi: 10.1101/gad.1021202

Knuesel, M. T., Meyer, K. D., Bernecky, C., & Taatjes, D. J. (2009). *"The human CDK8 subcomplex is a molecular switch that controls Mediator coactivator function"*. Genes Dev, 23(4), 439-451. doi: 10.1101/gad.1767009

Ko, T. K., Kelly, E., & Pines, J. (2001). *"CrkRS: a novel conserved Cdc2-related protein kinase that colocalises with SC35 speckles"*. J Cell Sci, 114(Pt 14), 2591-2603.

Kohoutek, J., & Blazek, D. (2012). *"Cyclin K goes with Cdk12 and Cdk13"*. Cell Div, 7, 12. doi: 10.1186/1747-1028-7-12

Krasnoselsky, A. L., Whiteford, C. C., Wei, J. S., Bilke, S., Westermann, F., Chen, Q. R., & Khan, J. (2005). *"Altered expression of cell cycle genes distinguishes aggressive neuroblastoma"*. Oncogene, 24(9), 1533-1541. doi: 10.1038/sj.onc.1208341

Kruskal, W. H., & Wallis, W. A. (1952). *"Use of Ranks in One-Criterion Variance Analysis"*. Journal of the American Statistical Association, 47(260), 39.

Larochelle, S., Amat, R., Glover-Cutter, K., Sanso, M., Zhang, C., Allen, J. J., Shokat, K. M., Bentley, D. L., & Fisher, R. P. (2012). *"Cyclin-dependent kinase control of the initiation-to-elongation switch of RNA polymerase II"*. Nat Struct Mol Biol, 19(11), 1108-1115. doi: 10.1038/nsmb.2399

Li, Y., Choi, P. S., Casey, S. C., Dill, D. L., & Felsher, D. W. (2014). *"MYC through miR-17-92 suppresses specific target genes to maintain survival, autonomous proliferation, and a neoplastic state"*. Cancer Cell, 26(2), 262-272. doi: 10.1016/j.ccr.2014.06.014

Liang, K., Gao, X., Gilmore, J. M., Florens, L., Washburn, M. P., Smith, E., & Shilatifard, A. (2015). *"Characterization of human cyclin-dependent kinase 12 (CDK12) and CDK13 complexes in C-terminal domain phosphorylation, gene transcription, and RNA processing"*. Mol Cell Biol, 35(6), 928-938. doi: 10.1128/MCB.01426-14

Liang, L., Zeng, J. H., Wang, J. Y., He, R. Q., Ma, J., Chen, G., Cai, X. Y., & Hu, X. H. (2017). *"Down-regulation of miR-26a-5p in hepatocellular carcinoma: A qRT-PCR and bioinformatics study"*. Pathol Res Pract, 213(12), 1494-1509. doi: 10.1016/j.prp.2017.10.001

Lim, S., & Kaldis, P. (2013). *"Cdks, cyclins and CKIs: roles beyond cell cycle regulation"*. Development, 140(15), 3079-3093. doi: 10.1242/dev.091744

Lin, C. Y., Loven, J., Rahl, P. B., Paranal, R. M., Burge, C. B., Bradner, J. E., Lee, T. I., & Young, R. A. (2012). *"Transcriptional amplification in tumor cells with elevated c-Myc"*. Cell, 151(1), 56-67. doi: 10.1016/j.cell.2012.08.026

Lindqvist, A., van Zon, W., Karlsson Rosenthal, C., & Wolthuis, R. M. (2007). *"Cyclin B1-Cdk1 activation continues after centrosome separation to control mitotic progression"*. PLoS Biol, 5(5), e123. doi: 10.1371/journal.pbio.0050123

Liu, B., Wu, X., Liu, B., Wang, C., Liu, Y., Zhou, Q., & Xu, K. (2012). *"MiR-26a enhances metastasis potential of lung cancer cells via AKT pathway by targeting PTEN"*. Biochim Biophys Acta, 1822(11), 1692-1704. doi: 10.1016/j.bbadis.2012.07.019

Liu, Z., Xie, D., & Zhang, H. (2018). *"Long noncoding RNA neuroblastoma-associated transcript 1 gene inhibits malignant cellular phenotypes of bladder cancer through miR-21/SOCS6 axis"*. Cell Death Dis, 9(10), 1042. doi: 10.1038/s41419-018-1090-z

Loschmann, N., Michaelis, M., Rothweiler, F., Zehner, R., Cinatl, J., Voges, Y., Sharifi, M., Riecken, K., Meyer, J., von Deimling, A., Fichtner, I., Ghafourian, T., Westermann, F., & Cinatl, J., Jr. (2013). *"Testing of SNS-032 in a Panel of Human Neuroblastoma Cell Lines with Acquired Resistance to a Broad Range of Drugs"*. Transl Oncol, 6(6), 685-696.

Lutz, W., Stohr, M., Schurmann, J., Wenzel, A., Lohr, A., & Schwab, M. (1996). *"Conditional expression of N-myc in human neuroblastoma cells increases expression of alpha-prothymosin and ornithine decarboxylase and accelerates progression into S-phase early after mitogenic stimulation of quiescent cells"*. Oncogene, 13(4), 803-812.

Majello, B., Napolitano, G., Giordano, A., & Lania, L. (1999). *"Transcriptional regulation by targeted recruitment of cyclin-dependent CDK9 kinase in vivo"*. Oncogene, 18(32), 4598-4605. doi: 10.1038/sj.onc.1202822

Malumbres, M. (2014). *"Cyclin-dependent kinases"*. Genome Biol, 15(6), 122.

Malumbres, M., & Barbacid, M. (2001). *"To cycle or not to cycle: a critical decision in cancer"*. Nat Rev Cancer, 1(3), 222-231. doi: 10.1038/35106065

Malynn, B. A., de Alboran, I. M., O'Hagan, R. C., Bronson, R., Davidson, L., DePinho, R. A., & Alt, F. W. (2000). *"N-myc can functionally replace c-myc in murine development, cellular growth, and differentiation"*. Genes Dev, 14(11), 1390-1399.

Mandegar, M. A., Huebsch, N., Frolov, E. B., Shin, E., Truong, A., Olvera, M. P., Chan, A. H., Miyaoka, Y., Holmes, K., Spencer, C. I., Judge, L. M., Gordon, D. E., Eskildsen, T. V., Villalta, J. E., Horlbeck, M. A., Gilbert, L. A., Krogan, N. J., Sheikh, S. P., Weissman, J. S., Qi, L. S., So, P. L., & Conklin, B. R. (2016). *"CRISPR Interference Efficiently Induces Specific and Reversible Gene Silencing in Human iPSCs"*. Cell Stem Cell, 18(4), 541-553. doi: 10.1016/j.stem.2016.01.022

Martin, M. (2011). *"Cutadapt removes adapter sequences from high-throughput sequencing reads"*. EMBnet.journal, 17(1). doi: DOI:10.14806/ej.17.1.200

Matthay, K. K., Maris, J. M., Schleiermacher, G., Nakagawara, A., Mackall, C. L., Diller, L., & Weiss, W. A. (2016). *"Neuroblastoma"*. Nat Rev Dis Primers, 2, 16078. doi: 10.1038/nrdp.2016.78

McKenzie, P. P., Guichard, S. M., Middlemas, D. S., Ashmun, R. A., Danks, M. K., & Harris, L. C. (1999). *"Wild-type p53 can induce p21 and apoptosis in neuroblastoma cells but the DNA damage-induced G1 checkpoint function is attenuated"*. Clin Cancer Res, 5(12), 4199-4207.

Megiorni, F., Colaiacovo, M., Cialfi, S., McDowell, H. P., Guffanti, A., Camero, S., Felsani, A., Losty, P. D., Pizer, B., Shukla, R., Cappelli, C., Ferrara, E., Pizzuti, A., Moles, A., & Dominici, C. (2017). *"A sketch of known and novel MYCN-associated miRNA networks in neuroblastoma"*. Oncol Rep, 38(1), 3-20. doi: 10.3892/or.2017.5701

Megison, M. L., Stewart, J. E., Nabers, H. C., Gillory, L. A., & Beierle, E. A. (2013). *"FAK inhibition decreases cell invasion, migration and metastasis in MYCN amplified neuroblastoma"*. Clin Exp Metastasis, 30(5), 555-568. doi: 10.1007/s10585-012-9560-7

Mena, M. A., Garcia de Yebenes, J., Dwork, A., Fahn, S., Latov, N., Herbert, J., Flaster, E., & Slonim, D. (1989). *"Biochemical properties of monoamine-rich human neuroblastoma cells"*. Brain Res, 486(2), 286-296.

Mestdagh, P., Fredlund, E., Pattyn, F., Schulte, J. H., Muth, D., Vermeulen, J., Kumps, C., Schlierf, S., De Preter, K., Van Roy, N., Noguera, R., Laureys, G., Schramm, A., Eggert, A., Westermann, F., Speleman, F., & Vandesompele, J. (2010). *"MYCN/c-MYC-induced microRNAs repress coding gene networks associated with poor outcome in MYCN/c-MYC-activated tumors"*. Oncogene, 29(9), 1394-1404. doi: 10.1038/onc.2009.429

Miyake, I., Hakomori, Y., Shinohara, A., Gamou, T., Saito, M., Iwamatsu, A., & Sakai, R. (2002). *"Activation of anaplastic lymphoma kinase is responsible for hyperphosphorylation of ShcC in neuroblastoma cell lines"*. Oncogene, 21(38), 5823-5834. doi: 10.1038/sj.onc.1205735

Mogilyansky, E., & Rigoutsos, I. (2013). *"The miR-17/92 cluster: a comprehensive update on its genomics, genetics, functions and increasingly important and numerous roles in health and disease"*. Cell Death Differ, 20(12), 1603-1614. doi: 10.1038/cdd.2013.125

Molenaar, J. J., Ebus, M. E., Geerts, D., Koster, J., Lamers, F., Valentijn, L. J., Westerhout, E. M., Versteeg, R., & Caron, H. N. (2009). *"Inactivation of CDK2 is synthetically lethal to MYCN over-expressing cancer cells"*. Proc Natl Acad Sci U S A, 106(31), 12968-12973. doi: 10.1073/pnas.0901418106

Molenaar, J. J., Ebus, M. E., Koster, J., van Sluis, P., van Noesel, C. J., Versteeg, R., & Caron, H. N. (2008). *"Cyclin D1 and CDK4 activity contribute to the undifferentiated phenotype in neuroblastoma"*. Cancer Res, 68(8), 2599-2609. doi: 10.1158/0008-5472.CAN-07-5032

Molenaar, J. J., Koster, J., Ebus, M. E., van Sluis, P., Westerhout, E. M., de Preter, K., Gisselsson, D., Ora, I., Speleman, F., Caron, H. N., & Versteeg, R. (2012). *"Copy number defects of G1-cell cycle genes in neuroblastoma are frequent and correlate with high expression of E2F target genes and a poor prognosis"*. Genes Chromosomes Cancer, 51(1), 10-19. doi: 10.1002/gcc.20926

Monclair, T., Brodeur, G. M., Ambros, P. F., Brisse, H. J., Cecchetto, G., Holmes, K., Kaneko, M., London, W. B., Matthay, K. K., Nuchtern, J. G., von Schweinitz, D., Simon, T., Cohn, S. L., Pearson, A. D., & Force, I. T. (2009). *"The International Neuroblastoma Risk Group (INRG) staging system: an INRG Task Force report"*. J Clin Oncol, 27(2), 298-303. doi: 10.1200/JCO.2008.16.6876

Mosse, Y. P., Laudenslager, M., Longo, L., Cole, K. A., Wood, A., Attiyeh, E. F., Laquaglia, M. J., Sennett, R., Lynch, J. E., Perri, P., Laureys, G., Speleman, F., Kim, C., Hou, C., Hakonarson, H., Torkamani, A., Schork, N. J., Brodeur, G. M., Tonini, G. P., Rappaport, E., Devoto, M., & Maris, J. M. (2008). *"Identification of ALK as a major familial neuroblastoma predisposition gene"*. Nature, 455(7215), 930-935. doi: 10.1038/nature07261

Muth, D., Ghazaryan, S., Eckerle, I., Beckett, E., Pohler, C., Batzler, J., Beisel, C., Gogolin, S., Fischer, M., Henrich, K. O., Ehemann, V., Gillespie, P., Schwab, M., & Westermann, F. (2010). *"Transcriptional repression of SKP2 is impaired in MYCN-amplified neuroblastoma"*. Cancer Res, 70(9), 3791-3802. doi: 10.1158/0008-5472.CAN-09-1245

Natrajan, R., Wilkerson, P. M., Marchio, C., Piscuoglio, S., Ng, C. K., Wai, P., Lambros, M. B., Samartzis, E. P., Dedes, K. J., Frankum, J., Bajrami, I., Kopec, A., Mackay, A., A'Hern, R., Fenwick, K., Kozarewa, I., Hakas, J., Mitsopoulos, C., Hardisson, D., Lord, C. J., Kumar-Sinha, C., Ashworth, A., Weigelt, B., Sapino, A., Chinnaiyan, A. M., Maher, C. A., & Reis-Filho, J. S. (2014). *"Characterization of the genomic features and expressed fusion genes in micropapillary carcinomas of the breast"*. J Pathol, 232(5), 553-565. doi: 10.1002/path.4325

Neri, F., Zippo, A., Krepelova, A., Cherubini, A., Rocchigiani, M., & Oliviero, S. (2012). *"Myc regulates the transcription of the PRC2 gene to control the expression of developmental genes in embryonic stem cells"*. Mol Cell Biol, 32(4), 840-851. doi: 10.1128/MCB.06148-11

Nie, Z., Hu, G., Wei, G., Cui, K., Yamane, A., Resch, W., Wang, R., Green, D. R., Tessarollo, L., Casellas, R., Zhao, K., & Levens, D. (2012). *"c-Myc is a universal*

amplifier of expressed genes in lymphocytes and embryonic stem cells". Cell, 151(1), 68-79. doi: 10.1016/j.cell.2012.08.033

Nowell, P. C. (1976). *"The clonal evolution of tumor cell populations"*. Science, 194(4260), 23-28.

O'Donnell, K. A., Wentzel, E. A., Zeller, K. I., Dang, C. V., & Mendell, J. T. (2005). *"c-Myc-regulated microRNAs modulate E2F1 expression"*. Nature, 435(7043), 839-843. doi: 10.1038/nature03677

Oberthuer, A., Juraeva, D., Hero, B., Volland, R., Sterz, C., Schmidt, R., Faldum, A., Kahlert, Y., Engesser, A., Asgharzadeh, S., Seeger, R., Ohira, M., Nakagawara, A., Scaruffi, P., Tonini, G. P., Janoueix-Lerosey, I., Delattre, O., Schleiermacher, G., Vandesompele, J., Speleman, F., Noguera, R., Piqueras, M., Benard, J., Valent, A., Avigad, S., Yaniv, I., Grundy, R. G., Ortmann, M., Shao, C., Schwab, M., Eils, R., Simon, T., Theissen, J., Berthold, F., Westermann, F., Brors, B., & Fischer, M. (2015). *"Revised risk estimation and treatment stratification of low- and intermediate-risk neuroblastoma patients by integrating clinical and molecular prognostic markers"*. Clin Cancer Res, 21(8), 1904-1915. doi: 10.1158/1078-0432.CCR-14-0817

Ortega, S., Prieto, I., Odajima, J., Martin, A., Dubus, P., Sotillo, R., Barbero, J. L., Malumbres, M., & Barbacid, M. (2003). *"Cyclin-dependent kinase 2 is essential for meiosis but not for mitotic cell division in mice"*. Nat Genet, 35(1), 25-31. doi: 10.1038/ng1232

Pardee, A. B. (1974). *"A restriction point for control of normal animal cell proliferation"*. Proc Natl Acad Sci U S A, 71(4), 1286-1290.

Peifer, M., Hertwig, F., Roels, F., Dreidax, D., Gartlgruber, M., Menon, R., Kramer, A., Roncaioli, J. L., Sand, F., Heuckmann, J. M., Ikram, F., Schmidt, R., Ackermann, S., Engesser, A., Kahlert, Y., Vogel, W., Altmuller, J., Nurnberg, P., Thierry-Mieg, J., Thierry-Mieg, D., Mariappan, A., Heynck, S., Mariotti, E., Henrich, K. O., Gloeckner, C., Bosco, G., Leuschner, I., Schweiger, M. R., Savelyeva, L., Watkins, S. C., Shao, C., Bell, E., Hofer, T., Achter, V., Lang, U., Theissen, J., Volland, R., Saadati, M., Eggert, A., de Wilde, B., Berthold, F., Peng, Z., Zhao, C., Shi, L., Ortmann, M., Buttner, R., Perner, S., Hero, B., Schramm, A., Schulte, J. H., Herrmann, C., O'Sullivan, R. J., Westermann, F., Thomas, R. K., & Fischer, M. (2015). *"Telomerase activation by genomic rearrangements in high-risk neuroblastoma"*. Nature, 526(7575), 700-704. doi: 10.1038/nature14980

Pelengaris, S., Littlewood, T., Khan, M., Elia, G., & Evan, G. (1999). *"Reversible activation of c-Myc in skin: induction of a complex neoplastic phenotype by a single oncogenic lesion"*. Mol Cell, 3(5), 565-577.

Pelletier, J., Thomas, G., & Volarevic, S. (2018). *"Ribosome biogenesis in cancer: new players and therapeutic avenues"*. Nat Rev Cancer, 18(1), 51-63. doi: 10.1038/nrc.2017.104

Peukert, K., Staller, P., Schneider, A., Carmichael, G., Hanel, F., & Eilers, M. (1997). *"An alternative pathway for gene regulation by Myc"*. EMBO J, 16(18), 5672-5686. doi: 10.1093/emboj/16.18.5672

Popova, T., Manie, E., Boeva, V., Battistella, A., Goundiam, O., Smith, N. K., Mueller, C. R., Raynal, V., Mariani, O., Sastre-Garau, X., & Stern, M. H. (2016). *"Ovarian Cancers Harboring Inactivating Mutations in CDK12 Display a Distinct Genomic Instability Pattern Characterized by Large Tandem Duplications"*. Cancer Res, 76(7), 1882-1891. doi: 10.1158/0008-5472.CAN-15-2128

Prochownik, E. V., & Vogt, P. K. (2010). *"Therapeutic Targeting of Myc"*. Genes Cancer, 1(6), 650-659. doi: 10.1177/1947601910377494

Puissant, A., Frumm, S. M., Alexe, G., Bassil, C. F., Qi, J., Chanthery, Y. H., Nekritz, E. A., Zeid, R., Gustafson, W. C., Greninger, P., Garnett, M. J., McDermott, U., Benes, C. H., Kung, A. L., Weiss, W. A., Bradner, J. E., & Stegmaier, K. (2013). *"Targeting MYCN in neuroblastoma by BET bromodomain inhibition"*. Cancer Discov, 3(3), 308-323. doi: 10.1158/2159-8290.CD-12-0418

Rader, J., Russell, M. R., Hart, L. S., Nakazawa, M. S., Belcastro, L. T., Martinez, D., Li, Y., Carpenter, E. L., Attiyeh, E. F., Diskin, S. J., Kim, S., Parasuraman, S., Caponigro, G., Schnepp, R. W., Wood, A. C., Pawel, B., Cole, K. A., & Maris, J. M. (2013). *"Dual CDK4/CDK6 inhibition induces cell-cycle arrest and senescence in neuroblastoma"*. Clin Cancer Res, 19(22), 6173-6182. doi: 10.1158/1078-0432.CCR-13-1675

Rao, D. D., Senzer, N., Cleary, M. A., & Nemunaitis, J. (2009). *"Comparative assessment of siRNA and shRNA off target effects: what is slowing clinical development"*. Cancer Gene Ther, 16(11), 807-809. doi: 10.1038/cgt.2009.53

Robinson, M. D., & Oshlack, A. (2010). *"A scaling normalization method for differential expression analysis of RNA-seq data"*. Genome Biol, 11(3), R25. doi: 10.1186/gb-2010-11-3-r25

Ross, R. A., Spengler, B. A., & Biedler, J. L. (1983). *"Coordinate morphological and biochemical interconversion of human neuroblastoma cells"*. J Natl Cancer Inst, 71(4), 741-747.

Ryl, T., Kuchen, E. E., Bell, E., Shao, C., Florez, A. F., Monke, G., Gogolin, S., Friedrich, M., Lamprecht, F., Westermann, F., & Hofer, T. (2017). *"Cell-Cycle Position of Single MYC-Driven Cancer Cells Dictates Their Susceptibility to a Chemotherapeutic Drug"*. Cell Syst, 5(3), 237-250 e238. doi: 10.1016/j.cels.2017.07.005

Sabo, A., Kress, T. R., Pelizzola, M., de Pretis, S., Gorski, M. M., Tesi, A., Morelli, M. J., Bora, P., Doni, M., Verrecchia, A., Tonelli, C., Faga, G., Bianchi, V., Ronchi, A., Low, D., Muller, H., Guccione, E., Campaner, S., & Amati, B. (2014). *"Selective transcriptional regulation by Myc in cellular growth control and lymphomagenesis"*. Nature, 511(7510), 488-492. doi: 10.1038/nature13537

Sambrook J, R. D. (2002). "*Molecular cloning, a laboratory manual"*: CSHL press.

Sanso, M., & Fisher, R. P. (2013). *"Pause, play, repeat: CDKs push RNAP II's buttons"*. Transcription, 4(4), 146-152.

Savelyeva, L., Corvi, R., & Schwab, M. (1994). *"Translocation involving 1p and 17q is a recurrent genetic alteration of human neuroblastoma cells"*. Am J Hum Genet, 55(2), 334-340.

Schleiermacher, G., Mosseri, V., London, W. B., Maris, J. M., Brodeur, G. M., Attiyeh, E., Haber, M., Khan, J., Nakagawara, A., Speleman, F., Noguera, R., Tonini, G. P., Fischer, M., Ambros, I., Monclair, T., Matthay, K. K., Ambros, P., Cohn, S. L., & Pearson, A. D. (2012). *"Segmental chromosomal alterations have prognostic impact in neuroblastoma: a report from the INRG project"*. Br J Cancer, 107(8), 1418-1422. doi: 10.1038/bjc.2012.375

Schlesinger, H. R., Gerson, J. M., Moorhead, P. S., Maguire, H., & Hummeler, K. (1976). *"Establishment and characterization of human neuroblastoma cell lines"*. Cancer Res, 36(9 pt.1), 3094-3100.

Schramm, A., Koster, J., Marschall, T., Martin, M., Schwermer, M., Fielitz, K., Buchel, G., Barann, M., Esser, D., Rosenstiel, P., Rahmann, S., Eggert, A., & Schulte, J. H. (2013). *"Next-generation RNA sequencing reveals differential expression of MYCN target genes and suggests the mTOR pathway as a promising therapy target in MYCN-amplified neuroblastoma"*. Int J Cancer, 132(3), E106-115. doi: 10.1002/ijc.27787

Schulte, J. H., Horn, S., Otto, T., Samans, B., Heukamp, L. C., Eilers, U. C., Krause, M., Astrahantseff, K., Klein-Hitpass, L., Buettner, R., Schramm, A., Christiansen, H., Eilers, M., Eggert, A., & Berwanger, B. (2008). *"MYCN regulates oncogenic MicroRNAs in neuroblastoma"*. Int J Cancer, 122(3), 699-704. doi: 10.1002/ijc.23153

Schwab, M. (2004). *"MYCN in neuronal tumours"*. Cancer Lett, 204(2), 179-187. doi: 10.1016/S0304-3835(03)00454-3

Schwab, M., Alitalo, K., Klempnauer, K. H., Varmus, H. E., Bishop, J. M., Gilbert, F., Brodeur, G., Goldstein, M., & Trent, J. (1983). *"Amplified DNA with limited*

homology to myc cellular oncogene is shared by human neuroblastoma cell lines and a neuroblastoma tumour". Nature, 305(5931), 245-248.

Schwab, M., Varmus, H. E., & Bishop, J. M. (1985). *"Human N-myc gene contributes to neoplastic transformation of mammalian cells in culture"*. Nature, 316(6024), 160-162.

Seyfried, T. N., & Huysentruyt, L. C. (2013). *"On the origin of cancer metastasis"*. Crit Rev Oncog, 18(1-2), 43-73.

Shen, W., Song, M., Liu, J., Qiu, G., Li, T., Hu, Y., & Liu, H. (2014). *"MiR-26a promotes ovarian cancer proliferation and tumorigenesis"*. PLoS One, 9(1), e86871. doi: 10.1371/journal.pone.0086871

Sherr, C. J. (2004). *"Principles of tumor suppression"*. Cell, 116(2), 235-246.

Sherr, C. J., & Roberts, J. M. (1999). *"CDK inhibitors: positive and negative regulators of G1-phase progression"*. Genes Dev, 13(12), 1501-1512.

Smith, V., & Foster, J. (2018). *"High-Risk Neuroblastoma Treatment Review"*. Children (Basel), 5(9). doi: 10.3390/children5090114

Song, Y., Song, C., & Yang, S. (2018). *"Tumor-Suppressive Function of miR-30d-5p in Prostate Cancer Cell Proliferation and Migration by Targeting NT5E"*. Cancer Biother Radiopharm, 33(5), 203-211. doi: 10.1089/cbr.2018.2457

Sternberg, S. H., Redding, S., Jinek, M., Greene, E. C., & Doudna, J. A. (2014). *"DNA interrogation by the CRISPR RNA-guided endonuclease Cas9"*. Nature, 507(7490), 62-67. doi: 10.1038/nature13011

Stewart, B. W., & Wild, C. P. (2014). World Cancer Report 2014. Lyon: International Agency for Research on Cancer,.

Sugimoto, T., Tatsumi, E., Kemshead, J. T., Helson, L., Green, A. A., & Minowada, J. (1984). *"Determination of cell surface membrane antigens common to both human neuroblastoma and leukemia-lymphoma cell lines by a panel of 38 monoclonal antibodies"*. J Natl Cancer Inst, 73(1), 51-57.

Thakore, P. I., D'Ippolito, A. M., Song, L., Safi, A., Shivakumar, N. K., Kabadi, A. M., Reddy, T. E., Crawford, G. E., & Gersbach, C. A. (2015). *"Highly specific epigenome editing by CRISPR-Cas9 repressors for silencing of distal regulatory elements"*. Nat Methods, 12(12), 1143-1149. doi: 10.1038/nmeth.3630

Theissen, J., Oberthuer, A., Hombach, A., Volland, R., Hertwig, F., Fischer, M., Spitz, R., Zapatka, M., Brors, B., Ortmann, M., Simon, T., Hero, B., & Berthold, F. (2014). *"Chromosome 17/17q gain and unaltered profiles in high resolution array-CGH are prognostically informative in neuroblastoma"*. Genes Chromosomes Cancer, 53(8), 639-649. doi: 10.1002/gcc.22174

Toyoshima, M., Howie, H. L., Imakura, M., Walsh, R. M., Annis, J. E., Chang, A. N., Frazier, J., Chau, B. N., Loboda, A., Linsley, P. S., Cleary, M. A., Park, J. R., & Grandori, C. (2012). *"Functional genomics identifies therapeutic targets for MYC-driven cancer"*. Proc Natl Acad Sci U S A, 109(24), 9545-9550. doi: 10.1073/pnas.1121119109

Trigg, R. M., & Turner, S. D. (2018). *"ALK in Neuroblastoma: Biological and Therapeutic Implications"*. Cancers (Basel), 10(4). doi: 10.3390/cancers10040113

Trochet, D., Bourdeaut, F., Janoueix-Lerosey, I., Deville, A., de Pontual, L., Schleiermacher, G., Coze, C., Philip, N., Frebourg, T., Munnich, A., Lyonnet, S., Delattre, O., & Amiel, J. (2004). *"Germline mutations of the paired-like homeobox 2B (PHOX2B) gene in neuroblastoma"*. Am J Hum Genet, 74(4), 761-764. doi: 10.1086/383253

Trompeter, H. I., Abbad, H., Iwaniuk, K. M., Hafner, M., Renwick, N., Tuschl, T., Schira, J., Muller, H. W., & Wernet, P. (2011). *"MicroRNAs MiR-17, MiR-20a, and MiR-106b act in concert to modulate E2F activity on cell cycle arrest during neuronal lineage differentiation of USSC"*. PLoS One, 6(1), e16138. doi: 10.1371/journal.pone.0016138

Tumilowicz, J. J., Nichols, W. W., Cholon, J. J., & Greene, A. E. (1970). *"Definition of a continuous human cell line derived from neuroblastoma"*. Cancer Res, 30(8), 2110-2118.

Tweddle, D. A., Malcolm, A. J., Cole, M., Pearson, A. D., & Lunec, J. (2001). *"p53 cellular localization and function in neuroblastoma: evidence for defective G(1) arrest despite WAF1 induction in MYCN-amplified cells"*. Am J Pathol, 158(6), 2067-2077. doi: 10.1016/S0002-9440(10)64678-0

van de Wetering, M., Oving, I., Muncan, V., Pon Fong, M. T., Brantjes, H., van Leenen, D., Holstege, F. C., Brummelkamp, T. R., Agami, R., & Clevers, H. (2003). *"Specific inhibition of gene expression using a stably integrated, inducible small-interfering-RNA vector"*. EMBO Rep, 4(6), 609-615. doi: 10.1038/sj.embor.embor865

van Limpt, V., Schramm, A., van Lakeman, A., Sluis, P., Chan, A., van Noesel, M., Baas, F., Caron, H., Eggert, A., & Versteeg, R. (2004). *"The Phox2B homeobox gene is mutated in sporadic neuroblastomas"*. Oncogene, 23(57), 9280-9288. doi: 10.1038/sj.onc.1208157

Vijayaraghavan, S., Moulder, S., Keyomarsi, K., & Layman, R. M. (2018). *"Inhibiting CDK in Cancer Therapy: Current Evidence and Future Directions"*. Target Oncol, 13(1), 21-38. doi: 10.1007/s11523-017-0541-2

Vlachos, I. S., Paraskevopoulou, M. D., Karagkouni, D., Georgakilas, G., Vergoulis, T., Kanellos, I., Anastasopoulos, I. L., Maniou, S., Karathanou, K., Kalfakakou, D., Fevgas, A., Dalamagas, T., & Hatzigeorgiou, A. G. (2015). *"DIANA-TarBase v7.0: indexing more than half a million experimentally supported miRNA:mRNA interactions"*. Nucleic Acids Res, 43(Database issue), D153-159. doi: 10.1093/nar/gku1215

Vlachos, I. S., Zagganas, K., Paraskevopoulou, M. D., Georgakilas, G., Karagkouni, D., Vergoulis, T., Dalamagas, T., & Hatzigeorgiou, A. G. (2015). *"DIANA-miRPath v3.0: deciphering microRNA function with experimental support"*. Nucleic Acids Res, 43(W1), W460-466. doi: 10.1093/nar/gkv403

Vogel, C. L., Cobleigh, M. A., Tripathy, D., Gutheil, J. C., Harris, L. N., Fehrenbacher, L., Slamon, D. J., Murphy, M., Novotny, W. F., Burchmore, M., Shak, S., Stewart, S. J., & Press, M. (2002). *"Efficacy and safety of trastuzumab as a single agent in first-line treatment of HER2-overexpressing metastatic breast cancer"*. J Clin Oncol, 20(3), 719-726. doi: 10.1200/JCO.2002.20.3.719

Wahlstrom, T., & Henriksson, M. A. (2015). *"Impact of MYC in regulation of tumor cell metabolism"*. Biochim Biophys Acta, 1849(5), 563-569. doi: 10.1016/j.bbagrm.2014.07.004

Wang, Z., Yao, W., Li, K., Zheng, N., Zheng, C., Zhao, X., & Zheng, S. (2017). *"Reduction of miR-21 induces SK-N-SH cell apoptosis and inhibits proliferation via PTEN/PDCD4"*. Oncol Lett, 13(6), 4727-4733. doi: 10.3892/ol.2017.6052

Weinstein, I. B. (2002). *"Cancer. Addiction to oncogenes--the Achilles heal of cancer"*. Science, 297(5578), 63-64. doi: 10.1126/science.1073096

Weinstein, I. B., & Joe, A. K. (2006). *"Mechanisms of disease: Oncogene addiction--a rationale for molecular targeting in cancer therapy"*. Nat Clin Pract Oncol, 3(8), 448-457. doi: 10.1038/ncponc0558

Weiss, W. A., Aldape, K., Mohapatra, G., Feuerstein, B. G., & Bishop, J. M. (1997). *"Targeted expression of MYCN causes neuroblastoma in transgenic mice"*. EMBO J, 16(11), 2985-2995. doi: 10.1093/emboj/16.11.2985

Westermann, F., Henrich, K. O., Wei, J. S., Lutz, W., Fischer, M., Konig, R., Wiedemeyer, R., Ehemann, V., Brors, B., Ernestus, K., Leuschner, I., Benner, A., Khan, J., & Schwab, M. (2007). *"High Skp2 expression characterizes high-risk neuroblastomas independent of MYCN status"*. Clin Cancer Res, 13(16), 4695-4703. doi: 10.1158/1078-0432.CCR-06-2818

Westermann, F., Muth, D., Benner, A., Bauer, T., Henrich, K. O., Oberthuer, A., Brors, B., Beissbarth, T., Vandesompele, J., Pattyn, F., Hero, B., Konig, R., Fischer, M., & Schwab, M. (2008). *"Distinct transcriptional MYCN/c-MYC activities are associated with spontaneous regression or malignant progression in neuroblastomas"*. Genome Biol, 9(10), R150. doi: 10.1186/gb-2008-9-10-r150

Westermark, U. K., Wilhelm, M., Frenzel, A., & Henriksson, M. A. (2011). *"The MYCN oncogene and differentiation in neuroblastoma"*. Semin Cancer Biol, 21(4), 256-266. doi: 10.1016/j.semcancer.2011.08.001

Wu, S., Cetinkaya, C., Munoz-Alonso, M. J., von der Lehr, N., Bahram, F., Beuger, V., Eilers, M., Leon, J., & Larsson, L. G. (2003). *"Myc represses differentiation-induced p21CIP1 expression via Miz-1-dependent interaction with the p21 core promoter"*. Oncogene, 22(3), 351-360. doi: 10.1038/sj.onc.1206145

Wu, X., Scott, D. A., Kriz, A. J., Chiu, A. C., Hsu, P. D., Dadon, D. B., Cheng, A. W., Trevino, A. E., Konermann, S., Chen, S., Jaenisch, R., Zhang, F., & Sharp, P. A. (2014). *"Genome-wide binding of the CRISPR endonuclease Cas9 in mammalian cells"*. Nat Biotechnol, 32(7), 670-676. doi: 10.1038/nbt.2889

Wu, Y., Zhang, J., Hou, S., Cheng, Z., & Yuan, M. (2017). *"Non-small cell lung cancer: miR-30d suppresses tumor invasion and migration by directly targeting NFIB"*. Biotechnol Lett, 39(12), 1827-1834. doi: 10.1007/s10529-017-2428-9

Wu, Y. M., Cieslik, M., Lonigro, R. J., Vats, P., Reimers, M. A., Cao, X., Ning, Y., Wang, L., Kunju, L. P., de Sarkar, N., Heath, E. I., Chou, J., Feng, F. Y., Nelson, P. S., de Bono, J. S., Zou, W., Montgomery, B., Alva, A., Team, P. S. C. I. P. C. D., Robinson, D. R., & Chinnaiyan, A. M. (2018). *"Inactivation of CDK12 Delineates a Distinct Immunogenic Class of Advanced Prostate Cancer"*. Cell, 173(7), 1770-1782 e1714. doi: 10.1016/j.cell.2018.04.034

Xu, L. F., Wu, Z. P., Chen, Y., Zhu, Q. S., Hamidi, S., & Navab, R. (2014). *"MicroRNA-21 (miR-21) regulates cellular proliferation, invasion, migration, and apoptosis by targeting PTEN, RECK and Bcl-2 in lung squamous carcinoma, Gejiu City, China"*. PLoS One, 9(8), e103698. doi: 10.1371/journal.pone.0103698

Yuan, Y., Niu, F., Nolte, I. M., Koerts, J., de Jong, D., Rutgers, B., Osinga, J., Azkanaz, M., Terpstra, M., Bystrykh, L., Diepstra, A., Visser, L., Dzikiewicz-Krawczyk, A., Kok, K., Kluiver, J., & van den Berg, A. (2018). *"MicroRNA High Throughput Loss-of-Function Screening Reveals an Oncogenic Role for miR-21-5p in Hodgkin Lymphoma"*. Cell Physiol Biochem, 49(1), 144-159. doi: 10.1159/000492850

Zeid, R., Lawlor, M. A., Poon, E., Reyes, J. M., Fulciniti, M., Lopez, M. A., Scott, T. G., Nabet, B., Erb, M. A., Winter, G. E., Jacobson, Z., Polaski, D. R., Karlin, K. L., Hirsch, R. A., Munshi, N. P., Westbrook, T. F., Chesler, L., Lin, C. Y., & Bradner, J. E. (2018). *"Enhancer invasion shapes MYCN-dependent transcriptional amplification in neuroblastoma"*. Nat Genet, 50(4), 515-523. doi: 10.1038/s41588-018-0044-9

Zhang, R., Xu, J., Zhao, J., & Bai, J. (2017). *"Mir-30d suppresses cell proliferation of colon cancer cells by inhibiting cell autophagy and promoting cell apoptosis"*. Tumour Biol, 39(6), 1010428317703984. doi: 10.1177/1010428317703984

Zhang, S., Wang, M., Li, Q., & Zhu, P. (2017). *"MiR-101 reduces cell proliferation and invasion and enhances apoptosis in endometrial cancer via regulating PI3K/Akt/mTOR"*. Cancer Biomark, 21(1), 179-186. doi: 10.3233/CBM-170620

Zhang, T., Kwiatkowski, N., Olson, C. M., Dixon-Clarke, S. E., Abraham, B. J., Greifenberg, A. K., Ficarro, S. B., Elkins, J. M., Liang, Y., Hannett, N. M., Manz, T., Hao, M., Bartkowiak, B., Greenleaf, A. L., Marto, J. A., Geyer, M., Bullock, A. N., Young, R. A., & Gray, N. S. (2016). *"Covalent targeting of remote cysteine residues to develop CDK12 and CDK13 inhibitors"*. Nat Chem Biol, 12(10), 876-884. doi: 10.1038/nchembio.2166

Zimmerman, K. A., Yancopoulos, G. D., Collum, R. G., Smith, R. K., Kohl, N. E., Denis, K. A., Nau, M. M., Witte, O. N., Toran-Allerand, D., Gee, C. E., & et al. (1986). *"Differential expression of myc family genes during murine development"*. Nature, 319(6056), 780-783. doi: 10.1038/319780a0

6.1 Supplementary Figures and Tables

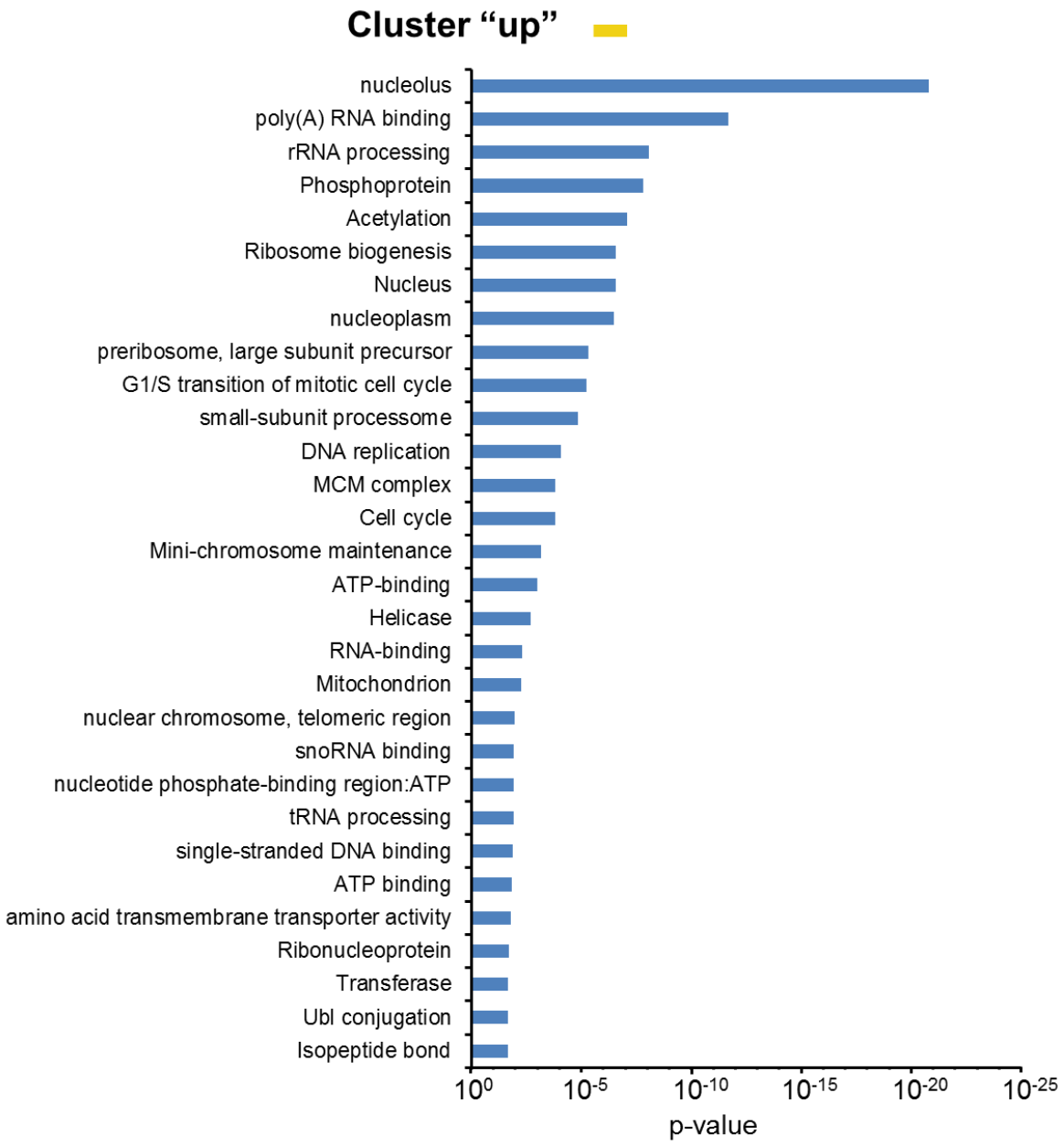

Figure S 1: Gene Enrichment Analysis of mRNAs Grouped Together by Unsupervised Clustering
Differentially expressed mRNAs detected comparing synchronized MYCN high and low IMR-5-75 cells were submitted to K-means clustering and subsequent cluster-specific gene enrichment analysis. List shows most significant terms (max. 30) of cluster "constitutively up" (yellow line, $p \leq 0.05$).

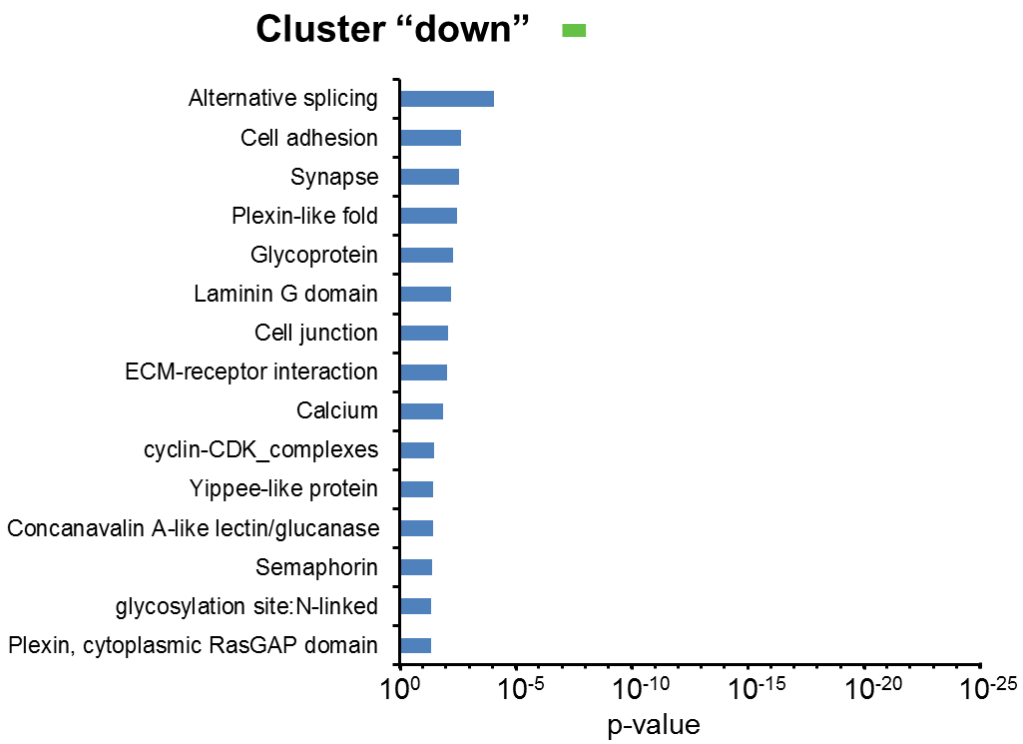

Figure S 2: Gene Enrichment Analysis of mRNAs Grouped Together by Unsupervised Clustering
Differentially expressed mRNAs detected comparing synchronized MYCN high and low IMR-5-75 cells were submitted to K-means clustering and subsequent cluster-specific gene enrichment analysis. List shows most significant terms (max. 30) of cluster "constitutively down" (green line, $p \leq 0.05$).

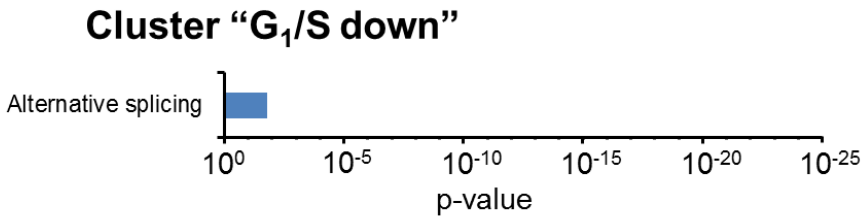

Figure S 3: Gene Enrichment Analysis of mRNAs Grouped Together by Unsupervised Clustering
Differentially expressed mRNAs detected comparing synchronized MYCN high and low IMR-5-75 cells were submitted to K-means clustering and subsequent cluster-specific gene enrichment analysis. List shows significant terms of cluster "G_1/S down" ($p \leq 0.05$).

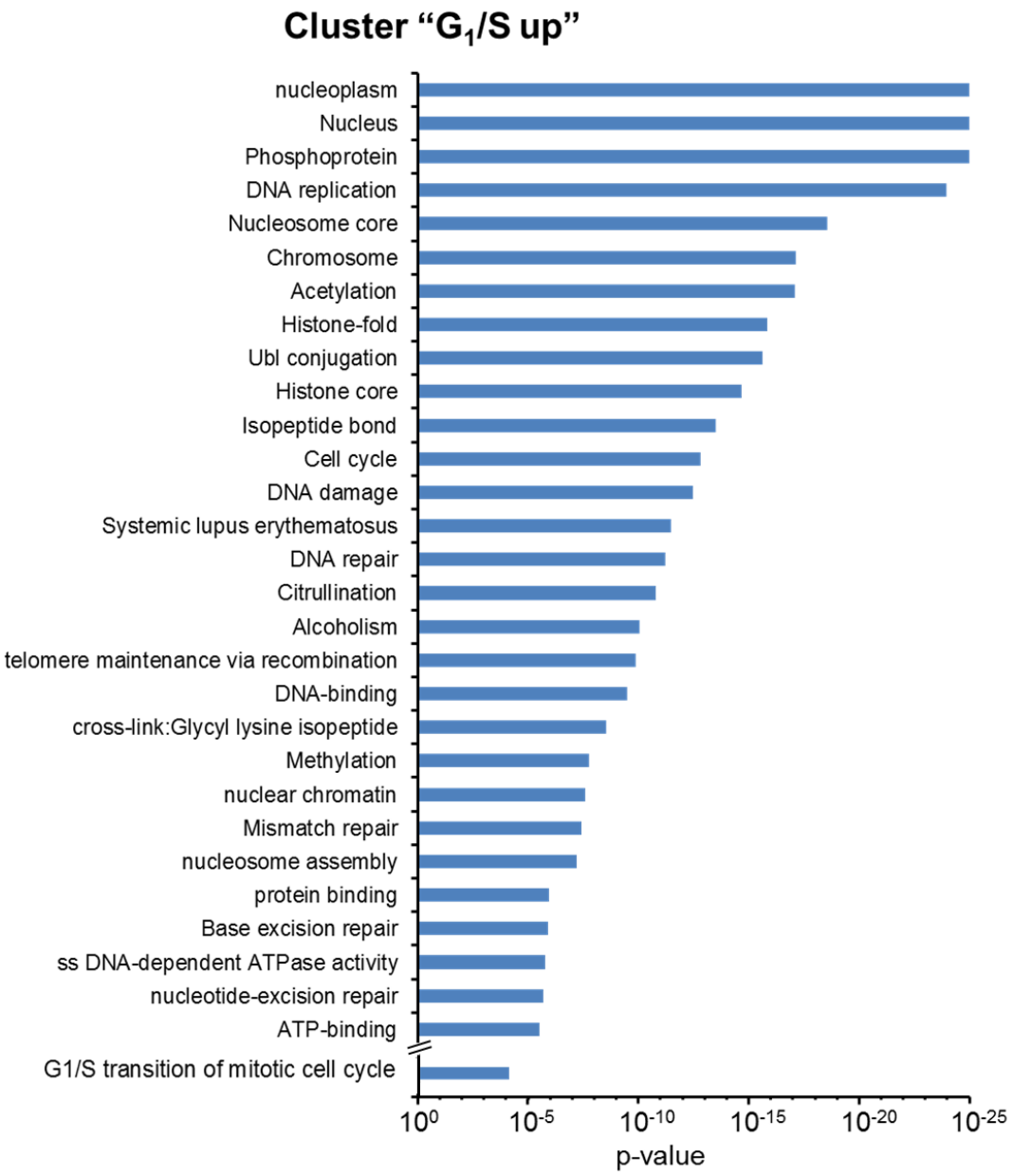

Figure S 4: Gene Enrichment Analysis of mRNAs Grouped Together by Unsupervised Clustering
Differentially expressed mRNAs detected comparing synchronized MYCN high and low IMR-5-75 cells were submitted to K-means clustering and subsequent cluster-specific gene enrichment analysis. List shows most significant terms (max. 30) of cluster "G_1/S up" ($p \leq 0.05$).

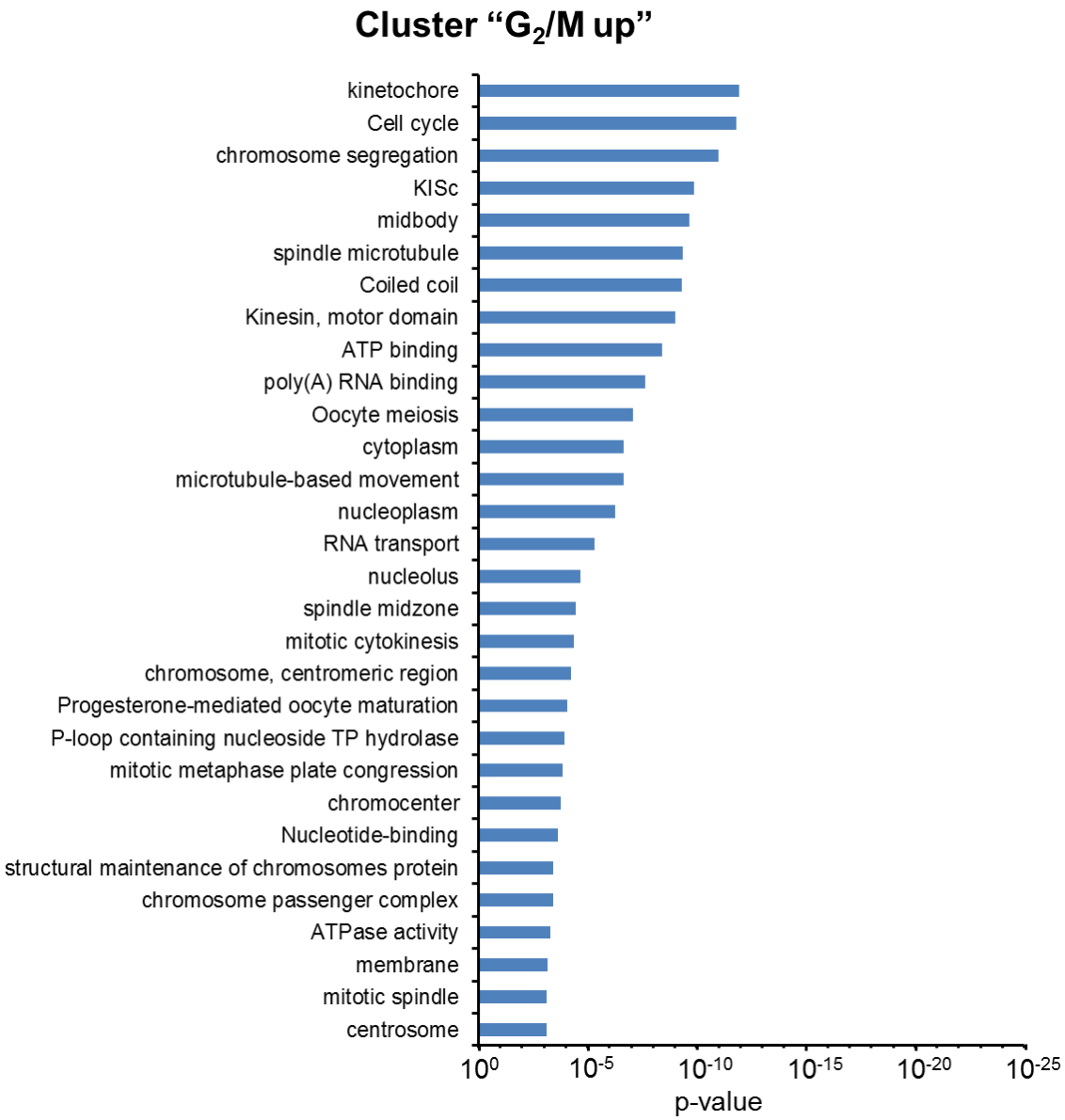

Figure S 5: Gene Enrichment Analysis of mRNAs Grouped Together by Unsupervised Clustering
Differentially expressed mRNAs detected comparing synchronized MYCN high and low IMR-5-75 cells were submitted to K-means clustering and subsequent cluster-specific gene enrichment analysis. List shows most significant terms (max. 30) of cluster "G_2/M up" ($p \leq 0.05$).

Table S 1: Intersection of Differentially MYCN-regulated miRNAs in the Time Course Experiment and the Literature *

consistently upregulated	reported as upregulated, downregulated in this study	consistently downregulated	reported as downregulated, not consistently down in this study
miR-18a-5p	miR-16-2-3p	miR-30c-2-3p	miR-3065-3p
miR-20b-3p	miR-181-5p	miR-149-5p	miR-628-5p
miR-20b-5p	let-7b-5p	miR-330-5p	miR-1291
miR-20a-5p		miR-26a-5p	miR-26b-5p
miR-9-5p		miR-30a-5p	miR-137
miR-106a-5p		miR-328-3p	miR-1908-5p**
miR17-5p			
miR-93-5p			
mir-221-3p			
mir-221-5p			

*(Megiorni *et al.*, 2017; Mestdagh *et al.*, 2010; Schulte *et al.*, 2008)
**consistently upregulated in this study

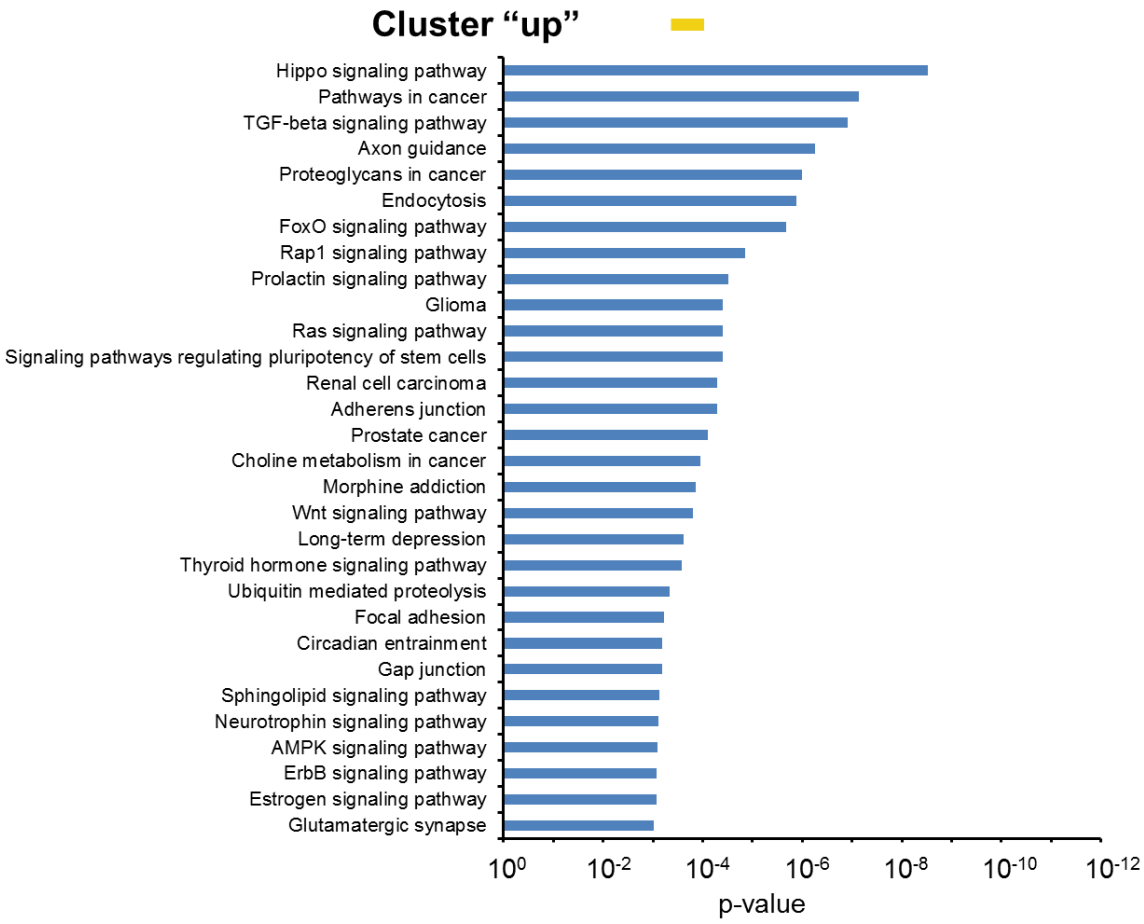

Figure S 6: KEGG Analysis of miRNAs Grouped Together by Unsupervised Clustering
Differentially expressed miRNAs detected comparing synchronized MYCN high and low IMR-5-75 cells were submitted to K-means clustering and subsequent cluster-specific KEGG analysis. List shows most significant terms (max. 30) for cluster "constitutively up" ($p \leq 0.05$).

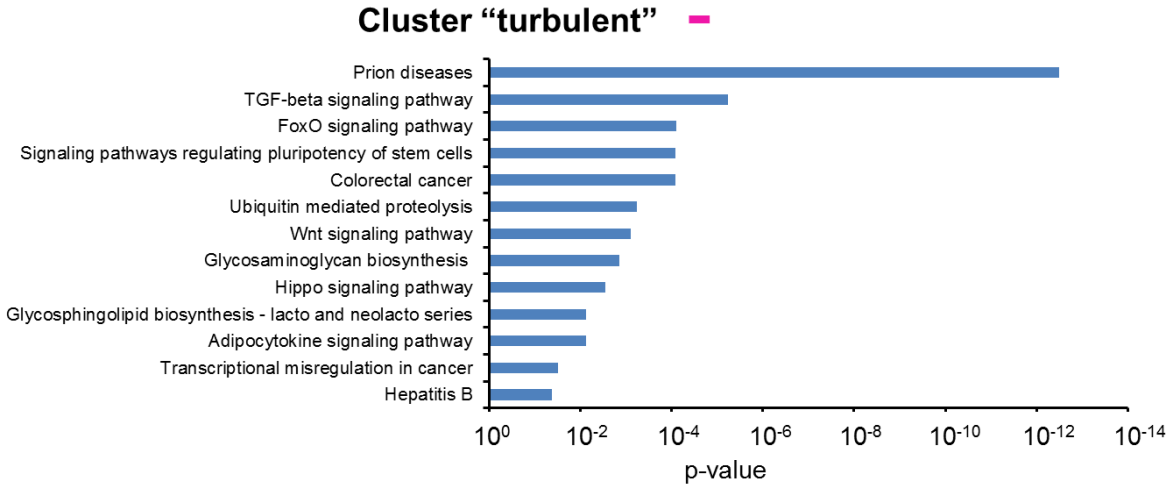

Figure S 7: KEGG Analysis of miRNAs Grouped Together by Unsupervised Clustering
Differentially expressed miRNAs detected comparing synchronized MYCN high and low IMR-5-75 cells were submitted to K-means clustering and subsequent cluster-specific KEGG analysis. List shows most significant terms (max. 30) for cluster "turbulent" ($p \leq 0.05$).

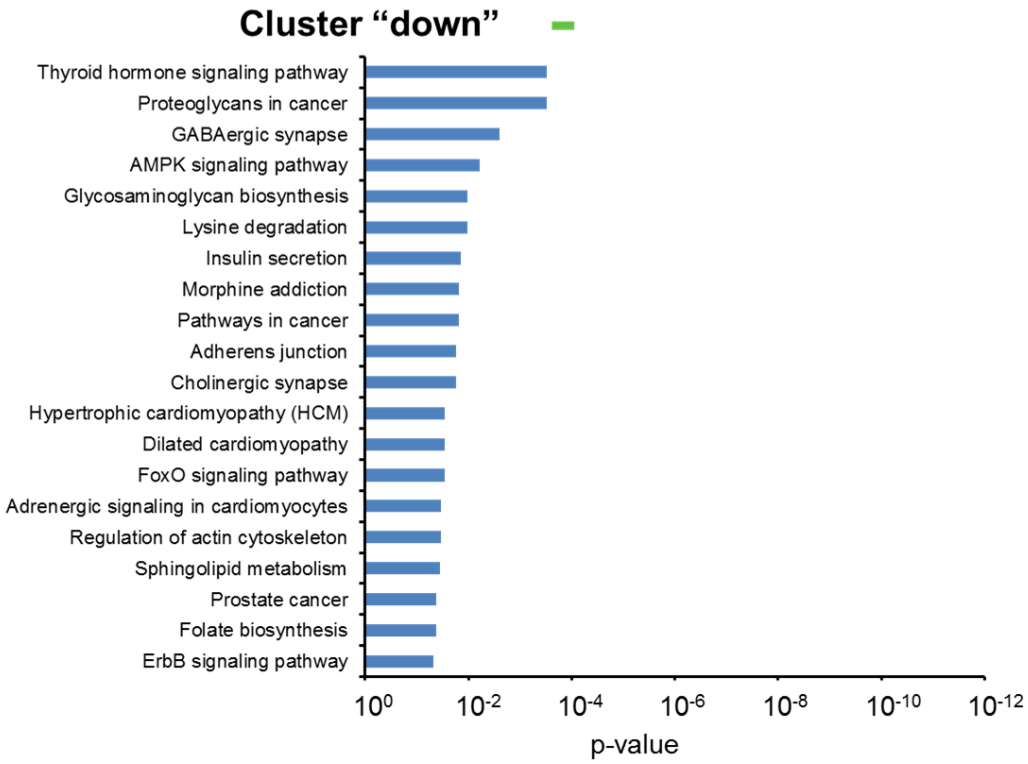

Figure S 8 KEGG Analysis of miRNAs Grouped Together by Unsupervised Clustering
Differentially expressed miRNAs detected comparing synchronized MYCN high and low IMR-5-75 cells were submitted to K-means clustering and subsequent cluster-specific KEGG analysis. List shows most significant terms (max. 30) for cluster "constitutively down" ($p \leq 0.05$).

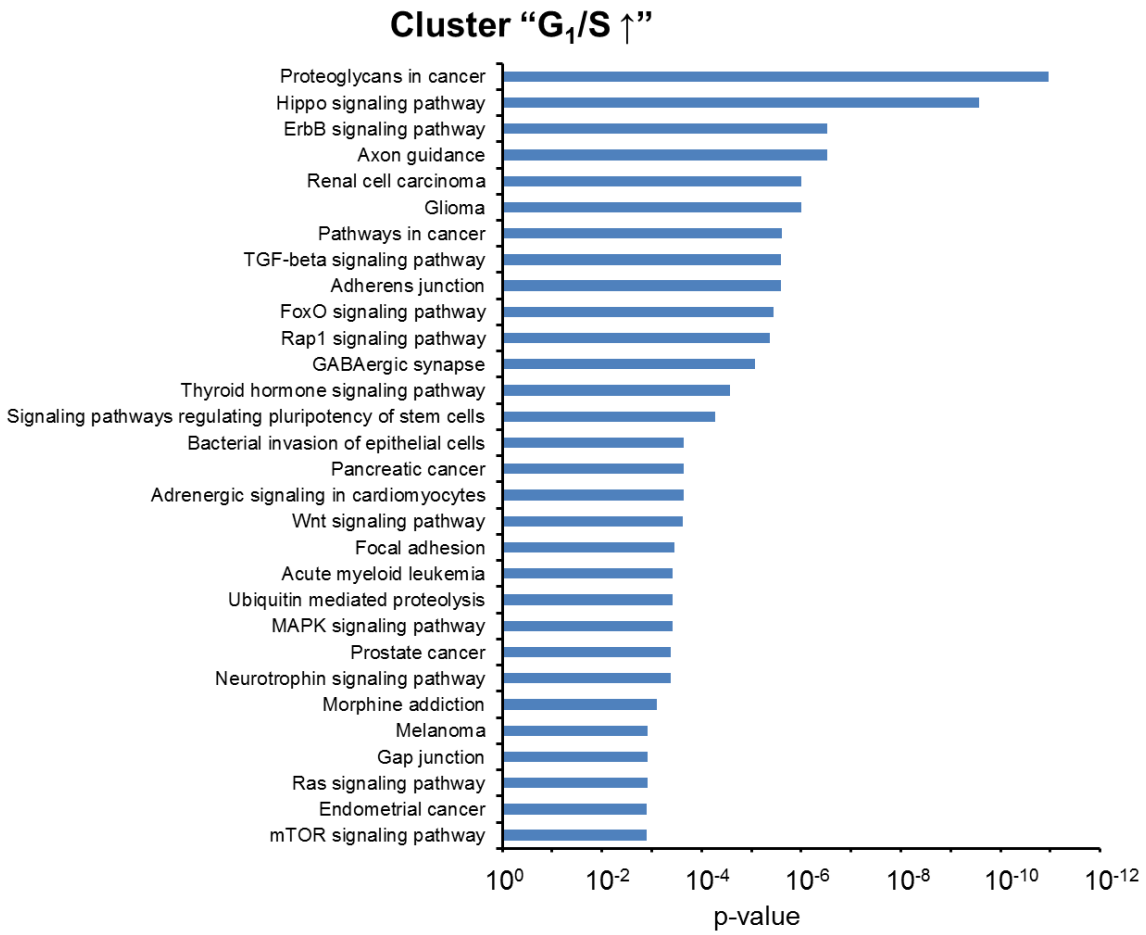

Figure S 9: KEGG Analysis of miRNAs Grouped Together by Unsupervised Clustering
Differentially expressed miRNAs detected comparing synchronized MYCN high and low IMR-5-75 cells were submitted to K-means clustering and subsequent cluster-specific KEGG analysis. List shows most significant terms (max. 30) for cluster "G_1/S up" ($p \leq 0.05$).

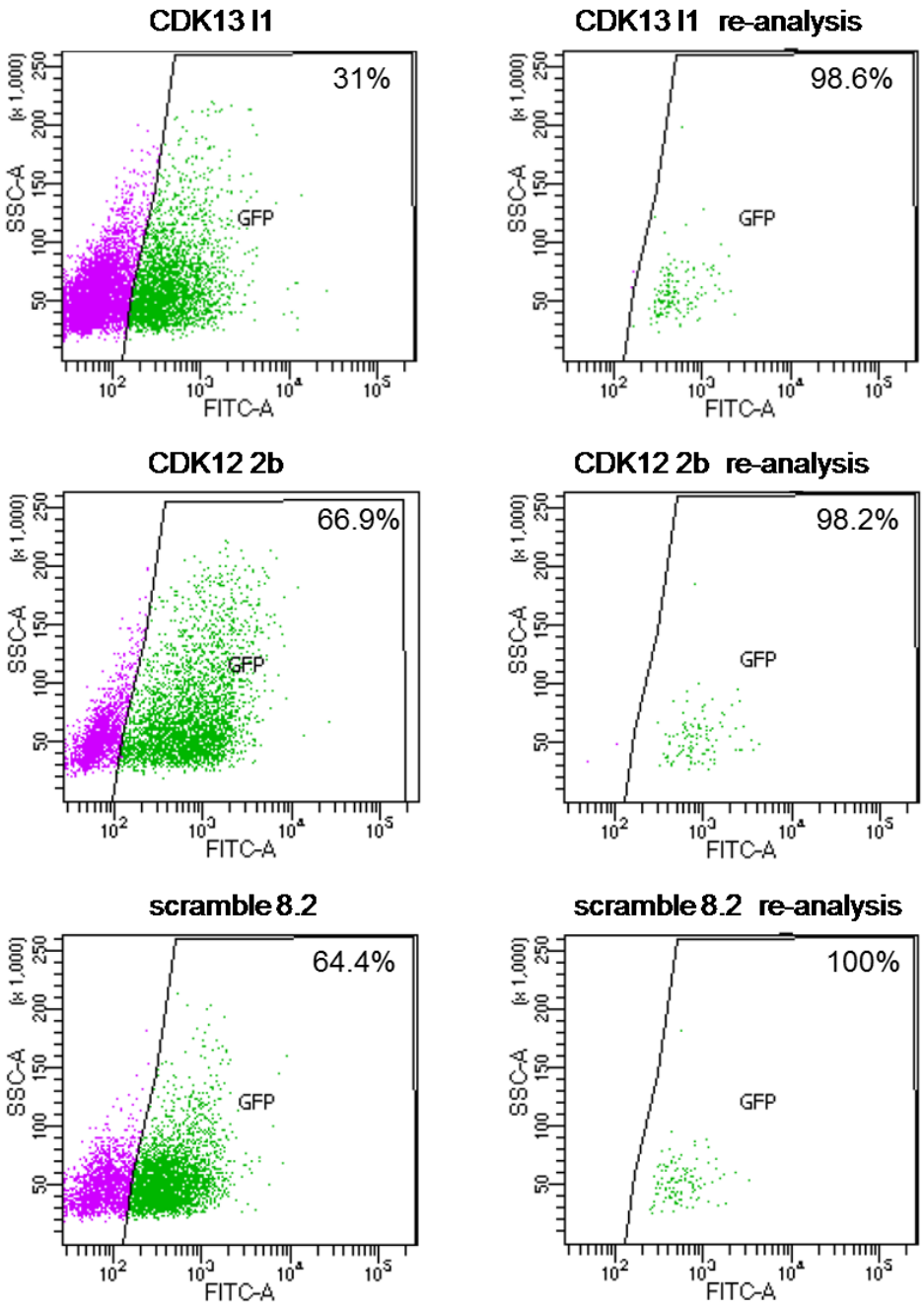

Figure S 10: Enrichment of GFP-Positive IMR-5-75 CRISPR Clones
IMR-5-75 cells were lentivirally transduced with CRISPR vectors containing Cas9, a specific sgRNA (CDK13, CDK12, scramble) and GFP. Transduced cells were taken into long-term culture and expanded. Fluorescence-activated cell sorting (FACS) was used to determine the percentage of transduced cells with GFP expression of each polyclonal culture (left graphs) and to sort GFP-positive cells, achieving > 98 % positive cells in the re-analysis (right graphs).

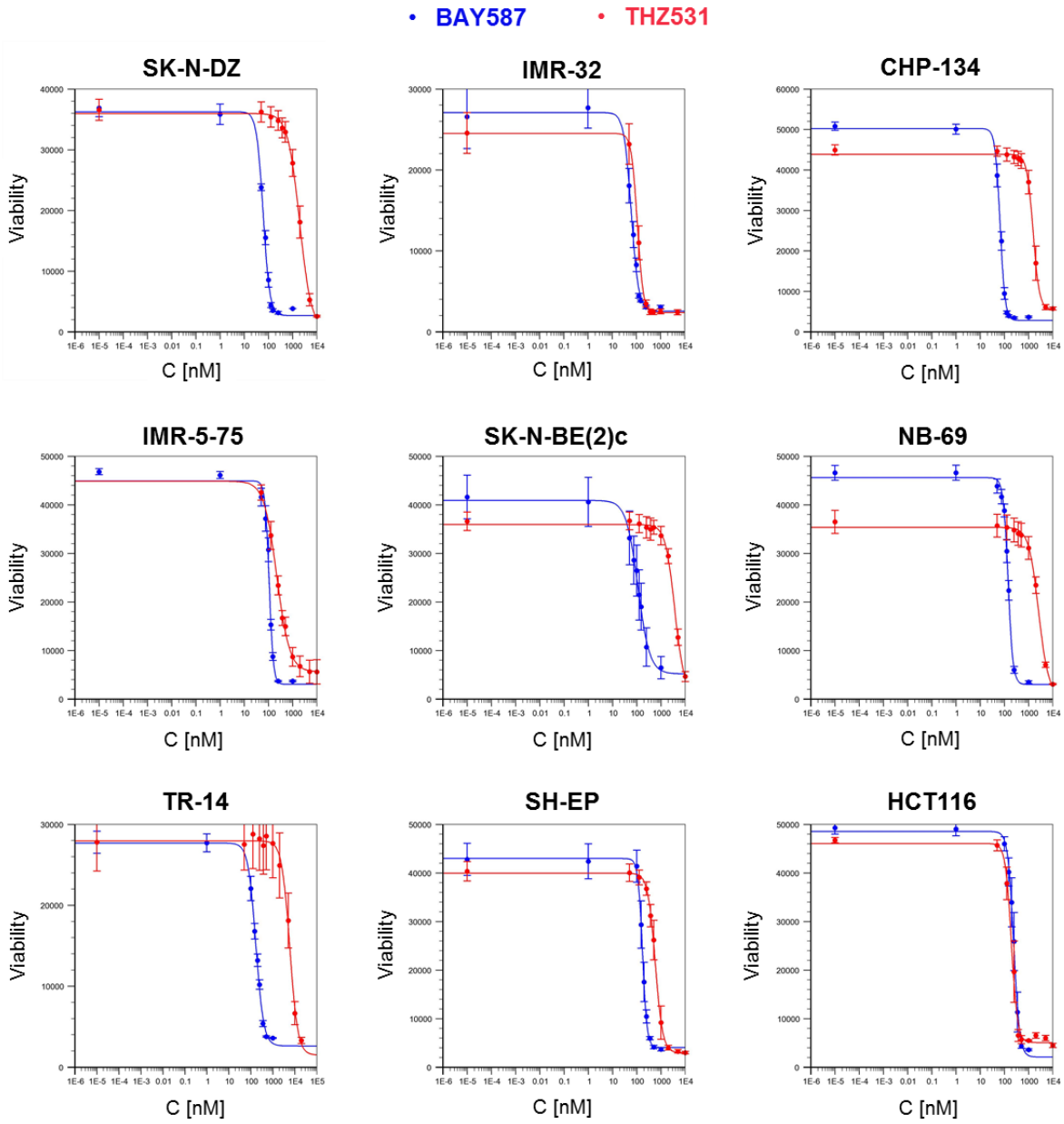

Figure S 11: Determination of Cell Line-Specific IC50 Values
Cells were seeded and treated with a dilution series of the inhibitors after 24 hours. Another 96 hours later, a CTB assay was performed to determine viability. IC50 values for BAY-587 (blue) and THZ531 (red) were determined with the "IC50 Calculator" by AAT Bioquest. mean ± SEM, n = 3-4.

6.2 Publications

Ryl, T., Kuchen, E. E., Bell, E., Shao, C., Florez, A. F., Monke, G., Gogolin, S., Friedrich, M., Lamprecht, F., Westermann, F., & Höfer, T. (2017). *"Cell-Cycle Position of Single MYC-Driven Cancer Cells Dictates Their Susceptibility to a Chemotherapeutic Drug"*. Cell Systems.

ACKNOWLEDGMENTS

Zunächst bedanke ich mich bei Frank Westermann für die Gelegenheit, in seiner Arbeitsgruppe zu promovieren, für die Betreuung während dieser Zeit, seinen überzeugenden Optimismus, selbst wenn es mal (wieder) nicht so gut lief und die Ermöglichung der Teilnahme an Konferenzen und Summer Schools im Ausland.
Mein Dank geht ebenfalls an alle, die sich freundlicherweise als Prüfer oder TAC-Mitglieder in das Projekt Doktorarbeit eingebracht und ihre Zeit geopfert haben: Thomas Höfer, Peter Angel, Matthias Selbach und Jan Lohmann.
Ich danke jedem Einzelnen der B087er für die gute und hilfsbereite Atmosphäre, die dafür sorgte, dass ich mich hier immer wohlgefühlt habe. Vielen Dank, Sina, für deine Unterstützung – sei es durch das Korrekturlesen dieser Arbeit oder in jeglichen experimentellen Fragen. Danke, Lena, dass du dich so detailliert der Einleitung dieser Arbeit angenommen hast. Elisa, dir danke ich für deine ausdauernde Hilfe bei Fragen aller Art – ohne dich würde unser Labor ganz sicher im Chaos untergehen! Danke auch, weil du eine wunderbare Büronachbarin bist. Mein Dank geht auch an Jochen für die frühmorgendliche Hilfe bei den Synchronisationsexperimenten. Ebenso möchte ich allen Azubis danken, die mich bei Experimenten unterstützten, sowie Umut und Chunxuan für die Auswertung der RNA Expressionsdaten. Ich danke auch Emma für die gute Einarbeitung zu Beginn meiner Promotion.
Vielen Dank an alle Mitleidenden – Moritz, Alica, Lea, Sabine, Selina, Ines und Karo – die Möglichkeit, Frust abzulassen, sich gegenseitig Mut zuzusprechen und zu versichern, dass es anderen auch nicht unbedingt besser ergeht, war wirklich Gold wert. Die gemeinsamen Reisen nach Australien, Bali, San Francisco und Spetses und viele andere feuchtfröhliche Aktivitäten außerhalb des Labors werden mir auf jeden Fall in guter Erinnerung bleiben.
Vielen Dank an Sylvia Fessler, Friederike Herbst und Anna Lena Ostermann-Parucha für die Möglichkeit zur und Unterstützung bei der Durchführung viraler Transduktionen in ihrer Arbeitsgruppe. Außerdem möchte ich unseren Kooperationspartnern bei Bayer, insbesondere Gerhard Siemeister, für die gute Zusammenarbeit danken.
Viel, viel Dank gebührt meiner Familie und meinen Freunden, und dabei ganz besonders meinen Eltern, die mich auf meinem ganzen bisherigen Lebensweg mit allen Kräften unterstützten und immer an mich glaubten.
Zu guter Letzt, aber doch allen voran danke ich dir, Josef, denn du bist mein verlässlicher Rückhalt und sicherer Hafen. Danke, dass du dir Tag für Tag geduldig irgendwelche experimentellen Details oder Sorgen anhörst und dich mit mir über alle noch so kleinen Fortschritte freust!